Dissertation

Consequences of intestinal CGI-58/ATGL deficiency and ATGL overexpression on gut lipid homeostasis

Submitted by

Melanie Korbelius, BSc. MSc.

For the Academic Degree of

Doctor of Philosophy

(PhD)

At the

Medical University of Graz

Gottfried Schatz Research Center for Cell Signaling, Metabolism and Aging

Molecular Biology and Biochemistry

Under the supervision of

Univ.-Prof. Mag. Dr.rer.nat. Dagmar Kratky

2019

Statutory Declaration

I hereby declare that this dissertation is my own original work and that I have fully acknowledged by name all of those individuals and organisations that have contributed to the research for this dissertation. Due acknowledgement has been made in the text to all other material used. Throughout this dissertation and in all related publications I followed the guidelines of “Good Scientific Practice“.

Graz, ...

Melanie Korbelius

Disclosures

Please note that parts of this thesis have already been published:

ATGL/CGI-58-Dependent Hydrolysis of a Lipid Storage Pool in Murine Enterocytes. **Korbelius, M**.; Vujic, N.; Sachdev, V.; Obrowsky, S.; Rainer, S.; Gottschalk, B.; Graier, WF.; Kratky, D. Cell Reports 2019. 28, 1-12. doi: 10.1016/j.celrep.2019.07.030

During my PhD thesis I also contributed to the following publications:

- *Lysosomal acid lipase regulates fatty acid channeling in brown adipose tissue to maintain thermogenesis.* Duta-Mare, M; Sachdev, V; Leopold, C; Kolb, D; Vujic, N; **Korbelius, M**; Hofer, DC; Xia, W; Huber, K; Auer, M; Gottschalk, B; Magnes, C; Graier, WF; Prokesch, A; Radovic, B; Bogner-Strauss, JG; Kratky, D. Biochim Biophys Acta. 2018; 1863(4):467-478. doi: 10.1016/j.bbalip.2018.01.011

- *Lysosomal lipid hydrolysis provides substrates for lipid mediator synthesis in murine macrophages.* Schlager, S; Vujic, N; **Korbelius, M**; Duta-Mare, M; Dorow, J; Leopold, C; Rainer, S; Wegscheider, M; Reicher, H; Ceglarek, U; Sattler, W; Radovic, B; Kratky, D. Oncotarget. 2017; 8(25):40037-40051. doi: 10.18632/oncotarget.16673

- *Monoglyceride lipase deficiency affects hepatic cholesterol metabolism and lipid-dependent gut transit in ApoE-/- mice.* Vujic, N; **Korbelius, M**; Leopold, C; Duta-Mare, M; Rainer, S; Schlager, S; Goeritzer, M; Kolb, D; Eichmann, TO; Diwoky, C; Zimmer, A; Zimmermann, R; Lass, A; Radovic, B; Kratky, D. Oncotarget. 2017; 8(20):33122-33136. doi: 10.18632/oncotarget.16529

- *Lysosomal acid lipase regulates VLDL synthesis and insulin sensitivity in mice.* Radović, B; Vujić, N; Leopold, C; Schlager, S; Goeritzer, M; Patankar, JV; **Korbelius, M**; Kolb, D; Reindl, J; Wegscheider, M; Tomin, T; Birner-Gruenberger, R; Schittmayer, M; Groschner, L; Magnes, C; Diwoky, C; Frank, S; Steyrer, E; Du, H; Graier, WF; Madl, T; Kratky, D. Diabetologia. 2016; 59(8):1743-1752. doi: 10.1007/s00125-016-3968-6

- *Active autophagy but not lipophagy in macrophages with defective lipolysis.* Goeritzer, M; Vujic, N; Schlager, S; Chandak, PG; **Korbelius, M**; Gottschalk, B; Leopold, C; Obrowsky, S; Rainer, S; Doddapattar, P; Aflaki, E; Wegscheider, M; Sachdev, V; Graier, WF; Kolb, D; Radovic, B; Kratky, D. Biochim Biophys Acta. 2015; 1851(10):1304-1316. doi: 10.1016/j.bbalip.2015.06.005

Co-authors who contributed to this thesis and my publication:

Nemanja Vujic[1], Vinay Sachdev[1,2], Sascha Obrowsky[1,3], Silvia Rainer[1], Benjamin Gottschalk[1], Wolfgang F. Graier[1,4], and Dagmar Kratky[1,4]

[1] Gottfried Schatz Research Center, Molecular Biology and Biochemistry, Medical University of Graz; 8010 Graz, Styria, Austria

[2] present address: Department of Medical Biochemistry, Academic Medical Center, University of Amsterdam, 1105 Amsterdam, Netherlands

[3] present address: EVER Neuro Pharma; 4866 Unterach am Attersee, Upper Austria, Austria

[4] BioTechMed-Graz; 8010 Graz, Styria, Austria

Hereby I acknowledge the contribution of the following persons to my research work:

- All fluorescent images were taken in cooperation with Benjamin Gottschalk.
- FPLC analysis was performed by Anton Ibovnik.
- All *in vivo* studies were performed with the help of Nemanja Vujic and Silvia Rainer.

I confirm that all co-authors have agreed to use their data in my thesis.

Für meine Eltern.

Acknowledgements

PhD student Melanie Korbelius received funding from the Austrian Science Fund (FWF P27070, P30882, DK-MCD W1226) and the Medical University of Graz through the PhD Program Molecular Medicine (MOLMED).

Danksagung

An dieser Stelle möchte ich mich bei allen bedanken, die mir die letzten Jahre über zur Seite gestanden sind und mich während meiner Dissertation unterstützt haben.

Ein ganz besonderer Dank gilt meinen Eltern und meinem Bruder, die mich stets ermutigt und jeder erdenklicher Art und Weise unterstützt haben. Die letzten Jahre waren sie rund um die Uhr für mich da und haben mich nicht nur emotional, sondern auch Nahrungs- und EDV-technisch unglaublich unterstützt ☺.

Ein riesengroßes Dankeschön richtet sich auch an meine Betreuerin Prof. Dagmar Kratky, die mich bereits schon seit meiner Masterarbeit Jahre hindurch motiviert und unterstützt hat. Dagmar hat mir nicht nur auf fachlicher, sondern auch auf persönlicher Ebene viel beigebracht, hatte jederzeit ein offenes Ohr für jede Art von Gesprächen und hat mir dadurch einen unvergleichlichen Arbeitsplatz ermöglicht.

Ich möchte mich auch besonders bei meinen großartigen Co-Betreuern und Mitgliedern meines Dissertationskomitees Prof. Günter Hämmerle und Prof. Robert Zimmermann bedanken, die mich durch anregende Disskussionen fachlich enorm weiter gebracht und durch ein freundschaftliches Verhältnis immer eine gute Atmosphäre geschaffen haben.

Weiters bedanke ich mich auch sehr für die Unterstützung von Prof. Richard Lehner als meinen externen Berater, sowie meinen Mentor Prof. Peter Macheroux, die mich während meiner Dissertation fachlich und privat großartig unterstützt haben.

Ein großer Dank gilt natürlich auch all meinen Co-Autoren, ohne die eine Publikation in *Cell Reports* unmöglich gewesen wäre. Hier möchte ich besonders Nemo hervorheben, der mir nicht nur in der Praxis, sondern auch in der Theorie unglaublich geholfen hat.

Vor allem aber möchte ich meinen großartigen Arbeitskollegen der AG-Kratky für die tolle Zusammenarbeit und das einzigartige Arbeitsklima danken - ins Besondere Silvia, Sarah und Kati, die mir jeden Tag versüßt haben.

Ein besonderer Dank gilt natürlich auch meinem Freund Stefan, der mich durchgehend unterstützt, verköstigt und ermutigt hat, auch wenn es nicht so gut lief.

Table of Contents

Abbrevations and Definitions

ABC	ATP-binding cassette
ABCA1	ATP-binding cassette subfamily A member 1
ABCG5/8	ATP-binding cassette subfamily G member 5/8
ACAT 2	Acyl-CoA:cholesterol acyltransferase 2
ACSL	Acyl-CoA synthethase
AGPAT	Acylglycerophosphat acyltransferase
Apo	Apolipoprotein
ATGL	Adipose triglyceride lipase
Atgl iKO	Intestine-specific ATGL knock out
Atgl iTg	Intestine-specific ATGL overexpression
BSA	Bovine serum albumin
cAMP	Cyclic adenosine monophosphate
CathD	Cathepsin D
cDNA	Complementary desoxyribonucleic acid
CE	Cholesteryl ester
CEL	Carboxyl ester lipase
Ces	Carboxylesterase
CGI-58	Comparative gene identification-58
Cgi-58 iKO	Intestine-specific CGI-58 knock out
Cgi-58/Atgl iDKO	Intestine-specific CGI-58/ATGL double knock out
cLD	Cytosolic lipid droplet
CM	Chylomicron
CoA	Coenzyme A
COPI/II	Coatomer protein coat-complex I/II
Cre	Cyclization recombination
DG	Diglyceride
DGAT	Acyl-CoA:diacylglycerol-acyltransferase
DTT	Dithiothreitol
EDTA	Ethylenediaminetetraacetic acid
ER	Endoplasmic reticulum
FABP	Fatty acid-binding protein
FAO	Fatty acid oxidation
FAT/CD36	Fatty acid translocase / cluster determinant 36

FATP	Fatty acid transport protein
FC	Free cholesterol
FFA	Free fatty acid
FFD	Fat-free diet
FG	Free glycerol
Fig	Figure
FPLC	Fast protein liquid chromatography
FSP27	Fat-specific protein 27
g	Gram
G0S2	G0/G1 switch protein 2
G3P	Glycerol-3-phosphate
GPAT	Glycerol-3-phosphate acyltransferase
GPCR	G-protein coupled receptor
GSTK1	Glutathion-S-transferase kappa1
GSTM3	Glutathion-S-transferase mu 3
GSTT	Glutathion-S-transferase teta
h	Hour
HDL	High-density lipoprotein
HF/HCD	High-fat/high-cholesterol diet
HIG2	Hypoxia inducible gene 2
HILPDA	Hypoxia-inducible LD-associated protein
HRP	Horseradish peroxidase
HSL	Hormone-sensitive lipase
i.p.	Intraperitoneal
i.v.	Intravenous
IDL	Intermediate-density lipoprotein
kDa	Kilo dalton
KO	Knockout
LAL	Lysosomal acid lipase
LCAT	Lecithin-cholesterol-acyltransferase
LCFA	Long-chain fatty acid
LD	Lipid droplet
LDL	Low-density lipoprotein
LDL-R	Low-density lipoprotein receptor
loxP	Locus of X-over P1

Lp(a)	Lipoprotein (a)
LPA	Lysophosphatidic acid
LPAAT	Lysophosphatidic acid acyltransferase
LPL	Lipoprotein lipase
LRP	Low-density lipoprotein receptor related protein
LSDP5	Lipid storage droplet protein 5
LXR	Liver X receptor
MCFA	Medium-chain fatty acid
MG	Monoglyceride
MGAT	Acyl-coA:monoacylglycerol acyltransferase
MGL	Monoglyceride lipase
µl	Microliter
min	Minute
ml	Milliliter
mM	Millimolar
mRNA	Messenger ribonucleic acid
MTTP	Microsomal triglyceride transport protein
NEFA	Non-esterfied fatty acid
NLSDM/NLSDI	Neutral lipid storage disease with myopathy/ichtyosis
NPC1L1	Niemann-Pick C1-like protein 1
OA	Oleic acid
ORO	Oil Red O
PA	Palmitic acid
PAP	Phosphohydrolase
PBS	Phosphate-buffered saline
PCR	Polymerase-Chain-Reaction (Polymerasekettenreaktion)
PCTV	Prechylomicron transport vesicle
PEDF	Epithelium-derived factor
PI3K	Phosphatidyl inositol kinase-3
PIC	Protease inhibitor cocktail
PKA	Proteinkinase A
PKB/Akt	Protein kinase B/Akt
PL	Phospholipid
PLA2	Phospholipase A2
PLIN	Perilipin

PPAR	Peroxisome proliferator-activated receptor
PTL	Pancreatic triglyceride lipase
SCFA	Short-chain fatty acid
SD	Standard deviation
SDS	Sodium dodecyl sulphate
sec	Seconds
SEM	Standard error of mean
SI	Small intestine
SR-B2	Scavenger receptor-B2
TC	Total cholesterol
TG	Triglyceride
TLC	Thin layer chromatography
TO	Triolein
TRL	Triglyceride-rich lipoprotein
VLDL	Very low-density lipoprotein
WAT	White adipose tissue
WT	Wildtype

List of Figures

List of Tables

Zusammenfassung

Die Aufrechterhaltung des Lipidgleichgewichts im Körper wird durch die Fettabsorption aus der Nahrung, die Lipoproteinsekretion des Darms sowie den schnellen hepatischen Abbau der Chylomikronen (CM) gewährleistet. Überschüssige Triglyceride (TG), die entweder apikal (Diät) oder basolateral (Lipoproteinreste) in den Darm aufgenommen werden, können vorübergehend als zytosolische Lipidtröpfchen (cLD) gespeichert werden. Die Mobilisierung dieses intrazellulären Lipidpools versorgt periphere Gewebe in interprandialen Perioden, wobei die Mechanismen und die beteiligten Enzyme noch unbekannt sind. Da Mäuse, denen die Adipose-TG-Lipase (ATGL) im Darm fehlt, massiv cLD akkumulieren, vermuten wir, dass der für den Abbau von intestinalen cLD verantwortliche Stoffwechselweg ATGL und ihren Co-Aktivator comparative gene identification-58 (CGI-58) miteinschließt.

Um systemische Effekte einer CGI-58/ATGL-Defizienz auszuschließen, generierten wir Mäuse, denen beide Proteine ausschließlich im Darm (iDKO) fehlen. Dies führte zu einer erhöhten cLD-Akkumulation in den Enterozyten, unabhängig von der Ernährung. In der frühen Absorptionsphase reicherten sich keine Nahrungslipide im Darm von iDKO-Mäusen an, sondern erst nach 2 h. Zusammen mit der Speicherung von cLD auch ohne alimentäre Lipidzufuhr deuten diese Ergebnisse auf das Vorhandensein eines Sekretions-/ Absorptionszykluses in Enterozyten hin. Die Ansammlung i.v. applizierter Lipide im Darm von iDKO Mäusen unterstrich die Rolle von CGI-58/ATGL in der Hydrolyse eines basolateralen Lipidpools.

Weiters gernerierten wir Mäuse, die ATGL spezifisch im Darm überexprimieren (Atgl iTg). Frühere Studien in Atgl iKO-Mäusen zeigten, dass ATGL eher für die Cholesterinabsorption als für die TG Aufnahme aus der Nahrung verantwortlich ist. In Übereinstimmung damit zeigten Atgl iTg-Mäuse eine beschleunigte Cholesterinabsorption, die hauptsächlich durch die Aktivierung von PPARα vermittelt wurde. Obwohl Atgl iTg-Mäuse eine leicht beeinträchtigte Sekretion von CM-TG und -cholesterin aufwiesen, scheint ATGL eine vernachlässigbare Rolle im intestinalen Lipoprotein-Metabolismus zu spielen.

Beide Studien zeigten, dass die Lipidhydrolyse im Darm weitaus komplexer ist als in früheren Modellen beschrieben. Wir identifizierten CGI-58 und ATGL als essentielle Enzyme im Abbau eines basolateralen, aber nicht alimentären intestinalen Lipidspeicherpools. Das Enzym, das für den Abbau von Nahrungslipiden verantwortlich ist, ist jedoch immer noch unbekannt. Die Identifizierung potenzieller Lipidhydrolasen und zukünftige Studien sollten zur Identifizierung neuer Wirkstoffziele zur Behandlung erhöhter Lipidspiegel in Blut und Darm führen.

Abstract

Systemic lipid levels are mainly determined by dietary lipid absorption and lipoprotein secretion by enterocytes of the small intestine (SI) as well as by rapid chylomicron (CM) clearance by the liver. Excessive triglycerides (TGs), originating from apical (diet) or basolateral (circulation) lipid uptake, are transiently stored in form of cytosolic lipid droplets (cLDs). Mobilization of this intracellular lipid pool is believed to sustain peripheral lipid supply in interprandial periods, however, the underlying mechanism(s) and enzyme(s) involved are still elusive. As mice lacking adipose TG lipase (ATGL) in the gut displayed massive accumulation of cLDs, we hypothesize that the enzymatic pathway accountable for the catabolism of intestinal cLDs involves ATGL and its coactivator comparative gene identification-58 (CGI-58).

To prevent systemic effects of CGI-58/ATGL deficiency, we generated mice lacking both proteins exclusively in the SI (Cgi-58/Atgl iDKO). Loss of intestinal CGI-58/ATGL resulted in increased cLD accumulation within enterocytes, independent of the diet. Alimentary lipids failed to accumulate in the SI of iDKO mice in the early phase of absorption, but got incorporated into cLDs 2 h post-gavage. These findings together with persistent cLD accumulation after restriction to endogenous lipids indicated the existence of a secretion/reuptake cycle in enterocytes. In line, accumulation of intravenously applied lipids in the proximal SI of iDKO mice highlighted the role of intestinal CGI-58/ATGL in the hydrolysis of a basolaterally-derived lipid pool.

To further investigate the contribution of solely ATGL to intestinal and whole-body lipid homeostasis, we also generated mice overexpressing ATGL (Atgl iTg) specifically in the SI. Previous studies in Atgl iKO mice revealed a role of ATGL in cholesterol absorption rather than in dietary TG metabolism. In line, Atgl iTg mice displayed accelerated cholesterol absorption, which was mainly mediated by the activation of PPARα. Although Atgl iTg mice displayed slightly impaired secretion of CM-TGs and –cholesterol, ATGL seems to play a neglible role in intestinal lipoprotein metabolism.

Both studies demonstrated that lipid hydolysis in the SI is by far more complex than described in previous models, highlighting the necessity to modify the current model of intestinal lipid metabolism. We could identify CGI-58 and ATGL as critical players in the catabolism of a basolaterally-derived intestinal lipid storage pool rather than alimentary lipids. However, the enzyme responsible for the catabolism of dietary lipids still remains elusive. Identification of potential lipid hydrolases in the SI and future studies in this field should lead to the identification of new drug targets to treat elevated lipid levels in blood and intestine.

1 Introduction

The increased incidence of metabolic disorders and cardiovascular diseases during the last decades are predominantly linked to an increase in dietary fat intake with a progressively increasing tendency of overweight and obese individuals worldwide. In this respect, a marked and prolonged postprandial hypertriglyceridemia, characterized by the accumulation of triglyceride (TG)-rich lipoproteins (TRLs), is a significant contributor to the development of dyslipidemia and a known risk factor for atherosclerosis. Despite all pathological aspects of systemic lipid metabolism, postprandial plasma lipid concentrations are primarily determined by dietary lipid absorption in the small intestine (SI). Consequently, enterocytes of the proximal SI are crucial players in whole body lipid homeostasis by mediating dietary lipid absorption and controling sustained lipid supply to other organs in the intraprandial periods. In this study, we therefore focused on alimentary absorbed lipids, subsequent neutral lipolysis in the SI, and effects on whole body lipid homeostasis.

Lipid metabolism comprises of anabolic (lipogenesis) and catabolic (lipolysis) processes, which are essential for energy homeostasis in the organism. Essentially all cells of the body are capable to store excess TGs within cytosolic lipid droplets (cLDs), which undergo neutral lipolysis to sustain lipid supply to peripheral tissues in negative energy balance states. Therefore, the lipid content of these cLDs is determined by the equilibrium of anabolic and catabolic pathways (**Figure 1**).

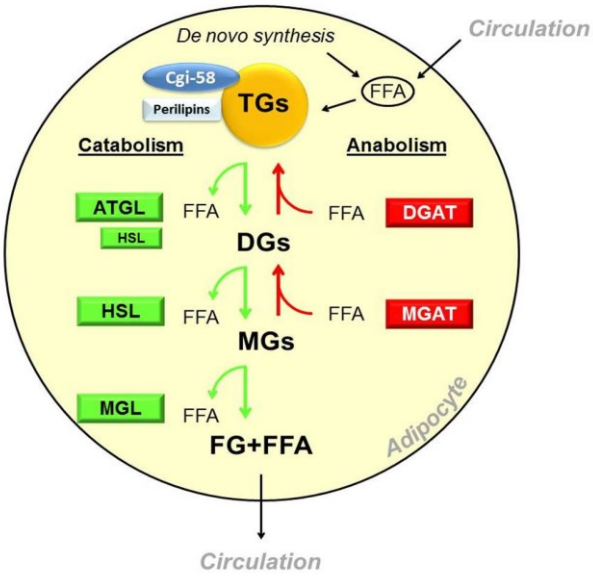

Figure 1: Anabolic and catabolic pathways in lipid metabolism.

Lipolysis (catabolic): Alimentary triglycerides (TGs) are initially hydrolyzed to diglycerides (DGs) by the action of adipose triglyceride lipase (ATGL) and hormone-sensitive lipase (HSL) and futher cleaved to monoglyceridesl (MGs) by the action of HSL. Final hydrolysis of MGs by MG lipase (MGL) results in free glycerol (FG) and free fatty acids (FFA). In each step, one FFA is released from the glycerol backbone. Lipogenesis (anabolic): TG synthesis via the MG-pathway involves acyl-coA: monoacylglycerol acyltransferase (MGAT) and acyl-coA:diacylglycerol acyltransferase (DGAT) to produce new TGs from MG and FFA.

1.1 Intestinal lipid absorption

Dietary lipid absorption in the SI is very efficient, with more than 95% of alimentary lipids taken up. Fecal lipid loss of >5% like steatorrhea already indicates a state of malabsorption. TGs make up the bulk of vegetable and animal oils and therefore represent the main component of dietary lipids (>95%) with the rest as phospholipids (PLs), lipid-soluble vitamins, sterols and other lipophilic compounds. Although all enterocytes along the SI are capable to absorb luminal lipids, dietary lipid absorption mainly occurs in the duodenum and the proximal jejunum, while bile acids and vitamin B12 are rather absorbed in the very distal SI [reviewed in (Caspary, 1992, Yen et al., 2015, Mu and Hoy, 2004)].

The absorption of dietary lipids like TGs, cholesteryl esters (CEs), and PLs already starts in the mouth and stomach, where oral and gastric lipases partially break down and emulsify dietary ingredients by peristalsis. Lingual and gastric lipases hydrolyze short- (SCFA) and medium-chain fatty acids (MCFA), which can directly enter the circulation through passive diffusion. Both lipases preferentially cleave FAs at the *sn*3 position, resulting in *sn*1,2-DGs [reviewed in (Caspary, 1992, Mu and Hoy, 2004)]. Within the stomach, 10-30% of the dietary lipids are hydrolyzed and this partially digested food (chyme) is subsequently mixed in the duodenal lumen with bile acids, deriving from either the gall bladder or directly from the liver, together with pancreatic juices (**Figure 2**).

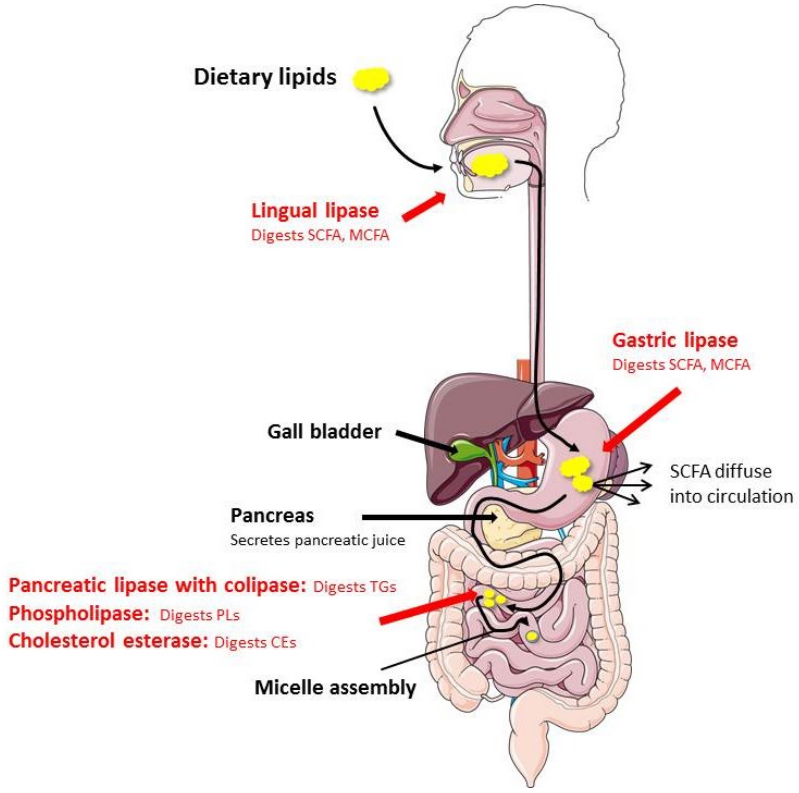

Figure 2: Dietary lipid digestion. After hydrolysis by oral and gastric lipases, dietary lipids are mixed with bile acids (gall bladder) and pancreatic juices (pancreas) in the proximal SI to form micelles, which facilitate hydrolysis and dietary lipid absorption. Within the intestinal lumen, pancreatic lipase, phospholipase and cholesterol esterase hydrolyze alimentary TGs, PLs and CEs, respectively. (modified from https://smart.servier.com)

Gastric predigestion facilitates lipid breakdown in the duodenum by increasing the solublization of TGs and by the release of free fatty acids (FFAs) that trigger cholecystokinin release. For partial degradation of dietary lipids into smaller molecules like FFA, monoglycerides (MGs), free cholesterol (FC) and lysophospholipids, which get incorporated into micelles, pancreatic juices contain pancreatic TG lipase (PTL), carboxyl ester lipase (CEL), and phospholipase A2 (PLA2) among other proteins necessary for protein- or carbodhydrate breakdown (e.g. trypsinogen, chymotrypsinogen, carboxypeptidase, amylase, nucleases). The major digestion of dietary lipids, however, is achieved by PTL [reviewed in (Wang, 2007, Mu and Hoy, 2004, Phan and Tso, 2001, Caspary, 1992)].

Of note, beside dietary lipids, the gut can also take up chylomicron (CM) remnants from the circulation and recent findings indicate the existence of two different TG pools in enterocytes, shown by diverging fates of apically (diet) and basolaterally (circulation) absorbed lipids (Storch et al., 2008) (**Figure 3**).

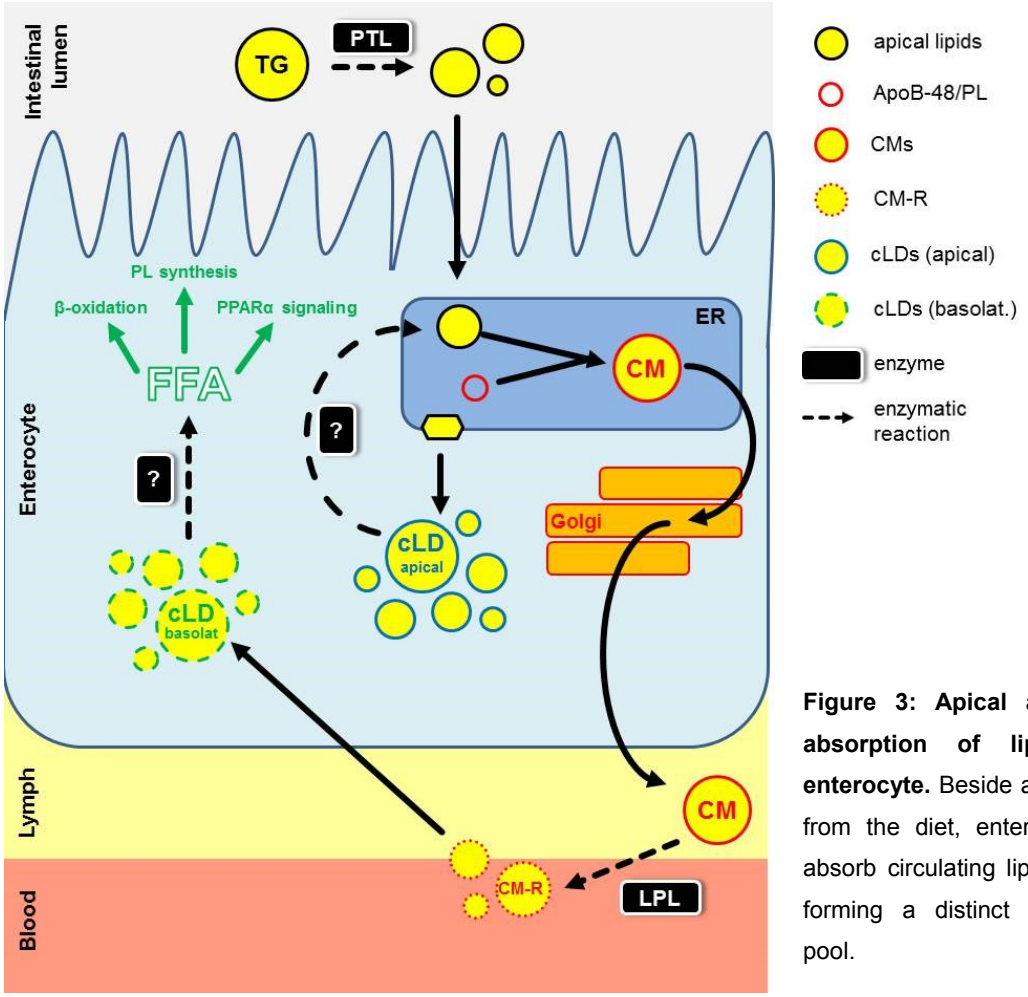

Figure 3: Apical and basolateral absorption of lipids into the enterocyte. Beside apical lipid uptake from the diet, enterocytes can also absorb circulating lipids basolaterally, forming a distinct intracellular lipid pool.

1.1.1 Absorption of alimentary TGs

The luminal digestion of dietary TGs is mainly mediated by PTL, which is secreted in ~100-fold excess than necessary after a fatty meal in response to the release of cholecystokinin [reviewed in (Caspary, 1992, Mu and Hoy, 2004)]. Dietary TGs get preferentially cleaved at the *sn*1- or *sn*3-position by PTL, thereby resulting in the formation of *sn*2-MG and FFA, which are taken up via the apical side of the enterocyte. The preference of PTL for FA at the *sn*1- or *sn*3-position is common to other lipases like hepatic lipase, endothelial lipase or lipoprotein lipase (LPL) (Yen et al., 2015). In an aqueous milieu, the isomerization of *sn*2-MG into *sn*1-MG can occur, but resorption of *sn*1-MG into the enterocyte takes longer than for *sn*2-MG (Borgstroem, 1964). Enzymatic action of PTL, but also cholesterol esterase, can lead to the production of FFA and free glycerol (FG), likely upon a rearrangement of *sn*2-MG into *sn*1(3)-MG. Depending on intra- and extracellular FFA concentrations, these hydrolysis products are subsequently taken up into the enterocyte, either via passive diffusion or by different transport proteins [reviewed in (Iqbal and Hussain, 2009, Mu and Hoy, 2004)]. Lthough enterocytes of all intestinal regions are capable to take up dietary lipids, the jejunum accounts for the majority of lipid aborption [reviewed in (D'Aquila et al., 2016)].

1.1.1.1 Passive diffusion

Passive diffusion into the enterocytes mainly occurs when extracellular FFA concentrations in the gut lumen exceed those inside the cell, while protein-mediated FFA absorption becomes more important when extracellular FFA levels are lower (Hussain, 2014). Although several transporters for long-chain FFA have been described, no transporter specific for *sn*2-MG is known so far. MG from digested lipids in the lumen is most likely taken up by passive diffusion (Pan and Hussain, 2012). Independent or partly dependent on protein-mediated FA uptake, a large amount of FFA can be absorbed through “flip-flop” across the plasma membrane, which is facilitated by the acidic microenvironment of the unstirred water layer at the apical brush border membrane (Niot et al., 2009). Unlike long-chain FAs (LCFA), MCFAs can be absorbed more easily as they are easier to hydrolyze and do not need bile salts to facilitate their absorption. Furthermore, they are hardly reesterified into TGs within the enterocyte, thus being transported directly into the liver via the portal vein without incorporation into CMs [reviewed in (Caspary, 1992, Mu and Hoy, 2004)].

1.1.1.2 Protein-mediated lipid uptake

Proteins mediating the uptake of FFA can be classified into three families: peripheral plasma membrane FA-binding proteins (FABPpm), FA transport proteins (FATP) and FA

translocases/cluster determinant 36 (FAT/CD36) [reviewed in (Pan and Hussain, 2012)]. The expression of FABPpm on the plasma membrane of intestinal microvilli indicated a role of this protein in dietary lipid absorption. However, its contribution to FA absorption in the SI has not yet been fully proven (Yen et al., 2015). Although FATP4 was believed to play an essential role in intestinal lipid absorption by facilitating the uptake of LCFAs (Stahl et al., 1999), the protein was recently ascribed a major role in skin lipid homeostasis, but a dispensable role in intestinal TG absorption (Shim et al., 2009). Another well established FA transporter at the apical brush border membrane of the enterocyte is CD36, now officially named scavenger receptor-B2 (SR-B2). This protein interacts extracellularly with FABPpm, therby acting as an FA acceptor and facilitating luminal FA uptake. Partitioning of dietary FA into lipid rafts in the outer leaflet of the plasma membrane bilayer further facilitates the "flip-flop" process of LCFA to the inner leaflet of the plasma membrane. Once inside the cell, CD36 provides a docking site for intracellular transport proteins to promote cytoplasmic FA transport [reviewed in (Glatz and Luiken, 2017)]

1.1.2 Cholesterol absorption in the SI

While luminal hydrolysis of TGs yields FFAs and MGs, cholesterol gets degraded to free cholesterol and FFAs [reviewed in (Hussain, 2014)]. Cholesterol that gets absorbed from the luminal side of the enterocyte either derives from the diet, bile or sloughing of the intestinal epithelium. Only unesterified cholesterol can be packed into micelles, therefore de-esterification of dietary CEs is a very important step in intestinal cholesterol absorption. However, the amount of non-esterified cholesterol is much larger than the amount of CEs, with only 15% of the dietary cholesterol being esterified [reviewed in (Wang, 2007)]. Cholesterol absorption is mediated by several proteins, including Niemann-Pick C1-like 1 (NPC1L1), ATP-binding cassette proteins (ABC) or CD36. Within the enterocyte, free cholesterol either gets secreted or esterified to CEs by the action of acyl-CoA:cholesterol-acyltransferase 2 (ACAT2). Cholesterol can be incorporated either in apolipoprotein B-48 (ApoB-48)-rich CMs or into high-density lipoproteins (HDLs) rich in ApoA1, which is mediated by ABCA1. Excess cholesterol gets excreted back into the intestinal lumen via ABCG5 and ABCG8. All proteins are strictly regulated via the transcription factor liver X receptor (LXR), which indirectly measures intracellular cholesterol levels and thereby regulates transcription of ABCG5, ABCG8, ABCA1, and NPC1L1. Usually, only 50% of dietary cholesterol gets absorbed [reviewed in (Iqbal and Hussain, 2009, Masson et al., 2010)].

1.2 Intracellular lipid trafficking

Within the enterocyte, MGs, FFAs or FGs are transported across the aqueous cytoplasm to the smooth endoplasmic reticulum (ER), where FAs get activated to fatty acyl-CoAs by acyl-CoA synthethases within 30 sec [reviewed in (D'Aquila et al., 2016)]. For this purpose, two intracellular transport proteins are expressed in enterocytes: intestinal FABP (I-FABP, FABP2) and liver FABP (L-FABP, FABP1). While I-FABP primarily plays a role in targeting absorbed FA to TG synthesis, L-FABP can also bind and channel MG to TG synthesis, regulates intracellular CM metabolism, and plays a role in FA oxidation (**Figure 4**) (Gajda and Storch, 2015, Lagakos et al., 2013).

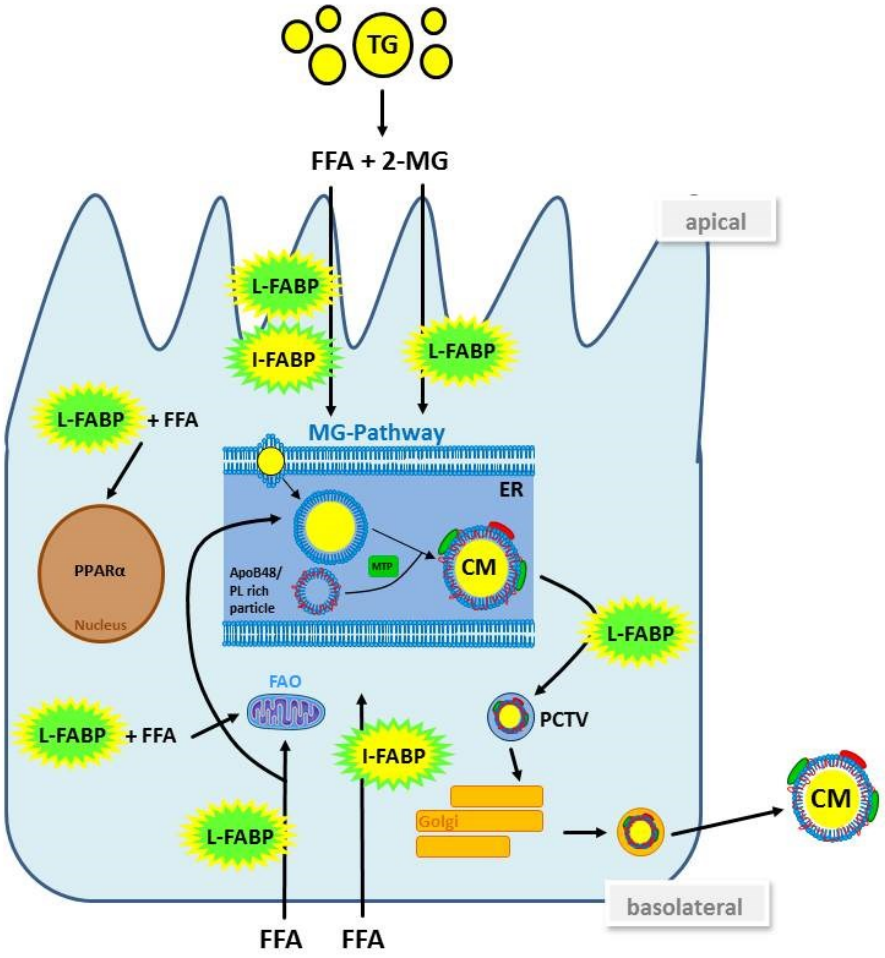

Figure 4: Role of FABPs within the enterocyte. FFA and 2-MG deriving from PTL-mediated lipolysis of dietary TGs are taken up either via L-FABP (FFA + 2-MG) or I-FABP and shuttled to the ER for resynthesis of TGs mainly via the 2-MG pathway. Beside dietary lipid uptake, L-FABP also plays a role in budding of prechylomicron transport vesicles (PCTVs), FA oxidation (FAO), and PPARα activiation. I-FABP directs mainly FFA from dietary or basolateral sources to TG synthesis.

1.2.1 I-FABP

I-FABP was shown to preferentially bind FFA deriving from the apical side, however, binding was minor compared to L-FABP-bound lipids (FFA-binding ratio between L-FABP/I-FABP = 3.3). FFA transported by I-FABP are mainly incorporated into TGs via the 2-MG pathway (**Figure 4**) (Alpers et al., 2000). Interestingly, loss of I-FABP (I-FABP KO mice) leads to enhanced fat mass loss during fasting, which was most likely attributable to increased lipid oxidation (Lagakos et al., 2013).

1.2.2 L-FABP

In contrast to I-FABP, L-FABP is also expressed in hepatocytes and to a lesser extent in kidneys. Its expression in enterocytes is highest in the duodenum and jejunum and possesses a unique feature among all FABPs as it has two binding sites: Beside high affinity binding of LCFA, L-FABP also binds other ligands like prostaglandins, FA acyl-CoAs, MGs, and lysophosholipids. L-FABP is not only responsible for trafficking of lipid substrates throughout the cytosol, but also regulates genes involved in FA oxidation by close interaction with PPARα (**Figure 4**). Increased lipid availability, like after an oral lipid load or high-fat feeding, increases the expression of L-FABP via increased substrate availability for PPARα and shifts the localization of L-FABP expression from the apical side to the cytosol [reviewed in (Gajda and Storch, 2015)]. Shuttling of dietary MG toward TG resynthesis via the 2-MG pathway implies a role of L-FABP in intracellular lipoprotein metabolism. Indeed, L-FABP was shown to be critically involved in the budding of prechylomicron transport vesicles (PCTV) from the ER (Siddiqi et al., 2010). Mice globally lacking L-FABP (L-FABP KO) display impaired hepatic and intestinal FA oxidation (FAO) and defective intestinal lipid secretion. Characterization of L-FABP KO mice revealed that L-FABP shuttles dietary MGs toward TG synthesis and directs basolaterally- as well as apically-derived FFAs toward catabolic pathways like FAO (Lagakos et al., 2013, Newberry et al., 2003).

1.3 Intestinal TG synthesis

Within the ER, absorbed hydrolysis products are used for TG re-synthesis. The rate of TG synthesis corresponds with the absorption of alimentary lipids throughout the intestine and is highly active in the epithelial layer (absorptive enterocytes), rather than in the crypt cells (Shiau et al., 1980) (**Figure 5**).

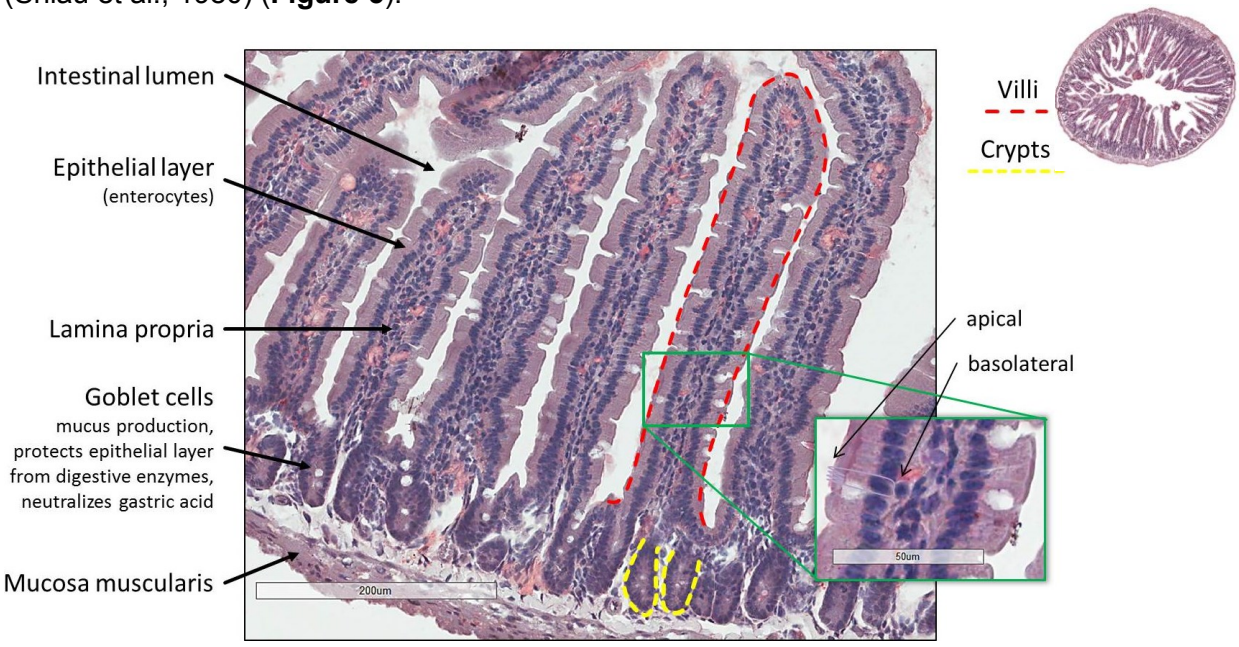

Figure 5: Histology of the SI. Magnification of a cross section of the jejunum (right corner), highlighting distinct villi. Each villus is coated by the epithelial layer consisting of the absorptive cells (enterocytes), which protects the lamina propria containing blood vessels, immune cells, and one lacteal. Magnification of the epithelial layer allows identification of the polarization of the enterocytes with the apical side facing the intestinal lumen and the basolateral side facing the lamina propria.

Enzymes involved in intestinal TG synthesis are not dependent on FA, but on their activation via acyl-CoA synthetases (ACSL), with ACSL5 being the most abundant ACSL in intestinal tissue (Grevengoed et al., 2014).

In contrast to other tissues, approximately 80% of intestinal TG synthesis is conducted via the MG-pathway, with the rest being executed by the glycerol-3-phosphate (G3P)/Kennedy pathway. The resynthesis stereospecifically favors the reacylation of the *sn*1 position. TGs synthesized from dietary MG are rapidly used for CM synthesis, whereas TGs formed from glucose-derived G3P primarily get stored in the cytosol [reviewed in (Pan and Hussain, 2012, Mu and Hoy, 2004)]. The two pathways are illustrated in **Figure 6**.

1.3.1 *sn*2-MG pathway

In the first step of TG resynthesis, acyl coA:monoacylglycerol acyltransferase (MGAT) covalently joins MG and FFA to form diglycerides (DGs), which further gets acylated by acyl coA:diacylglycerol acyltransferases 1 and 2 (DGAT1/2) to finally synthesize TGs (**Figure 6**) [reviewed in (Pan and Hussain, 2012)].

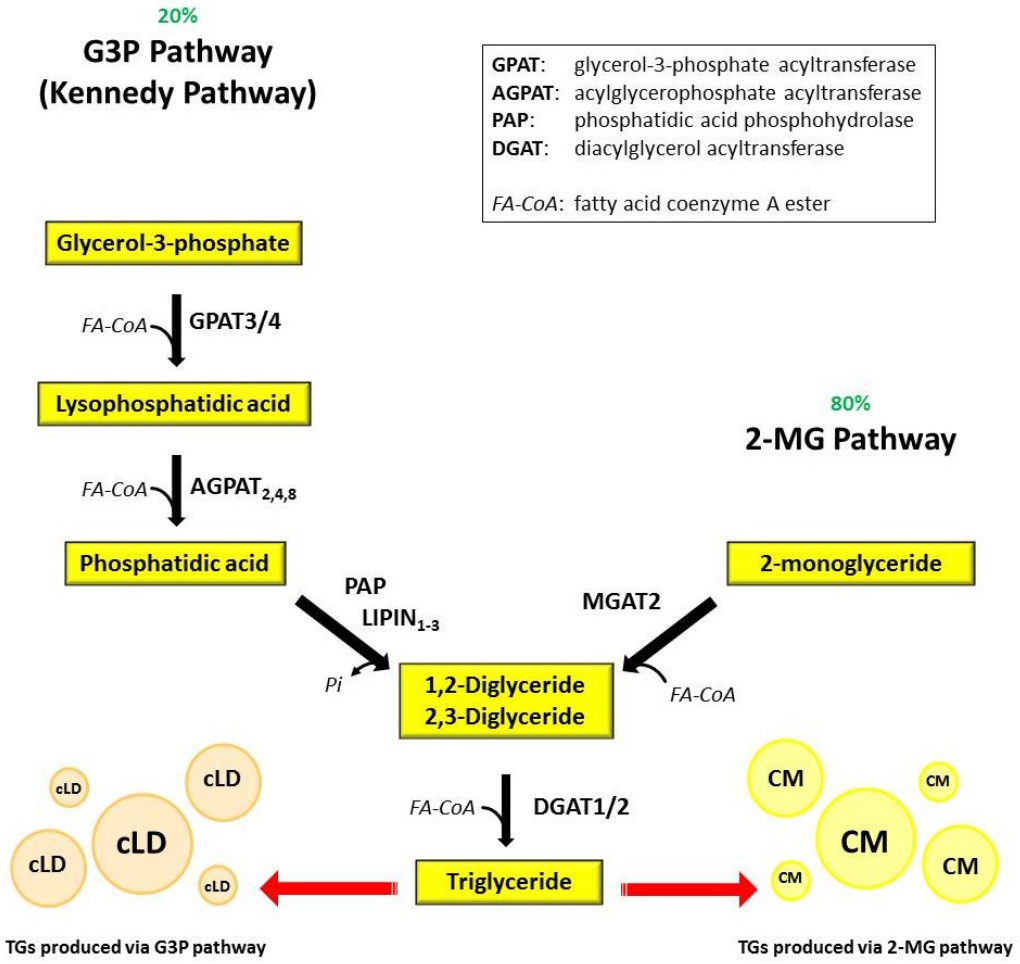

Figure 6: Resynthesis of TGs within enterocytes. As luminal hydrolysis of dietary TG results in the uptake of FFA and 2-MG, TG synthesis in the SI is mainly executed by the 2-MG pathway, involving MGAT2 and DGAT1 to synthesize 1,2- or 2,3- DG and finally TGs. The residual 20% of intestinal TGs are synthesized via the Kennedy Pathway with the initial acylation of glycerol-3-phosphate (G3P) to lysophosphatidic acid (LPA). Acylation of LPA to phosphatidic acid and further dephosphorylation yields DGs, which further get acylated by DGAT1 to form TGs. Both pathways share the last step.

1.3.1.1 MGAT

Three isoforms of MGAT are known, with MGAT2, encoded by the gene *Mogat2*, being the sole MGAT expressed in the murine SI. MGAT1 is not expressed in human or mouse intestinal tissue and MGAT3 is only found in human but not murine intestine (Nelson et al., 2014). Mice lacking global MGAT2 display lower plasma TGs, impaired metabolic efficiency, and are protected from diet-induced obesity and associated disorders. This phenotype is likely due to the observed delayed intestinal lipid absorption, leading to a redistribution of lipids rather toward energy generation (increased energy expenditure) than storage within adipocytes (Yen et al., 2009). Rescue of MGAT2 expression solely in the SI of MGAT2 KO mice only partially restored metabolic efficiency, but corrected intestinal fat absorption and weight gain upon high-fat feeding (Gao et al., 2013). Intestine-specific deletion of MGAT2 resembled the phenotype of global MGAT2 KO mice, although protection from diet-induced obesity was less pronounced (Nelson et al., 2014, Gao et al., 2013).

1.3.1.2 DGAT

The acylation of DGs via the action of DGAT enzymes is the final step of TG synthesis and the point at which the *sn*2-MG and the Kennedy pathway converge. By now, two enzymes with DGAT activity are known. Althrough both, DGAT1 and DGAT2, catalyze the same reaction, they do not belong to the same gene family and differ in terms of biochemical properties, expression patterns, and structure [reviewed in (D'Aquila et al., 2016)]. In contrast to humans, who only express DGAT1 in enterocytes, mice express both DGAT1 and DGAT2 in the intestine. Both enzymes are located in the ER of murine intestine, with DGAT1 showing activity toward the luminal and the cytosolic side and DGAT2 mainly facing the cytosol [reviewed in (Yen et al., 2015)].

Global loss of DGAT1 in mice led to massive TG accumulation within the SI, but less TG deposition in all other tissues, resulting in resistance to diet-induced obesity. Although postprandial TG secretion (1 h post gavage) was impaired in these mice, most probably caused by increased intestinal TG deposition, CM secretion *per se* was not affected, most likely due to a compensatory mechanism involving DGAT2 and DG transacylase. However, mice lacking DGAT1 display a 90% reduction in total DGAT activity, although DGAT2 is expressed in the murine SI (Buhman et al., 2002).

Due to residual TG synthesis in mice lacking DGAT1, the role of DGAT2, which is mainly expressed in liver and adipose tissue, was investigated. Whole body DGAT2 deficiency resulted in severe lipopenia and led to postnatal death within 24 h due to inavailability of

energy substrates and severe skin barrier defects. Interestingly, DGAT1 could not compensate for DGAT2 deficiency (Stone et al., 2004). *Dgat2* overexpression in whole body Dgat1 KO mice did not affect TG secretion or storage. However, co-localization of DGAT2 with Perilipin (PLIN) 2 on the surface of cLDs suggests a role of DGAT2 in directing TGs toward cLD expansion [reviewed in (D'Aquila et al., 2016)]. A recent study on human intestinal organoids deficient in DGAT1 revealed an unexpected contribution of DGAT2 to intestinal cLD formation. Overexpression of *Dgat2* in DGAT1-deficient organoids completely took over the function of DGAT1 to form cLDs in order to prevent lipotoxicity, although intestinal DGAT2 expression is lost in humans upon differentiation into enterocytes (van Rijn et al., 2019).

1.3.2 G3P/ Kennedy pathway

Beside the MG pathway, enterocytes can also synthesize TGs via the G3P or Kennedy pathway. In extraintestinal tissues like the liver, the G3P pathway is the major pathway for TG synthesis. G3P, deriving from dietary glucose, is acylated at the *sn*1 position to from lysophosphatidic acid (LPA) by G3P acyltransferase (GPAT) 3 or 4. *Sn*2 acylation of LPA to phosphatidic acid by acylglycerophosphat acyltransferase (AGPAT; also known as LPAAT) and subsequent dephosphorylation by phosphatidic acid phosphohydrolase (PAP; also known as LIPIN) finally yields DGs. Both pathways share the last step executed by DGAT1 or 2, which acylate DGs to synthesize TGs (**Figure 6**) [reviewed in (Pan and Hussain, 2012)]. Deficiency in GPAT3, which is highly expressed in the jejunum, results in impaired TG secretion into the circulation and elevated intracellular TG levels [reviewed in (D'Aquila et al., 2016)].

1.3.3 CMs versus cLDs

As TG is hydrophobic, assistance for its transport or storage within the aqueous cytoplasm is needed. Therefore, newly synthesized TGs in the ER are either incorporated into CMs or serve as a transient lipid storage as cLDs [reviewed in (D'Aquila et al., 2016)]. Beside CMs, the rodent SI can also secrete very low-density lipoprotein (VLDL) particles. While CMs are the predominant lipoproteins secreted following an oral lipid load, VLDLs are the major lipoproteins secreted in the fasting state (Ockner et al., 1969, Tso et al., 1984). In addition, previous publications also described the appearance of HDL particles in the mesenteric lymph, one containing ApoB and one enriched with ApoA-I and ApoA-IV [reviewed in (Mu and Hoy, 2004)]. Although liporoteins and cLDs share some similarities, they both possess unique features, which are summarized in **Table 1**.

Table 1: Differences between CMs and intestinal cLDs.

	CMs	Intestinal cLDs
Size	75 – 1200 nm	< 6 µm *
Lipid composition	Neutral lipid core (TGs, CEs) surrounded by PL monolayer	
Localization	ER lumen, golgi, extracellular (lymphatics, blood)	cytosol
Function	Lipid supply to periphery	Lipid storage
Apolipoproteins	ApoB-48 (not exchangeable), ApoA-I, ApoA-II, ApoA-IV, ApoC-I, ApoC-II, ApoC-III ApoE	none
Perilipins	none	PLIN2, PLIN3

* Size of cLDs varies drastically, ranging from 0.1 µm in yeast up to > 100 µm in white adipocytes [reviewed in (Walther and Farese, 2009)]

1.3.3.1 CMs

CMs from enterocytes and VLDLs from hepatocytes represent the two main TG sources for peripheral cells and tissues and are characteristics of postprandial hypertriglyceridemia. Within the enterocyte, newly synthesized TGs in the ER get assembled with ApoB-48 via the action of microsomal TG transport protein (MTTP) to form pre-CMs. The main components of CMs are TGs, CEs, FCs and PLs. The neutral core of CMs composes TGs and CEs, which is surrounded by a PL monolayer containing FC and proteins. Pre-CMs are formed by expansion of the lipid core of primordial CM particles, most likely via the addition of TGs from luminal cLDs within the ER. L-FABP together with protein kinase Cζ mediate the budding of pre-CM transport vesicles PCTVs from the ER surface. After fusion of PCTVs with the cis-Golgi, pre-CMs are further modified by glycosylation of ApoB-48 and addition of ApoA-I, before mature CMs are finally released via exocytosis into the lymphatics on the basolateral side of the enterocyte. Finally, CMs are released into the circulation (left subclavian vein) via the thoracial duct [reviewed in (Demignot et al., 2014, D'Aquila et al., 2016)]. However, not only TGs absorbed from the diet, but also FAs from the bile or from VLDL particles, which were transported to the SI, are transported in the lymphatics, making data obtained from lymph collection difficult to interpret. Beside the lymphatics, dietary lipids can also directly enter the portal vein, depending on their chain length, level of unsaturation, and structure [reviewed in (Mu and Hoy, 2004)].

1.3.3.2 cLDs

In case of excess dietary TGs, lipids can also be incorporated into cLDs to sustain lipid supply to peripheral tissues in interprandial periods. Over the past years, several models of cLD formation were proposed with the model involving ER budding being the most supported one. In this model, TG accumulation within the PL-bilayer of the ER membrane finally leads to budding of a cLD with the outer ER membrane leaflet forming its PL monolayer. Once in the cytosol, cLDs are able to furher increase in size either by TG synthesis localized on the cLD surface or by fusion of cLDs. An important aspect in the growth of cLDs is an upregulation in PL synthesis to also expand the PL monolayer [reviewed in (Demignot et al., 2014, D'Aquila et al., 2016].

Beside structural proteins (e.g. PLIN) and chaperones, proteins involved in lipid metabolism, membrane transport, signal transduction, or other metabolic pathways are located on the cLD surface, raising the question how these cLD-associated proteins are targeted to the droplet. Usually transmembrane proteins possess water-soluble domains on each side of the membrane bilayer, which makes it difficult to target these proteins to the monolayer of a cLD. Previous studies demonstrated that especially two proteins, caveolin and DGAT2, are located to the bilayer of the ER membrane and the PL monolayer of cLDs. Both proteins possess a long hydrophopic stretch, which is embedded in the membrane with both termini facing the aqueous cytoplasm [reviewed in (Walther and Farese, 2009)].
The mobilization of TG stores within cLDs of the adipose tissue already becomes clearer with adipose TG lipase (ATGL) mediating the first step in neutral lipid degradation (Zimmermann et al., 2004). In the SI, the current hypothesis states that intestinal cLDs optimize lipid absorption during food intake and provide sustained lipid supply during fasting, however, knowledge about the enzymes involved in the catabolism of cLDs within the SI is limited [reviewed in (Beilstein et al., 2016)].

1.3.4 Lipoprotein assembly in other tissues

The rodent intestine is able to secrete also VLDL and HDL particles beside CMs, whereas hepatic cells secrete VLDL and HDL. Intermediate-density lipoprotein (IDL) and low-density lipoprotein (LDL) originate from lipolysis of CMs and VLDLs within the circulation. Circulating lipoproteins are classified according to their density, resulting from their lipid to protein ratio: e.g. HDL particles posses more proteins than incorporated lipids and are therefore high-densitiy particles due to the lower buoyant density of lipids compared to proteins. **Table 2** summarizes the differences of circulating lipoproteins. Beside the major lipoproteins listed in

Table 2, lipids can also be transported within the bloodstream in form of lipoprotein(a) [Lp(a)] with ApoB-100 and Apo(a) as predominant proteins or as FA bound to albumin (Vance and Vance, 2002).

Table 2: Properties of circulating lipoproteins. (Estrada-Luna et al., 2018)

	CM	**VLDL**	**IDL**	**LDL**	**HDL**
Origin	Intestine	Liver, (Intestine)	Plasma	Plasma	Liver, Intestine
Size	> 70 nm	30-70 nm	20-30 nm	19-23 nm	7.5-12.5 nm
Density [mg/ml]	<0.094	1.006-1.019	1.019-1.063	1.063-1.120	1.120-1.210
Protein content	1-2%	6-10%	20%	18-22%	45-55%
Lipid compostion					
TG	90-95%	45-65%	35%	4-8%	2-7%
Cholesterol	1-3%	4-8%	38%	50%	20-25%
PL	3-6%	15-20%	30%	18-24%	26-32%
Apolipoproteins	**ApoB-48**, ApoA-I, ApoA-II, ApoA-IV, ApoC-I, ApoC-II, ApoC-III ApoE	**ApoB-100**, ApoC-I, ApoC-II, ApoC-III ApoE	**ApoB-100**, ApoC-I, ApoC-II, ApoC-III ApoE	**ApoB-100**	ApoA-I, ApoA-II, ApoC-I ApoC-II, ApoC-III, ApoD, ApoE

The main difference between intestinal and hepatic lipoproteins is the isoform of ApoB, the only non-exchangeable protein of all lipoproteins. Of note, secretion of ApoB is strictly dependent on non-covalent binding of lipids in the ER lumen, therefore ApoB is only present in the plasma when bound to lipids (Vance and Vance, 2002). All other apolipoproteins can be exchanged within the circulation and possess different functions (**Table 3**).

Human as well as murine hepatocytes secrete ApoB-100, while the intestine primarily secretes the truncated form, ApoB-48, which consists only of the N-terminal 48% of full-length ApoB-100. In contrast to humans, rodent livers can secrete both froms of ApoB, making it difficult to distinguish between CMs and VLDLs by means of their ApoB variant. ApoB is amphiphatic with the non-polar side facing neutral lipids within the lipoprotein particles and the polar side facing the aequous environment of the bloodstream. As ApoB ist the only secretory protein known which needs lipid binding for secretion, intestinal as well as

hepatic cells express MTTP in the ER lumen to transfer TGs to nascent ApoB particles (Vance and Vance, 2002).

CMs containing dietary lipids are secreted via the basolateral side of the enterocytes into the lymphatics and finally into the bloodstream. Circulating nascent CMs mature through contact with ApoE and ApoC-II from circulating HDL particles. LPL-mediated hydrolysis of CM-TGs, activated by its cofactor ApoC-II, provides FFAs and glycerol for peripheral tissues. The remaining CM particles (CM remnants) containing ApoB-48, ApoE, CEs, and lipid-soluble vitamins bind to specific ApoE receptors in the liver and are removed from the circulation by endocytosis via the LDL-receptor-like protein (LRP). Within hepatocytes, lipids derived from CM remnants further serve as substrates for hepatic VLDL or HDL synthesis [reviewed in (Cooper, 1997)].

Table 3: Characteristics of apolipoproteins. (Wrensch et al., 2018, Vance and Vance, 2002)

	Function
ApoA-I	Cofactor of lecithin-cholesterin acyltransferase (LCAT), structural component of HDL, reverse cholesterol transport
ApoA-II	Unknown, activator of hepatic lipase (?), structural component of HDL
ApoA-IV	LCAT activator
ApoB-48	Assembly and secretion of CMs, structural component
ApoB-100	Assembly and secretion of VLDL, structural component of VLDL, IDL, LDL Ligand for LDL receptor (LDL-R)
ApoC-I	Ligand for LDL-R and LDL-R related protein (LRP), LCAT activator (?)
ApoC-II	LPL activator
ApoC-III	LPL inhibtor
ApoD	Associated with LCAT activation
ApoE	Facilitates uptake by LDL-R and LRP

1.4 Lipolysis in the SI

In essentially all cells of the body, TGs and sterol esters are stored within cLDs, which are surrounded by a PL monolayer. Whether they mainly contain TGs or sterol esters depends on the cell type. Adipocytes contain primarily TGs, whereas macrophage “foam cells” have higher CE concentrations (Walther and Farese, 2009). Generally, cytosolic cLDs play an important role in the prevention of lipotoxicity by reesterfication of FFAs into TGs, but also serve as a reservoir for hydrophobic molecules like vitamins, prostaglandins, and steroids [reviewed in (Demignot et al., 2014)]. Lipolysis is needed to mobilize stored lipids to release FFA, which can then be further used for energy generation, membrane biosynthesis and as ligands for transcription factors [reviewed in (Zechner et al., 2012)]. Despite their important physiological role, excess FFA are harmful to the organism. Elevated levels of FFA disrupt the stability of biological membranes, alter acid-base balance, and trigger the production of bioactive lipids. All these effects affect the membrane function and lead to lipotoxicity, including ER stress, mitochondrial dysfunction, inflammation, and cell death [reviewed in (Unger et al., 2010, Zechner et al., 2012)]. Glycerol as final end product of TG breakdown is mainly metabolized in the liver and shuttled to gluconeogenesis after phosphorylation to G3P and oxidation to dihydroxyacetone phosphate (Löffler et al., 2009).

1.4.1 Neutral lipolysis - ATGL and CGI-58

For white adipose tissue, the mechanism of lipolysis of TGs stored in cytosolic cLDs has already been well described. ATGL and its coactivator comparative gene identification-58 (CGI-58) mediate the initial and rate-limiting step of neutral lipolysis, degrading TGs into DGs and FFAs. Further degradation into MG and finally glycerol and FFA is accomplished by hormone-sensitive lipase (HSL) and monoglyceride lipase (MGL), respectively. This complex consisting of the three lipases including their regulatory proteins is known as the „lipolysome“ (Zimmermann et al., 2004, Yen and Farese, 2006).

Initially, HSL was believed to be the primarily responsible enzyme for intracellular TG catabolism. However, as HSL-deficient mice predominantly accumulated DGs in adipose tissue and muscle, HSL was ascribed a pivotal role in the degradation of DGs, but not TGs (Haemmerle et al., 2002). In 2004, three idependent research groups discovered the enzyme responsible for TG hydrolysis, named ATGL (Zimmermann et al., 2004), desnutrin (Villena et al., 2004) and iPLAζ (Jenkins et al., 2004). Studies on adipose ATGL and HSL revealed that 95% of total TG catabolism is executed by these two enzymes, with CGI-58 being a specific coactivator for ATGL but not HSL. Importantly, hormonal stimulation of lipolysis by forskolin

led to FFA release in both ATGL- and HSL-deficient adipose tissue, indicating that both enzymes are able to mobilize intracellular TG stores. While HSL was shown to be less efficient to induce TG hydrolysis than ATGL, ATGL could also not compensate for HSL-mediated degradation of DGs. This highlights the importance of ATGL-derived DGs as substrates for HSL to ensure efficient lipolysis (Schweiger et al., 2006).

1.4.1.1 Regulation of LD-associated lipolysis

Nutritional / hormonal regulation

Several growth factors, hormones, and (adipo-)cytokines are involved in endocrine regulation of ATGL activity. Increased catecholamine levels in response to fasting stimulate lipolysis by binding of catecholamines to β-adrenergic receptors (e.g. β_3 on adipocytes), followed by binding of G-proteins to G-protein coupled receptors (GPCRs) and subsequent activation of adenylate cyclase. Intracellular cyclic adenosine monophosphate (cAMP) levels rise in response to adenylate cyclase activation and in turn activate cAMP-dependent protein kinase A (PKA), which phosphorylates HSL as well as PLIN. HSL is phosphorylated on a non-activating site (Ser563) and two other sites (Ser659 and Ser660), leading to translocation of this lipase from the cytosol to the cLD surface. Phosphorylation of PLIN on Ser492 or Ser517 allows CGI-58 to dissociate from PLIN to bind and coactivate ATGL (**Figure 7**). This condition is reversible and can be returned to basal levels by lowering cellular cAMP levels. Other hormones leading to activation of PKA via GPCR stimulation beside catecholamines include glucagon, parathyroid hormones, thyrotropin, α-melanocyte stimulating hormone (α-MSH) and adrenocorticotropin [reviewed in (Duncan et al., 2007, Zechner et al., 2009)].

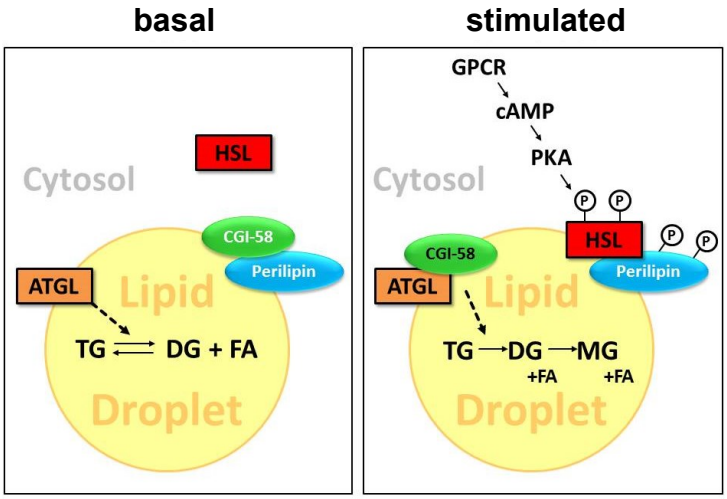

Figure 7: Hormonal stimulation of lipolysis. In the basal state, CGI-58 and perilipin are associated with each other bound to the LD surface. While HSL is predominantly localized in the cytosol, ATGL is located on LDs. Stimulation leads to phosphorylation-dependent dissociation of CGI-58 from PLIN and allows its binding to ATGL. Upon phosphorylation, HSL translocates to the surface of the LD and allows complete lipolysis.

However, insulin and insulin-like growth factor are considered inhibiting hormones of lipolysis. Thus, refeeding attenuates lipolytic action primarily through anti-lipolytic actions of insulin. This effect is mediated by cAMP-independent and cAMP-dependent mechanisms. Binding of insulin to its receptor results in autophosphorylation of the receptor, further leading to activation of phosphatidyl inositol kinase-3 (PI3K) and protein kinase B/Akt (PKB/Akt). Finally, phosphorylation and activation of phosphodiesterase 3B by PKB/Akt leads to degradation of intracellular cAMP, thereby inactivating PKA and decreasing lipolysis. Independent of cAMP, insulin can also impair lipolysis by stimulation of protein phosphatase 1, which dephosphorylates and inactivates HSL. Further, insulin decreases lipolysis by repressing *Atgl* mRNA expression. In addition, dietary compounds like calcium, caffeine, or ethanol are able to influence the rate of lipolysis, predominantly through the cAMP-dependent pathway [reviewed in (Duncan et al., 2007, Zechner et al., 2009)].

Regulation through proteins

Beside nutritional (fasting / refeeding; dietary compounds) or hormonal (catecholamines, insulin) regulation, lipolysis is controlled by direct or indirect interaction with different proteins. Along with CGI-58, which increases the lipolytic activity of ATGL up to 20-fold, PLINs as well as pigment epithelium-derived factor (PEDF) and certain transport proteins also play an essential role in the regulation of lipolysis. Interaction of PEDF with ATGL on the cLD surface was shown to stimulate ATGL-mediated lipid hydrolysis, although the underlying mechanism is controversial [reviewed in (Zechner et al., 2012)]. Probably the most important transport machinery mediating the transport of ATGL from the ER to the surface of cLDs is the ER-Golgi transport machinery with coatomer protein coat-complex I (COPI), small GTP-binding protein ARF1, and guanine-nucleotide exchange factor GBF1 as essential players. A study using GFB1 knockdown cells highlighted the role of this machinery in sequestration of ATGL as well as PLIN2 to nascent LDs, most probably due to the close proximity of ER exit sites, the ER-Golgi intermediate compartment, and cLDs. Furthermore, perturbances in the GBF1-ARF1-COPI transport machinery led to increased cLD accumulation, most likely due to impaired delivery of ATGL to the cLD surface (Soni et al., 2009).

1.4.1.2 The first step: ATGL and CGI-58

ATGL as the main regulator of LD-associated lipolysis was recently shown to also possess PLA_2 and retinyl ester hydrolase activities as well as transacylase activity to generate DGs from two MGs or TGs from DG and MG [reviewed in (Schreiber et al., 2019)]. Acylglycerol transacylase activity was shown to be dependent on MG as acyl donor and another MG or DG as acyl acceptor (Jenkins et al., 2004). For some time, it was believed that also CGI-58 possesses enzymatic activity and acts as a lysophosphatidic acid acyl transferase (LPAAT), thereby generating signaling lipids (Montero-Moran et al., 2010). In 2014, however, it was published that this LPAAT activity was due to a co-purification with plsC, the sole LPAAT in *E.coli* (McMahon et al., 2014). Interaction of the N-terminal region of CGI-58 with the patatin domain of ATGL (**Figure 8A**) stimulated the lipolytic activity of ATGL up to 20-fold (Lass et al., 2006).

Mice globally lacking ATGL displayed increased cLD accumulation in multiple tissues, leading to premature death within 14 weeks due to cardiac dysfunction. Impaired lipolysis and subsequent decreased availability of FFAs altered whole-body lipid and energy homeostasis with increased insulin sensitivity and glucose tolerance (Haemmerle et al., 2006). In humans, mutations of ATGL and CGI-58 lead to massive ectopic lipid accumulation, a autosomal-recessive rare disease called neutral lipid storage disease (NLSD). NLSD accompanied with ichtyosis (NLSDI), also known as Chanarin-Dorfman syndrome, is caused by mutations of CGI-58, leading to postnatal death of whole-body CGI-58 KO mice due to a severe skin barrier defect. In contrast, NLSD caused by mutations of ATGL is always accompanied by cardiomyopathy (NLSDM). Both diseases are characterized by lipid bodies within leukocytes (Jordans anomaly) and hepatic steatosis. Interestingly, obesity is not observed in patients suffering from NLSD [reviewed in (Lord and Brown, 2012, Schweiger et al., 2009)]. Different clinical manifestation and diverse phenotypes in mice lacking CGI-58 or ATGL point out distinct roles of these proteins in lipid metabolism (**Table 4**).

Table 4: Phenotypes of CGI-58 KO and ATGL KO mice. [reviewed in (Lord and Brown, 2012)]

Tissue	CGI-58 KO	ATGL KO
WAT	• 50% lower fat mass	• Higher fat pad weight (mildly obese) • 80% reduced TG hydrolase (TGH) activity
Skin	• Reduced dermal TGH activity • 80% reduced epidermal TGH acitivity • Severe skin barrier defect (lethal)	• Reduced dermal TGH activity • Unchanged epidermal TG hydrolase acitivity
Liver	• Severe hepatosteatosis • Newborns: 73% lower TGH activity • Liver-specific KD: VLDL secretion ↓ • DG, ceramides ↑	• Hepatosteatosis • Newborns: 46% lower TGH activity • Liver-specific KD: VLDL secretion unchanged ATGL-KO: VLDL secretion ↓ (due to increased clearance?) • DG, ceramides unchanged
SI	• Postprandial plasma TG ↓ • FA absorption & oxidation ↓ • Plasma & intestinal cholesterol ↑ • Hepatic cholesterol ↓	• FA absorption & oxidation unchanged • Plasma cholesterol ↓ • Intestinal cholesterol ↑ • Hepatic cholesterol unchanged

In fact, after lipolytic stimulation, only a small amount of CGI-58 remains on the LD to interact with ATGL, but the majority disperses into the cytosol, indicating another function of CGI-58 independent from ATGL. The main ATGL-independent function of CGI-58 was observed in the skin, leading to postnatal death of CGI-58 KO mice, while ATGL KO mice did not show any skin phenotype. Mice lacking CGI-58 specifically in the epidermis displayed impaired ω-O-acylceramide synthesis, resulting in severe dysfunction of the skin barrier. Restoring the skin phenotype by re-expressing CGI-58 in the skin of whole-body CGI-58 KO mice could reverse the skin barrier defect, indicating that epidermal CGI-58 is essential for lipid metabolism in the skin. As ATGL deficiency did not cause any changes in skin lipid metabolism, CGI-58 is believed to activate an unknown TG lipase, which provides FFAs as substrates for ω-O-acylceramide synthesis (Grond et al., 2017).

Furthermore, a recent study identified CGI-58 as a direct interaction parter for FABPs, making CGI-58 a crucial player in connecting intracellular lipolysis with shuttling of ATGL-derived FFAs through the cytosol. A-FABP was able to activate ATGL-mediated lipolysis by binding to CGI-58, but not directly to ATGL. Immediate capture of FFA released by ATGL or HSL by FABPs through interaction with CGI-58 further prevents feedback inhibition of ATGL, usually caused by increased levels of FFA. As FFA released by ATGL-mediated lipolysis are

also used for PPARα signaling, interaction of FABPs with CGI-58 likely plays an essential role in transporting FFA to the nucleus to activate PPARα (Hofer et al., 2015).

1.4.1.3 ATGL inhibitors

Opponent to CGI-58, ATGL activity can also be inhibited endogenously or pharmacologically. The first described endogenous inhibitor, G0/G1 switch gene 2 (G0S2), directly binds with its hydrophobic domain to the patatin domain of ATGL (**Figure 8A**), thereby preventing substrate accessibility and decreasing lipolysis (Yang et al., 2010). While ATGL expression is induced in adipose tissue and downregulated in liver upon fasting, expression of G0S2 is contrarily regulated. While mice lacking G0S2 globally or specifically in the liver displayed increased lipolysis accompanied by attenuated weight gain and resistance to high-fat diet (HFD)-induced hepatic steatosis, overexpression of G0S2 resulted in impaired hepatic FAO and sustained hepatic steatosis (Zhang et al., 2014b).

Recently, another endogenous inhibitor which shares structural similarity with G0S2 was identified. The PPARα target gene hypoxia-inducible LD-associated protein (HILPDA; also known as hypoxia inducible gene 2, HIG2) was shown to also directly bind to the patatin domain of ATGL (**Figure 8A**) with its N-terminal hydrophobic domain (Padmanabha Das et al., 2018). Liver-specific deletion of HILPDA led to attenuated lipid accumulation in hepatocytes due to increased lipolysis, accompanied by improved glucose tolerance. Conversely, expression of HILPDA promoted lipid accumulation in hepatocytes, indicating a major role in the control of hepatic cLD degradation (DiStefano et al., 2015). Interestingly, although HILPDA was also found on cLDs in the WAT, silencing or overexpression of HILPDA did not impact FFA or glycerol levels, indicating a negligible role of this protein in adipose cLD degradation (Dijk et al., 2017).

In addition, fat-specific protein 27 (FSP27) was shown to inhibit the lipolytic activity of ATGL, however, the underlying mechanism is questionable [reviewed in (Zechner et al., 2017)].
Recently, also lipid storage droplet protein 5 (LSDP5), a member of the PLIN family, was shown to negatively regulate ATGL-mediated lipolysis. Overexpression of LSDP5 led to increased cLD accumulation in the liver, whereas knock-down of this protein enhanced lipolysis, likely due to increased *Atgl* mRNA expression, and slightly triggered FAO (Li et al., 2012).

Although impaired ATGL activity in mice and humans led to increased ectopic lipid deposition and disease, ATGL might be a potential therapeutical target to ameliorate obesity-associated metabolic disorders caused by increased levels of circulating FFA. Pharmacological inhibition

of ATGL by the potent and ATGL-specific inhibitor Atglistatin potently diminished lipolysis in adipocytes and reduced weight gain, insulin resistance, and hepatosteatosis in HFD-fed mice. In contrast to genetic ATGL ablation, Atglistatin treatment did not cause ectopic lipid accumulation, thereby evading premature death due to cardiac steatosis. The limited effect of Atglistatin (inhibition of lipolysis up to 8 h *in vivo*) together with its diverse distribution into tissues might explain the beneficial phenotype in mice treated with Atglistatin compared to mice genetically lacking ATGL. Although human and murine ATGL share 84% similarity in their amino acid sequence, Atglistatin is only able to inhibit murine ATGL activity (Schweiger et al., 2017).

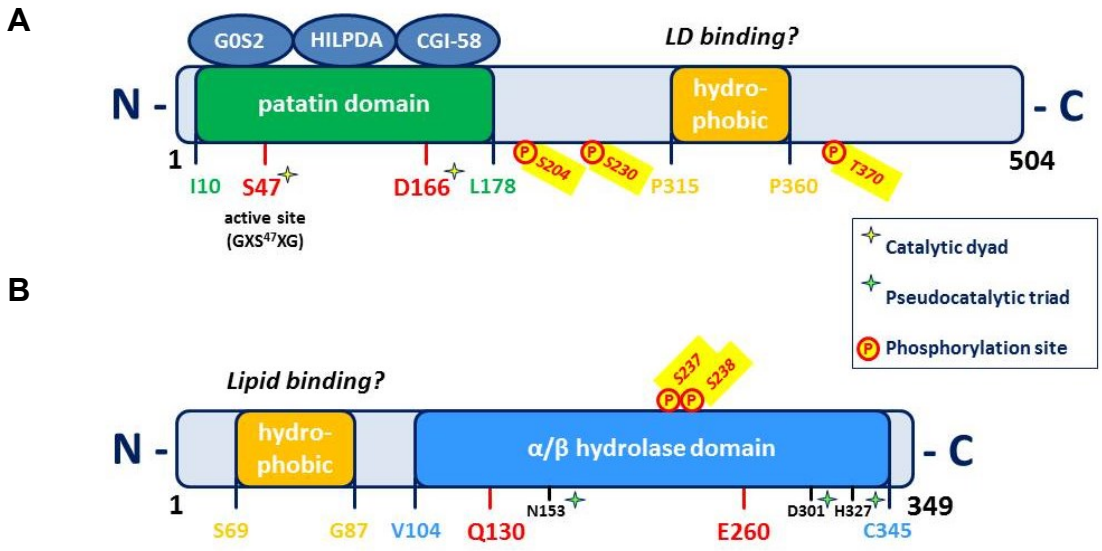

Figure 8: Structure of ATGL and CGI-58. (A) The human ATGL protein consists of 504 amino acids, containing an N-terminal patatin domain and a C-terminal hydrophobic stretch, which is supposed to function as an LD binding site. The active site is located in the patain domain and comprises a catalydic dyad (Ser47 and Asp166). (B) Human CGI-58 comprises 349 amino acids with a C-terminal α/β-hydrolase domain. The nucleophile serine in the esterase/lipase motif GXSXG is replaced by asparagine ($GXN^{153}XG$), thus CGI-58 does not possess hydrolase activity. [modified from (Missaglia et al., 2019, Schweiger et al., 2009)]

1.4.1.4 ATGL and CGI-58 in the SI

The physiological role of CGI-58 and ATGL in the SI still remains elusive. Previous studies on intestinal lipid turnover have shown that TGs stored in intestinal cLDs have the same FFA composition as TGs ingested in the previous meal (Seyer et al., 2013) and number and size of cLDs increase during dietary fat absorption with a maximum 3 h post gavage. Six hours post gavage, cLDs further decrease in size and become nearly depleted after 12 h digestion (Zhu et al., 2009). By then, it was still unclear if ATGL and CGI-58 are involved in the

hydrolysis of this intestinal TG pool. Recent findings of our group pointed out a role of ATGL in the hydrolysis of intestinal cLDs, as intestine-specific deletion of ATGL led to increased intracellular cLDs but unchanged TG absorption. This finding indicated that ATGL hydrolyzes TGs stored in cLDs but these lipids are not used for CM production (Obrowsky et al., 2013). However, intestine-specific deletion of HSL did not affect intestinal TG metabolism, but intracellular accumulation of CEs together with impaired *de novo* synthesis of cholesterol and accelerated intestinal lipid absorption from the diet identified intestinal HSL as a critical player in cholesterol homeostasis (Obrowsky et al., 2012). Interestingly, lack of intestinal CGI-58 led to large cLD accumulation in enterocytes even during the fasting state. Postprandial plasma TG levels were found to be decreased in these mice, indicating that CGI-58 is required for efficient postprandial CM secretion (Xie et al., 2014). Because of these diverging roles of CGI-58 and ATGL in lipid metabolism, this project focuses on the consequences of intestinal CGI-58/ATGL deficiency to elucidate the mechanisms behind cLD turnover in enterocytes and to point out the different roles of CGI-58 and ATGL in the SI.

1.4.2 Autophagy – acid lipolysis

Beside neutral lipolysis, degrading TGs stored within cLDs, lipids can also be transported to the lysosome to be degraded under acidic conditions. Although it was initially believed that lysosomal lipid degradation is limited to lipoprotein-derived TGs involving lipoprotein binding, internalization, and lysosomal recycling, the discovery of lipophagy in 2009 demonstrated that lysosomes also contribute to the catabolism of cLD-TGs. The enzyme responsible for acid lipid turnover within lysosomes is lysosomal acid lipase (LAL), having its optimal pH at 4.5 - 5. LAL is responsible for hydrolysis of not only TGs, but also DGs, CEs, and retinyl esters [reviewed in (Zechner et al., 2017)].

Lipophagy also plays an essential role in intracellular lipid distribution in the SI. Administration of dietary lipids induced a rapid autophagic response in enterocytes, immediately trapping newly synthesized TGs on the ER membrane by non-mature autophagosomal structures. Chemical inhibition of LAL led to massive cLD accumulation in enterocytes, highlighting an essential role of acid lipolysis in the degradation of neutral, cytosolic lipids. Of note, LDs within the SI vary drastically in their size and subcellular localization. After LD synthesis in the ER lumen, lipids are predominantly stored in cLDs. However, in parallel to the cytosolic storage, almost half of newly synthesized LDs is shuttled to the autophagic machinery and final degradation by lysosomes (Khaldoun et al., 2014).

1.5 Hypothesis and aims

Transient, postprandial storage of alimentary lipids within cLDs in enterocytes raised the question of their mobilization to sustain lipid supply to peripheral organs during interprandial periods. Massive accumulation of cLDs in mice lacking ATGL specifically in the SI (Obrowsky et al., 2013) indicated a crucial role of this enzyme in intestinal lipid turnover. I characterized mice lacking both ATGL and its coactivator CGI-58 as well as mice overexpressing intestinal ATGL to identify the underlying mechanism(s) in dietary and basolateral lipid absorption, lipoprotein metabolism, and whole-body lipid homeostasis.

2 Characterization of intestine-specific Cgi-58/Atgl KO mice

2.1 Materials and Methods

2.1.1 Animals

Mice carrying a LoxP-modified *Atgl* or *Cgi-58* allele (backcrossed onto C57BL/6 × N3) were generated in the laboratories of Erin Kershaw (Obrowsky et al., 2013) and Guenter Haemmerle (Zierler et al., 2013), respectively. To produce intestine-specific Atgl and Cgi-58 KO mice (herein designated as Atgl iKO and Cgi-58 iKO), floxed mice were interbred with transgenic mice expressing Cre recombinase under the control of the intestinal epithelial cell-specific Villin promoter (Madison et al., 2002). Intestine-specific Atgl and Cgi-58 double KO (Atgl/Cgi-58 iDKO) mice were generated by crossing Cgi-58 iKO and Atgl iKO mice.

Age- and sex-matched Atgl/Cgi-58 iDKO and $Atgl^{flox/flox}$/$Cgi\text{-}58^{flox/flox}$ littermates (WT controls) (Korbelius et al., 2019) were maintained in a temperature-controlled environment with unlimited access to food and water in a regular light-dark cycle (12h/12h). All experiments were performed using female mice aged between 13 and 14 weeks, unless stated otherwise. Mice were fed a standard chow diet (11.9% caloric intake from fat; Altromin, Lage, Germany) or challenged with either high-fat/high-cholesterol diet (HF/HC; 34% crude fat, 1% cholesterol; Ssniff®, Soest, Germany) or fat-free diet (FFD; 45% starch, 16.8% sugar, 0.2% crude fat; Ssniff®, Soest, Germany). Mice fed HF/HC diet were housed individually and food intake as well as fecal output were monitored over a period of 3 days. Food intake was calculated as g/day/mouse. To determine fecal fat weight, feces of HF/HC diet-fed mice were collected, weighed, and lipids were extracted by the method of Folch. Lipid extracts were then weighed again and the relative ratio of lipid weight to whole feces weight was calculated.

All experiments were performed in accordance with the European Directive 2010/63/EU, approved by the Division of Genetic Engineering and Animal Experiments, Austrian Federal Ministry of Education, Science and Research (Vienna, Austria; BMWFW-66.010/0057-WF/V/3b/2015).

2.1.2 Plasma lipid analysis

Blood was collected from the retroorbital plexus. To isolate plasma, blood was centrifuged for 7 min at 5,200 *x g* and 4°C. TG, total cholesterol (TC), FC, and non-esterified fatty acid (NEFA) concentrations were assayed in plasma from mice using enzymatic kits according to

manufacturer's protocols (DiaSys, Holzheim, Germany; Wako Chemicals GmbH, Neuss, Germany). Plasma CE concentrations were calculated by subtracting FC from TC.
To separate lipoproteins, 200 µl of pooled plasma were subjected to fast protein liquid chromatography (Pharmacia P-500) equipped with a Superose 6 column (Amersham Biosciences, Piscataway, NJ). (Korbelius et al., 2019)

2.1.3 Analysis of CM secretion and CM size

CM secretion was determined in chow-diet fed mice fasted for 16 h injected with tyloxapol (500 mg/kg body weight; Merck KGaA; Darmstadt, Germany) to inhibit peripheral lipolysis. Thirty minutes later, mice were gavaged with 200 µl olive oil. Blood was taken prior to the injection as well as 1, 2, 3, and 4 h post oil gavage. Plasma TG concentrations were measured as described above.

For analysis of CM size, mice were fasted for 4 h prior to injection of tyloxapol (500 mg/kg body weight). One hour later, mice were administered 200 µl oil, blood was collected 90 min post gavage and plasma was isolated. Pools (400 µl) of WT and iDKO plasma were mixed with 280 µl buffer (PBS, 2 mM benzamidine, 4 M KBr) and 4 ml of 0.9 % NaCl before ultracentrifugation for 45 min. CMs were isolated from the upper phase and size was measured in technical triplicate by light scattering (Malvern Zetasizer, Malvern Panalytical GmbH, Kassel, Germany). (Korbelius et al., 2019)

2.1.4 VLDL and postprandial TG secretion

To study VLDL secretion, mice fasted for 16 h were injected with 500 mg tyloxapol/kg body weight (Merck KGaA; Darmstadt, Germany) to prevent peripheral lipolysis. Blood was taken prior to injection as well as 1, 2, 3, and 4 h post injection. Due to slight differences in the last time point, VLDL secretion was repeated once with 0, 2, 4, and 6 h points. Plasma TG and TC concentrations were measured as described above.

For investigating the role of CGI-58 in postprandial TG secretion (Xie et al., 2014), Cgi-58 iKO and control mice on HF/HCD for six weeks were fasted overnight (16 h) and injected with 500 mg tyloxapol/kg body weight. Thirty minutes later, mice were gavaged with 500 µl olive oil and blood was taken prior to the gavage as well as 2, 4 and 6 h post-gavage. (Korbelius et al., 2019)

2.1.5 Tissue lipid analysis

Lipid parameters in the SI and liver of Cgi-58/Atgl iDKO and WT mice fed chow, HF/HC diet or FFD were analyzed in the refed state or after an indicated fasting period. Lipids were isolated from mucosal scrapings of the three parts of the SI (duodenum, jejunum, ileum) as well as from livers by folch extraction (Folch et al., 1957). Briefly, a chloroform/methanol (2:1) solution in 20-fold excess was added to the tissue lysates, which were then rotated for 2 h at room temperature. After centrifugation at 3,200 *x g* for 15 min, 0.2 parts of PBS were added to the supernatant. Samples were vortexed and centrifuged for 15 min at 800 *x g*. The lower phase was taken and dried under a stream of nitrogen. One hundred µl 2% Triton-X100 in chloroform was added and dried under nitrogen gas. Thereafter, the samples were dissolved in 100 µl ddH_2O, and TG, TC and FC concentrations were measured enzymatically with the above mentioned kits. CE concentrations were calculated by subtracting FC from TC. All values were normalized to protein concentrations. (Korbelius et al., 2019)

2.1.6 Histology and ORO staining

Duodenum, jejunum, ileum, and livers were isolated, fixed in 4% neutral-buffered formalin (Carl Roth GmbH, Vienna, Austria) for 48 h and stored in 30% sucrose before cryosectioning. Intestinal and hepatic sections of 5 µm were cut (HM 560 Cryo-Star; Microm International GmbH, Walldorf, Germany) and stained with Oil Red O (ORO) and Mayer's hematoxylin to visualize neutral lipids and nuclei. Microscopic images were taken in 40x magnification using the Aperio ScanScope AT (Leica Biosystems Nussloch GmbH, Nussloch, Germany). (Korbelius et al., 2019)

2.1.7 BODIPY® administration and immunofluorescence stainings

To trace the fate of dietary lipids, mice were fasted for 16 h prior to an oral administration of 100 µl oil containing 1 µg/g body weight BODIPY®-C_{16} (BODIPY® FL C_{16}; Molecular Probes Europe BV, Leiden, Netherlands). The administered volume was decreased to 100 µl to avoid toxic effects from DMSO and dilution of BODIPY® fluorescence. To investigate basolateral absorption of lipids, 20 µg BODIPY®-C_{16} was injected i.v. in 100 µl Intralipid. Thirty min and 2 h after gavage or injection, mice were euthanized and all three parts of the SI as well as the liver were fixed in 4% neutral-buffered formalin (Carl Roth GmbH, Vienna, Austria) for 12 h and stored in 30% sucrose. Cryosections (5 µm) were mounted using Vectashield® Mounting Medium with DAPI (Vector Laboratories, Inc., Burlingame, CA) or used for immunofluorescence staining. (Korbelius et al., 2019)

For co-staining with PLIN3 or cathepsin D (CathD), cryosections were rehydrated in Tris-buffered saline (TBS) and blocked either with 0.05% TBST containing 10% anti-goat serum or the M.O.M blocking reagent (Vector Laboratories, Inc., Burlingame, CA) for PLIN3 and CathD, respectively. Sections were incubated overnight at 4°C with the primary antibodies against PLIN3 (abs482; Merck KGaA, Darmstadt, Germany) or CathD (a6313; Abcam, Cambridge, UK) at a dilution of 1:200, followed by incubation with the corresponding Alexa Fluor 594-labeled secondary antibodies for PLIN3 (A11037; Thermo Fisher Scientific, Waltham, MA) and CathD (A11005; Thermo Fisher Scientific, Waltham, MA). Sections were mounted using Vectashield® Mounting Medium with DAPI and images were captured with a confocal spinning disk microscope (Axio Observer.Z1 from Zeiss, Gottingen, Germany) equipped with 100x objective lens (Plan-Fluor x100/1.45 Oil, Zeiss), a motorized filter wheel (CSUX1FW, Yokogawa Electric Corporation, Tokyo, Japan) on the emission side, AOTF-based laser merge module for laser line 405, 445, 473, 488, 561, and 561 nm (Visitron Systems) and a Nipkow-based confocal scanning unit (CSU-X1, Yokogawa Electric corporation). The BODIPY® and Alexa Fluor® 594 labeled structures were excited with 488 and 561 laser lines, respectively, and emission was acquired with a charged CCD camera (CoolSNAP-HQ, Photometrics, Tucson, AZ, USA). The software VisiView acquisition software (Universal Imaging, Visitron Systems) was used to acquire the imaging data. (Korbelius et al., 2019)

2.1.8 Western Blotting

Mucosal scrapings were lysed (Precellys; Bertin Instruments, Bretonneux, France) and subsequently sonicated (Labsonic B. Braun, Melsungen, Germany) for 10 sec. After centrifugation for 3 min at 18,000 *x g*, the supernatant was used for protein estimation according to the method of Lowry (BioRad Laboratories, Hercules, CA).

Eighty µg of protein were separated by SDS-PAGE and transferred onto a nitrocellulose or PVDF membrane to detect ATGL (Cell Signaling Technology; Danvers, MA; 1:200) and CGI-58 (Abnova; Taipei City, Taiwan; 1:500), respectively. Monoclonal anti-mouse β-actin (Santa Cruz Biotechnology, Heidelberg, Germany) was used as loading control. Secondary anti-rabbit (1:2,500) or anti-mouse (1:500) antibodies, conjugated with HRP (Dako, Glostrup, Denmark) were visualized using the Clarity™ Western ECL Substrate Kit (Bio Rad Laboratories; Hercules, CA) on a ChemiDoc™ MP imaging system (Bio Rad Laboratories; Hercules, CA). (Korbelius et al., 2019)

2.1.9 RNA isolation and quantitative real-time PCR

RNA was extracted using peqGOLD TriFast™ according to the manufacturer's protocol (Peqlab, Erlangen, Germany) and 2 µg of RNA were reverse transcribed using the High Capacity cDNA Reverse Transcription Kit (Applied Biosystems, Carlsbad, CA). Quantitative real-time PCR was performed on a Roche LightCycler 480 (Roche Diagnostics, Palo Alto, CA) using the GoTaq® qPCR Mastermix (Promega, Madison, WI). Samples were analyzed in duplicate and normalized to the expression of cyclophilin A as housekeeping gene. Expression profiles and associated statistical parameters were determined using the $2^{-\Delta\Delta CT}$ method. Primer sequences are listed in **Table 5**. (Korbelius et al., 2019)

Table 5: Primer sequences

Gene	Forward primer	Reverse primer
Abca1	CTCTTCATGACTCTAGCCTGGA	ACACAGACAGGAAGACGAACAC
Abcg5	AGAGGGCCTCACATCAACAGA	CTGACGCTGTAGGACACATGC
Abcg8	CTGTGGAATGGGACTGTACTTC	GTTGGACTGACCACTGTAGGT
Acc	GGACTTGGAGCAGAGAACCTTCG	CAAGCTGGTTGTTGGAGGTGTA
Acot2	GCACGAGCGTCACTTCTTGG	CCAGATACTCCAGAAGGCCAC
Acox1	TCCAGACTTCCAACATGAGGA	CTGGGCGTAGGTGCCAATTA
Atgl	GCCACTCACATCTACGGAGC	GACAGCCACGGATGGTGTTC
Cd36	GCAGGTCTATCTACGCTGTG	GGTTGTCTGGATTCTGGAGG
Ces1d	ATGGAGGTGGACTGGTGGTG	AGTGCAGCCACCTGGTCCAA
Ces1e	CCAGTGACAGGGCAAATAGTC	GTAGACAGGACCAGTCCATCATA
Ces1f	CAAGTGGCTGCTCTGCATTG	TCCAGGAATGAAGGCCACAC
Ces2a	GTGGACTGGTTGTAGGATCAGC	TTCTTCTGCACCCAGCGTAAG
Ces2c	CCTGTAGGACCACTGCGATT	GAGATACAGGCAGTCCTCAG
Ces2e	CTTGATCCTGCCTCCCATCT	GATAGCGACCACCACCACAT
Ces2f	GCCTACCATTATACCTGACTCCC	CACAGCAGGCATAAACCTGAA
Ces2g	AGGTCCAAGGCAGGCTCAT	GGCCCTCCATATTCATCGTAACA
Cgi-58	GGTTAAGTCTAGTGCAGC	AAGCTGTCTCACCACTTG
Cpt1α	CTCCGCCTGAGCCATGAAG	CACCAGTGATGATGCCATTCT
CyclophilinA	CCATCCAGCCATTCAGTCTT	TTCCAGGATTCATGTGCCAG
Ddhd2	GAGTCCAGAGCGAAATGTCATC	GGCGTCCATGTCTATGAGTTC
Dgat1	TCCGCCTCTGGGCATTC	GAATCGGCCCACAATCCA
Dgat1	TCCGCCTCTGGGCATTC	GAATCGGCCCACAATCCA
Dgat2	AGTGGCAATGCTATCATCATCGT	TCTTCTGGACCCATCGGCCCCAGGA

Dgat2	AGTGGCAATGCTATCATCATCGT	TCTTCTGGACCCATCGGCCCCAGGA
Fasn	GAAGCCGAACACCTCTGTGCAGT	GCTCCTTGCTGCCATCTGTATTG
G0s2	GTGAAGCTATACGTGCTGGG	CCGTCTCAACTAGGCCGAG
Gstk1	AAGCAGTTCTTCCAGGTTCC	CCAGAATGCTCTGATACTCC
Gstm3	ATGCCATCCTGCGCTACCTT	CCAGGAACTCAGAGTAGAGC
Hsl	GCTGGTGACACTCGCAGAAG	TGGCTGGTGTCTCTGTGTCC
I-Fabp	ACTAATCCAGACCTACACATATGAA GGA	GCTCCAGGCTCTGAGAAGTTGA
Lal	CGGCTTGCTGGCAGATTCTA	GTGCAGCCTTGAGAATGACC
Ldl-R	CATGTCTGTCACCTGTCAGTCC	CTTGTCCAAGCTGATGCACTCC
L-Fabp	CTTCTCCGGCAAGTACCAAT	GAACTCATTGCGGACCACTT
Lrp1	CCACTATGGATGCCCCTAAAAC	GCAATCTCTTTCACCGTCACA
Mcad	GCAACTGCCCGCAAGTTT	TACTCCCCGCTTTTGTCATATTC
Mgl	CGGACTTCCAAGTTTTTGTCAGA	GCAGCCACTAGGATGGAGATG
Mttp	GTCAACAGAGAGGCGAGAAG	CTAGCCAAGCCTCTCTTGAG
Npc1l1	GCAAGGTGATCAGGAGGTTGA	ATCCTCATCCTGGGCTTTGC
Pgc1α	CCCTGCCATTGTTAAGACC	TGCTGCTGTTCCTGTTTTC
Plin2	GACCTTGTGTCCTCCGCTTAT	CAACCGCAATTTGTGGCTC
Plin3	ATGTCTAGCAATGGTACAGATGC	CGTGGAACTGATAAGAGGCAGG
PPARα	TTCACAAGTGCCTGTCTGTC	GGCCTTGACCTTGTTCATGT
Ptl	GCCATTGGAAGGATCACAGG	CCTGGCATTTCGATTCCTCC
Scd-1	CCGGAGACCCCTTAGATCGA	TAGCCTGTAAAAGATTTCTGCAAACC
Srebp1c	CCATCGACTACATCCGCTTCTT	ACTTCGCAGGGTCAGGTTCTC
Vldl-R	GAGTCTGACTTCGTGTGCAAA	GAACCGTCTTCGCAATCAGGA

2.1.10 Triglyceride hydrolase activity

Tissues were lysed in lysis buffer (100 mM potassium phosphate, 250 mM sucrose, 1 mM EDTA, 1 mM DTT, pH 7), sonicated on ice (2x10 sec with 1 min interval), and centrifuged at 1,000 *x g* and 4°C for 10 min. The supernatant was again centrifuged at 20,000 *x g* for 30 min at 4°C and the lipid-free infranatant was used for protein estimation. Protein concentrations were measured using a Lowry assay (BioRad Laboratories, Hercules, CA). Fourty µg of protein from tissue lysates were diluted to a final volume of 100 µl with lysis buffer. To measure neutral TG hydrolase activity, the samples were mixed with 100 µl of TG substrate [0.3 mM triolein/sample, 0.5 µCi/sample [9,10-^{3}H(N)]-triolein (Perkin Elmer, Waltham, MA), 3.5 µg mixed micelles of phosphatidylcholine and phosphatidylinositol (3:1, w:w)]. Each substrate contained NEFA-free BSA at a final concentration of 2% in 100 mM phosphate buffer. After incubation in a water bath for 1 h at 37°C, the reaction was stopped by the addition of 3.25 ml stop solution (methanol:chloroform:n-heptane, 10:9:7, v:v:v) and 1 ml of 0.1 M potassium carbonate (pH 10.5, adjusted with boric acid). The tubes were vortexed for 10-15 sec and centrifuged at 800 *x g* for 15 min at 4°C. The radioactivity in 1 ml of the upper phase was determined by liquid scintillation counting, and the release of FAs was calculated. (Korbelius et al., 2019)

2.1.11 Dual meal study

After a 12 h fasting period, mice were gavaged with 200 µl oil containing 0.5 µCi [1-^{14}C]-triolein (Perkin Elmer, Waltham, MA). Blood was taken 2, 4, and 6 h post gavage. Six hours after the first bolus, mice were gavaged with 200 µl oil containing 2 µCi [9,10-^{3}H(N)]-triolein (Perkin Elmer, Waltham, MA) and blood was taken 2 and 4 h later. Four hours after the second bolus, which reflects 10 h post the ^{14}C-gavage, mice were sacrificed and stomach, duodenum, jejunum, ileum, liver, white and brown adipose tissue, kidneys, and heart were collected. Tissues were lyophilized, digested in 1 M NaOH and radioactivity was measured by liquid scintillation counting. For determination of the lipid distribution into different lipid classes, lipids were extracted from 20 mg of lyophilized tissue using chloroform:methanol (2:1). Lipid extracts were separated by thin-layer chromatography using n-hexane-diethylether-acetic acid (70:30:1, v/v/v), corresponding bands for PL, FC, FFA, TG, and CE were cut and radioactivity was determined by liquid scintillation counting. (Korbelius et al., 2019)

2.1.12 Apical lipid absorption

Chow-diet fed mice were fasted for 4 h, injected with 500 mg tyloxapol/kg body weight (Merck KGaA; Darmstadt, Germany), and gavaged with 200 µl corn oil containing 2 µCi [9,10-^{3}H(N)]-triolein (Perkin Elmer, Waltham, MA). Blood was collected 150 and 300 min post gavage and mice were sacrificed 5 h after the administration of the oil bolus. Duodenum, jejunum, ileum, stomach, and liver were collected and radioactivity was measured in lyophilized tissues using liquid scintillation counting.

To study the early absorption phase, overnight fasted mice were gavaged with 200 µl corn oil containing 2 µCi [9,10-^{3}H(N)]-triolein (Perkin Elmer, Waltham, MA) and sacrificed 30 min post gavage. Intestines, stomach, and livers were collected, lyophilized and radioactivity was determined by liquid scintillation counting (Korbelius et al., 2019).

2.1.13 Basolateral lipid absorption

TG uptake from the blood was measured as previously described (Obrowsky et al., 2013). Briefly, chow-diet fed mice were fasted for 4 h prior to an intraperitoneal (i.p.) injection of 500 µl 20 % Intralipid (Fresenius Kabi Austria GmbH, Graz, Austria) containing 7 µCi [9,10-^{3}H(N)]-oleic acid (Perkin Elmer, Waltham, MA). Plasma was collected 3 and 6 h post injection. Intestines, stomach, livers, and feces were collected after 6 h, lyophilized, and radioactivity was determined by liquid scintillation counting.

To identify the source of basolateral lipids, either BSA-bound FA or human VLDL particles were injected i.v. into experimental mice. For that purpose, 4 h fasted mice were injected i.v. with 200 µl PBS containing 5 µCi [9,10-3H(N)]-oleic acid (Perkin Elmer, Waltham, MA) complexed with Na-oleate and BSA (Vujic et al., 2017). For VLDL injection, 1 µCi [9,10-^{3}H(N)]-triolein (Perkin Elmer, Waltham, MA) was incorporated into human VLDL (2.44 mg TG) and administered i.v.. Blood was taken 30 sec after injection to determine the total dose of administered lipoprotein. Mice were sacrificed either 1 h post injection or 24 h after administration and a 12 h fasting period prior to sacrifice. At the time of sacrifice, blood was drawn and intestines and livers were collected. After lyophilization, radioactivity was determined by liquid scintillation counting (Korbelius et al., 2019).

2.1.14 Isolation of primary enterocytes and fatty acid oxidation

Isolation of enterocytes was performed as described previously (Khalifeh-Soltani et al., 2016). After washing the jejunal segment with Buffer A (115 mM NaCl, 5.4 mM KCl, 0.96 mM NaH_2PO_4, 26.19 mM $NaHCO_3$, 5.5 mM glucose), one end of the jejunum was tied and the lumen was filled with Buffer B (67.5 mM NaCl, 1.5 mM KCl, 0.96 mM NaH_2PO_4, 26.19 mM $NaHCO_3$, 27 mM sodium citrate, 5.5 mM glucose). The jejunum was incubated for 15 min in 0.9% NaCl at 37°C, the luminal content was discarded and filled with Buffer C (Buffer A plus 1.5 mM EDTA and 0.5 mM DTT). After incubation at 37°C for 10 min in 0.9% NaCl, the luminal content was collected, filtered, and centrifuged at 1,500 *x g* for 5 min at room temperature. All buffers were adjusted to pH 7.4 and aerated wit 95% O_2 and 5% CO_2 before use.

Cell pellets were resuspended in 1 ml DMEM containing 0.5 mM carnitine, 0.4 µCi [1-^{14}C]-palmitic acid (Perkin Elmer, Waltham, MA), and 100 µM palmitic acid. The filter in the center well in the cell culture flask was saturated with 50 µl 1 M NaOH, the flask was sealed with a rubber stopper and incubated for 90 min at 37°C. The reaction was terminated by the addition of 100 µl 70% perchloric acid and $^{14}CO_2$ was trapped for 2 h at 37°C. Radioactivity on the filter paper was counted by liquid scintillation counting. Results were normalized to protein content. (Korbelius et al., 2019)

2.1.15 Gut transit

Overnight fasted mice were gavaged with 200 µl Evans blue suspension (5% Evans blue, 5% gum Arabic in PBS). Afterwards, mice had free access to food and water and the time until the emergence of Evans blue in the feces was recorded. To determine oil-based gut transit time, overnight fasted mice were gavaged with 100 µl oil 30 min prior to Evans blue administration (Vujic et al., 2017).

2.1.16 Statistical analyses

Statistical analyses were performed using GraphPad Prism 5.0 software. Significance was calculated by unpaired Student's *t*-test or ANOVA followed by Bonferroni post-tests. Data are shown as mean ± SD for biological replicates or as mean ± SEM for technical replicates (e.g. quantification of cLDs). For statistical analysis of mRNA expression, values were calculated using the $2^{-\Delta\Delta CT}$ method and represented as mean + SD. The following levels of statistical significance were used: *, $p < 0.05$; **, $p \leq 0.01$; ***, $p \leq 0.001$.

2.2 Results

2.2.1 Expression of CGI-58 and ATGL

The gut plays a major role in maintaining lipid homeostasis by regulating absorption, trafficking, and transient storage of dietary lipids as well as their utilization for lipoprotein assembly (Abumrad and Davidson, 2012). For other cell types, like adipocytes (Zimmermann et al., 2004, Yamaguchi et al., 2007), (cardio-)myocytes (Zierler et al., 2013, MacPherson et al., 2013), hepatoma- (Brown et al., 2007) and hepatic stellate cells (Eichmann et al., 2015), it has already been well described that ATGL and CGI-58 are cLD-associated proteins and promote lipolysis of transiently stored TGs. Compared to the WAT, *Cgi-58* and *Atgl* mRNA expressions throughout the SI are about 35% to 50%, respectively (**Figure 9**).

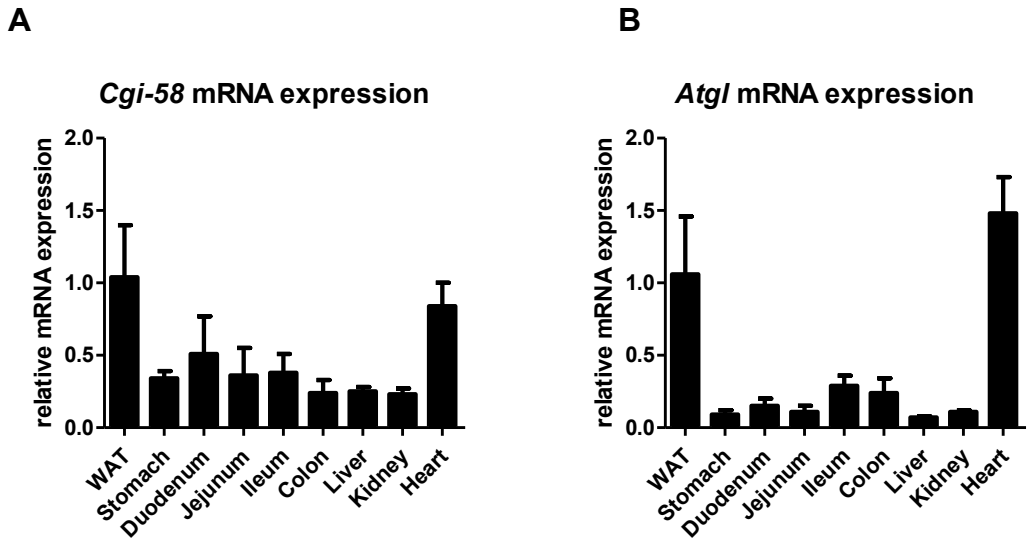

Figure 9: Expression of *Cgi-58* and *Atgl* in tissues.

Gene expression levels of (A) *Cgi-58* and (B) *Atgl*, normalized to *cyclophilin A* as internal control, were analyzed in tissues of 4 h-fasted WT mice. mRNA expression in the WAT was arbitrarily set to 1. Data represent mean values (n=5) + SD.

2.2.2 Efficient knock out of CGI-58 and ATGL in the SI

To confirm the intestine-specific deletion of CGI-58 and ATGL in the respective genotypes, we determined mRNA and protein expression levels. *Cgi-58* as well as *Atgl* mRNA expression levels were significantly downregulated in the respective iKO models, whereas hepatic expression levels remained comparable between WT and iKO mice (**Figure 10**).

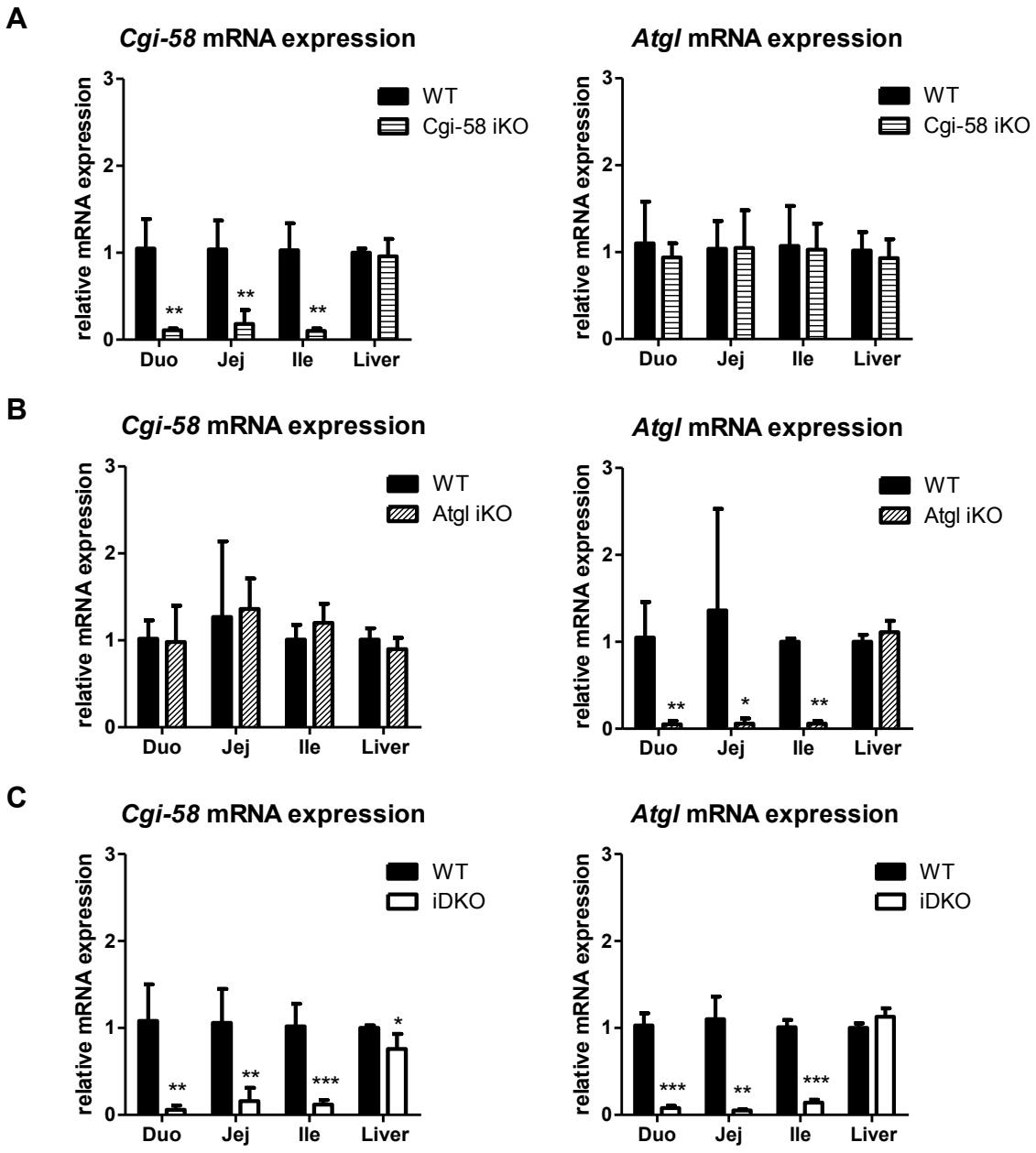

Figure 10: Efficient gene KO of CGI-58 and ATGL in the respective genotypes. mRNA expression of *Cgi-58* and *Atgl* in (A) Cgi-58 iKO, (B) Atgl iKO, and (C) Cgi-58/Atgl iDKO mice and their corresponding WT littermates. Expression levels were normalized to *cyclophilin A* as housekeeping gene. Mice were fasted 4 h prior to organ collection. Data represent mean values (n=3-4) + SD. *p < 0.05; **p ≤ 0.01; ***p ≤ 0.001.

Western Blot analysis of jejunal samples corroborated the efficient KO in the different mouse models (**Figure 11**). Due to enterocyte-specific deletion of CGI-58 and ATGL, faint bands in the iKO mice might origin from other cells of the SI (Korbelius et al., 2019).

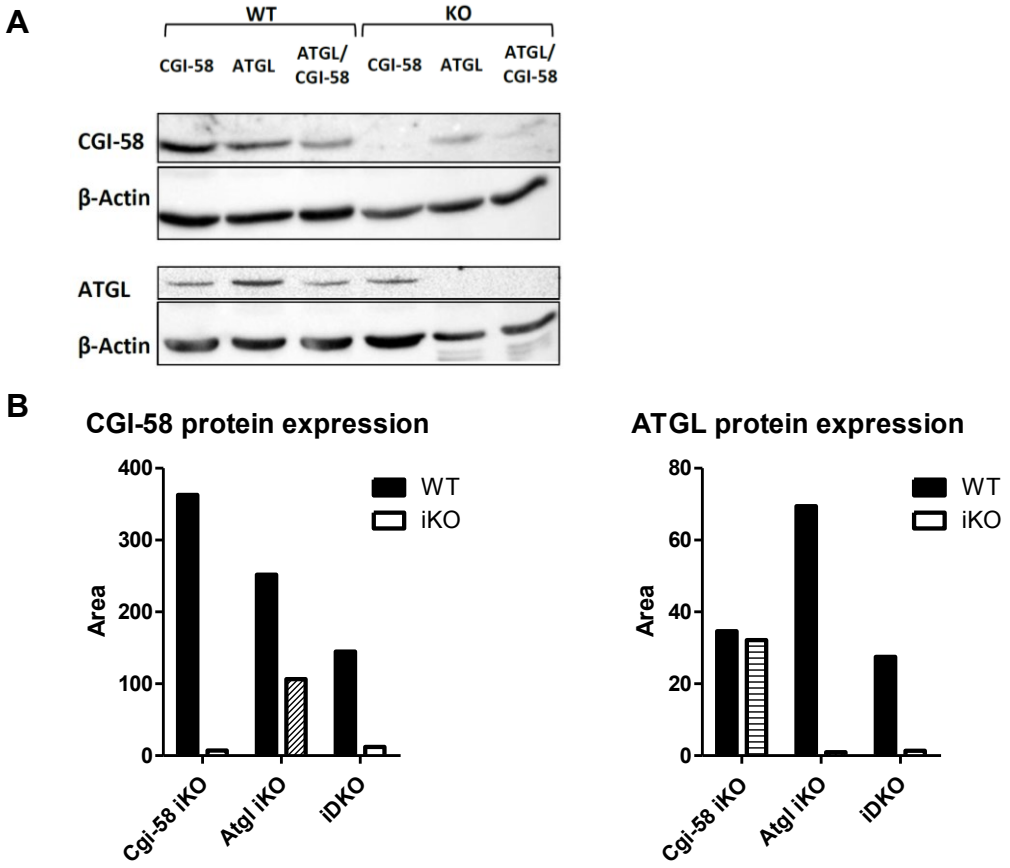

Figure 11: Efficient KO of CGI-58 and ATGL on protein level. (A) Protein expression of CGI-58 and ATGL in jejunal lysates of WT and Cgi-58 iKO, Atgl iKO and Cgi-58/Atgl iDKO mice with β-actin as loading control (Korbelius et al., 2019). (B) Quantification of CGI-58 and ATGL protein levels. All mice were fasted 4 h prior to organ collection. Data represent mean values (n=3-4) + SD.

Significantly decreased TG hydrolase activity in jejuna of refed or 4 h-fasted iDKO mice (**Figure 12**) already highlighted the importance of intestinal CGI-58 and ATGL in the hydrolysis of an intracellular transient lipid storage pool (Korbelius et al., 2019).

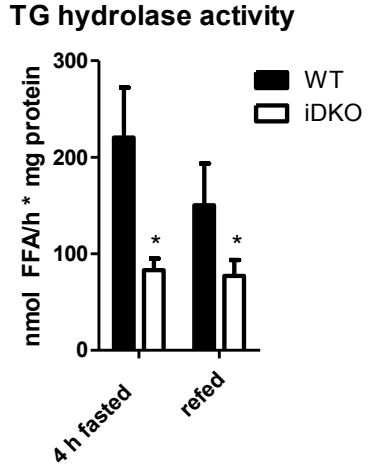

Figure 12: Lack of intestinal CGI-58 and ATGL impairs jejunal TGH activity.

Neutral TG hydrolase activity in jejuna of 4 h fasted and refed WT and iDKO mice. Data represent mean values (n=3-5) + SD. *p < 0.05. (Korbelius et al., 2019)

2.2.3 Impact of CGI-58/ATGL iDKO on expression of cLD-associated proteins

Under basal conditions, CGI-58 is associated with PLIN on the surface of the cLD in adipose tissue and is released through phosphorylation of perilipins by PKA to activate ATGL. Therefore, we next wondered how intestinal PLIN expression might be altered if CGI-58 and ATGL are absent in the SI. We found that jejunal expression levels of *Plin2* and *Plin3*, the sole perilipins expressed in the gut (Lee et al., 2009), are strongly regulated by nutrional statuses: In comparison to expression levels in the 4 h fasted state, *Plin2* expression was upregulated by 2.4- and 3.2-fold after prolonged fasting (16 h) and after an acute lipid load, respectively. The same effect was observed for *Plin3*, with a drastic increase after 16 h of fasting (81-fold) and post gavage (61-fold) (**Figure 13A**). Intestinal CGI-58/ATGL deficiency, however, did not alter mRNA expression of Plins or other cLD-associated proteins like *G0s2*, the endogenous inhibitor of ATGL (Yang et al., 2010) and *Cideb*, which was recently shown to play a role in the lipidation of CMs in the SI (Zhang et al., 2014a) in the 4 h fasted state (**Figure 13B**) or upon HF/HCD feeding (data not shown). In the refed state, Cgi-58/Atgl iDKO mice displayed a slight increase of *Plin2* accompanied by a significant 30% decrease of *Plin3* (**Figure 13C**).

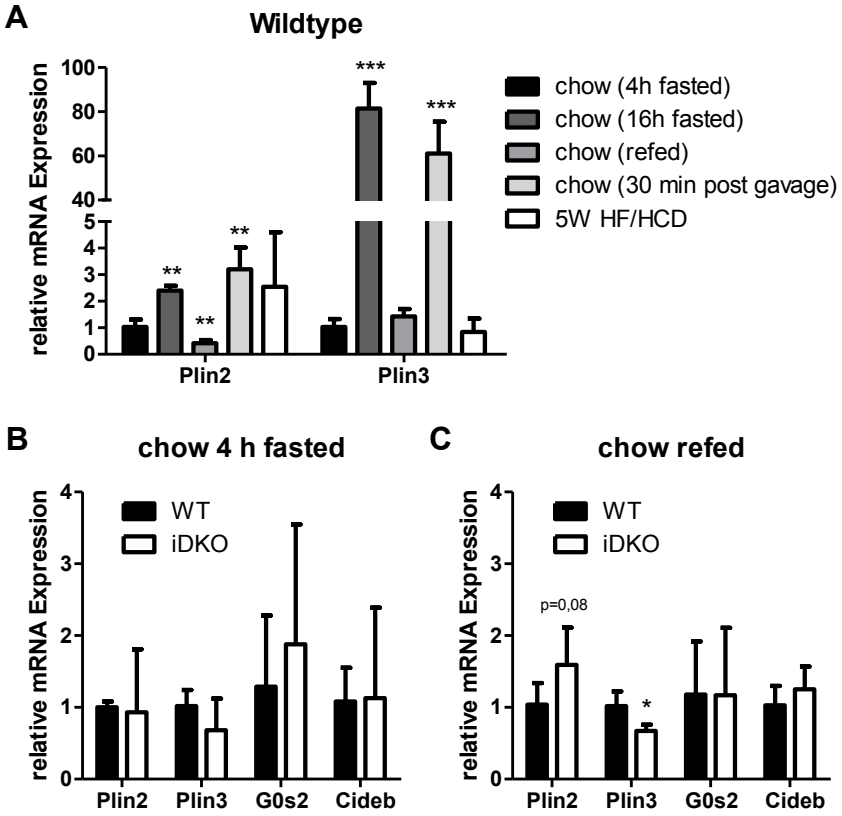

Figure 13: Effect of intestinal CGI-58/ATGL deficiency on mRNA expression of cLD-associated proteins. (A) Nutritional regulation of *Plin2* and *Plin3* expression in the jejunum of WT mice. mRNA expression of cLD-associated proteins in WT and iDKO mice (B) after a 4 h fasting period and (C) in the refed state. Gene expression was normalized to *cyclophilin A* as housekeeping gene. Data represent mean values (n=4-5) + SD. *p < 0.05; **p ≤ 0.01; ***p ≤ 0.001.

2.2.4 CGI-58/ATGL deficiency leads to massive cLD accumulation in the SI

To further investigate the role of intestinal CGI-58 and ATGL in sustaining intestinal lipid homeostasis, we next analyzed if the lack of these two proteins causes alterations in intracellular lipid levels. Previous work from our group already demonstrated that lack of solely ATGL in the SI caused a drastic increase in intracellular TG levels and cLD deposition (Obrowsky et al., 2013). In line, in Cgi-58 iKO mice, intracellular lipid levels were increased predominantly in the proximal SI, with 2.1- and 2.2-fold elevated TG levels in the duodenum of chow-fed Cgi-58 iKO mice in the refed (**Figure 14A**) and 4 h fasted state (**Figure 14B**), respectively. Intestinal lipid accumulation was even more pronounced in HF/HCD-fed Cgi-58 iKO with a 3.7-fold increase in intracellular TG levels (**Figure 14C**).

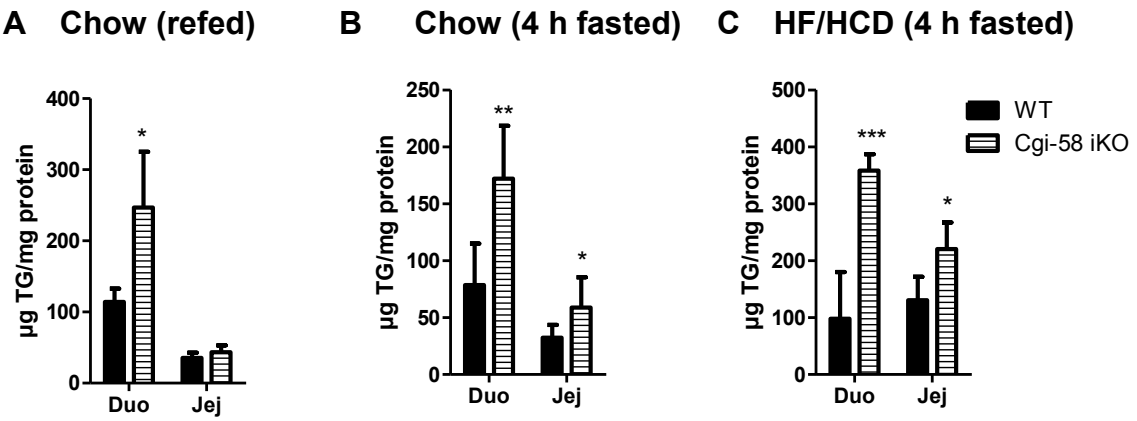

Figure 14: Intestinal CGI-58 deficiency provokes intestinal TG accumulation. Lipid extraction from duodena and jejunua of WT and Cgi-58 iKO mice on chow diet in (A) refed or (B) 4 h-fasted states. (C) Biochemical analysis of intestinal TG levels after 5 weeks of HF/HCD feeding. Data represent mean values (n=3-6) + SD. *p < 0.05; **p ≤ 0.01; ***p ≤ 0.001.

Mice lacking both ATGL and CGI-58 displayed massive accumulation of neutral lipids on chow diet as well as after HF/HCD feeding. While cholesterol levels remained comparable between the genotypes (data not shown), intestinal TG concentrations were drastically increased primarily in the very proximal part. Already on chow diet, duodenal TG levels were increased by 3.8-fold in the refed state (**Figure 15A**) and after a 4 h fasting period (**Figure 15B**), accompanied by only slightly elevated jejunal TG levels. Challenging mice with HF/HCD for 5 weeks resulted in 2.6- and 1.9-fold increased TG contents in duodena and jejuna of iDKO mice (**Figure 15C**). ORO stainings of the proximal SI (duodenum) further confirmed accumulation of neutral lipids in iDKO mice, with cLDs localizing chiefly within enterocytes and not in the lamina propria, where CMs are usually found upon secretion (Korbelius et al., 2019).

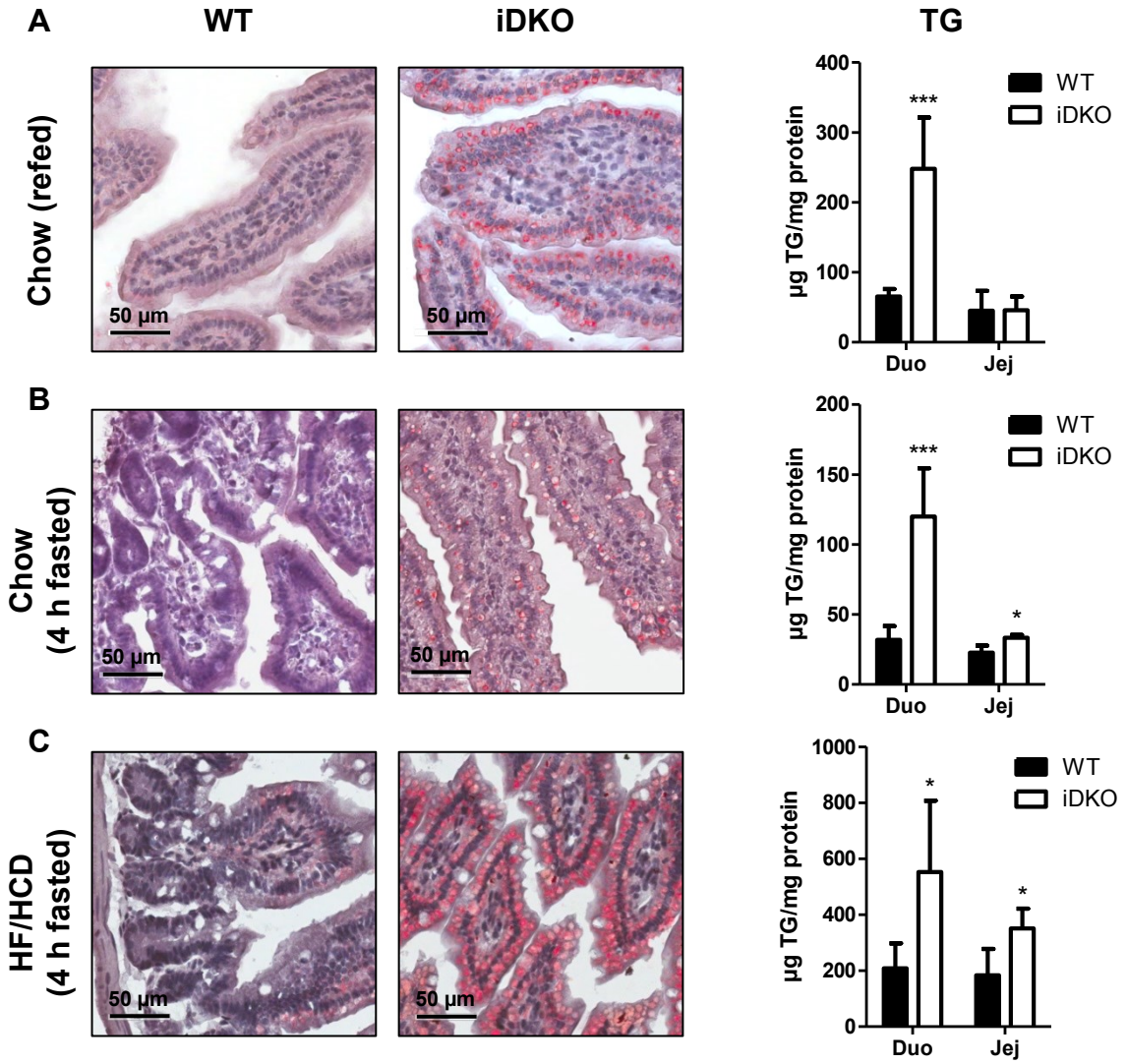

Figure 15: Intestinal lipid accumulation in Cgi-58/Atgl iDKO mice. ORO staining of duodenal sections and biochemical quantification of intestinal lipid levels in chow diet-fed WT and iDKO mice in (A) refed and (B) 4 h-fasted states. (C) Neutral lipid staining in the duodenum and biochemical analysis of intracellular TG concentrations after 5 weeks of HF/HCD feeding. Data represent mean values (n=5-6) + SD. *p < 0.05; ***p ≤ 0.001. Magnification, 40x; Scale bar, 50 µm. (Korbelius et al., 2019)

2.2.5 Intestinal CGI-58/ATGL are not contributing to systemic lipid supply

The remarkable lipid accumulation in mice deficient in intestinal CGI-58 and ATGL stressed a major role for both proteins in intestinal lipid metabolism. To elucidate if ATGL and its coactivator CGI-58 are involved in hydrolyzing dietary lipids to provide FFA as a substrate for CM synthesis, we analysed plasma lipid levels under various conditions. Circulating TG, cholesterol and FFA levels as well as body weights remained comparable between the genotypes in chow diet-, HF/HCD- and gavaged mice in the fasted or fed state (**Table 6**) (Korbelius et al., 2019).

Table 6: Comparison of body weight and plasma lipid parameters of WT and Cgi-58/Atgl iDKO mice.

	Chow (4 h fasted)		Chow (refed)		Chow refed (30 min post gavage)	
	WT	**iDKO**	**WT**	**iDKO**	**WT**	**iDKO**
BW (g)	21.9±1.95	20.8±2.26	21.2±0.21	20.1±2.15	22.3±1.78	21.7±1.10
TG (mg/dl)	85.2±20.4	83.2±19.10	57.2±6.73	53.6±17.6	90.2±27.8	82.4±6.32
TC (mg/dl)	68.1±9.14	58.4±7.81	54.4±7.71	56.0±4.36	70.9±11.4	62.4±7.58
FC (mg/dl)	13.8±3.48	13.5±2.84	18.7±2.25	19.7±2.09	25.6±3.59	25.0±2.37
CE (mg/dl)	53.9±6.60	46.1±6.54*	35.7±5.74	36.3±4.21	45.3±8.08	37.4±5.73
FFA (mmol/l)	0.48±0.36	0.45±0.37	0.20±0.05	0.17±0.02	0.48±0.09	0.45±0.10
n	9	9	5	5	4	4

	5 W HF/HCD (4 h fasted)		16 W HF/HCD (4 h fasted)	
	WT	**iDKO**	**WT**	**iDKO**
BW (g)	22.8±2.35	23.7±1.98	29.2±4.93	28.8±6.81
TG (mg/dl)	54.5±7.53	51.9±6.53	45.9±8.74	50.0±5.01
TC (mg/dl)	106±11.4	96.8±9.13	95.2±9.93	81.0±9.39
FC (mg/dl)	26.7±3.70	22.8±2.78	22.1±2.29	17.5±1.45
CE (mg/dl)	79.7±7.81	74.0±6.41	73.2±8.08	63.5±7.98
FFA (mmol/l)	0.58±0.05	0.63±0.10	n.d.	n.d.
n	5	5	5	5

Body weights and plasma parameters of sex- and age-matched WT and Cgi-58/Atgl iDKO mice. Data represent mean ± SD. BW, body weight; TG, triglyceride; TC, total cholesterol; FC, free cholesterol; CE, cholesteryl ester; FFA, free fatty acid; n.d., not determined. *p < 0.05. (Korbelius et al., 2019)

Next, we injected mice with tyloxapol to inhibit peripheral lipolysis, followed by an oral oil bolus to mimic postprandial CM secretion. We observed no difference in CM-TG or -cholesterol (**Figure 16A**) concentrations in Cgi-58/Atgl iDKO mice, indicating that CGI-58 and ATGL do not play an essential role in intestinal lipoprotein metabolism. In line, CM size (**Figure 16B**) and mRNA expression of *Mttp* (**Figure 16C**), the rate limiting enzyme for lipoprotein assembly in the proximal parts of the SI, were not affected by the loss of CGI-58 and ATGL (Korbelius et al., 2019).

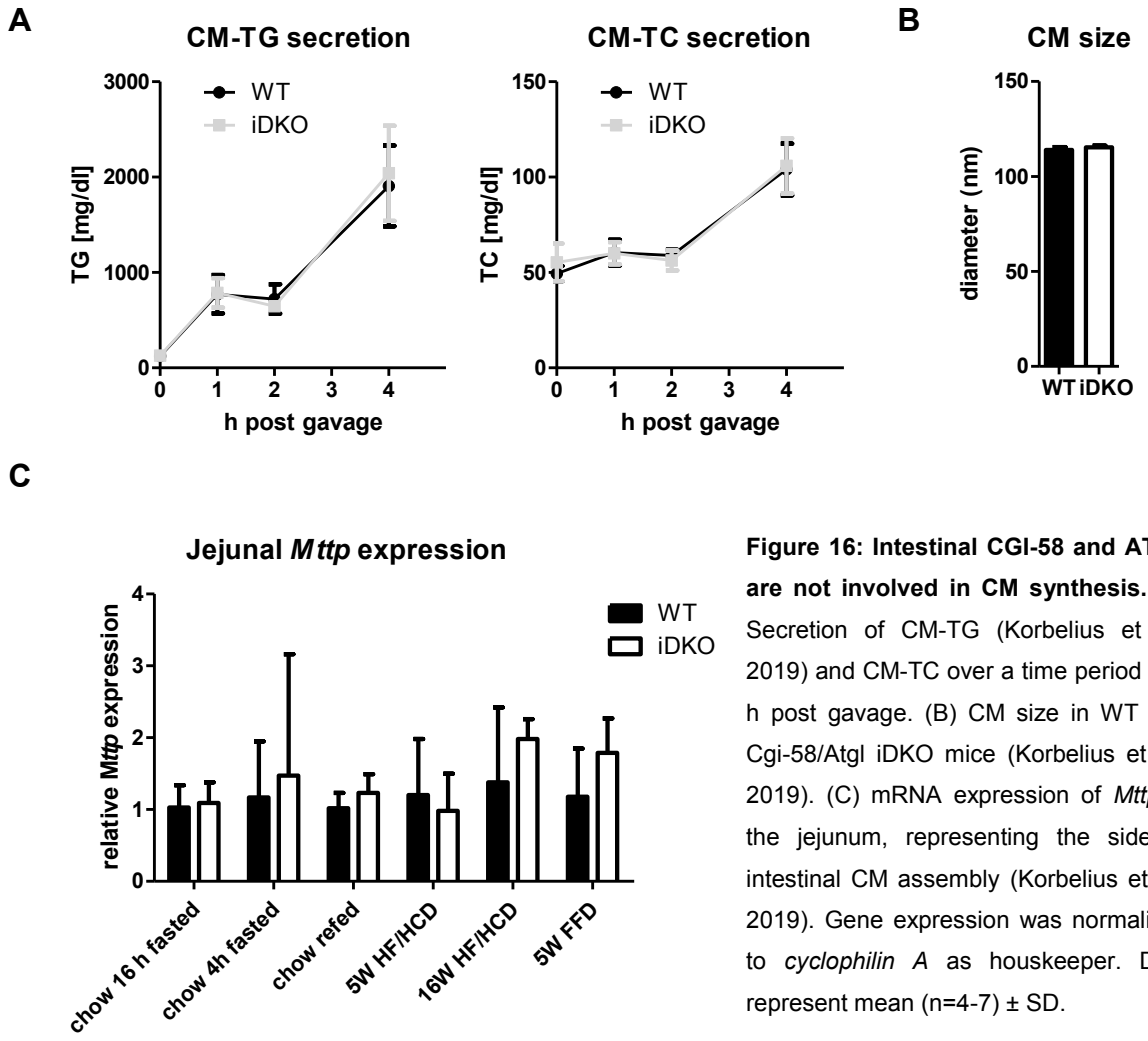

Figure 16: Intestinal CGI-58 and ATGL are not involved in CM synthesis. (A) Secretion of CM-TG (Korbelius et al., 2019) and CM-TC over a time period of 4 h post gavage. (B) CM size in WT and Cgi-58/Atgl iDKO mice (Korbelius et al., 2019). (C) mRNA expression of *Mttp* in the jejunum, representing the side of intestinal CM assembly (Korbelius et al., 2019). Gene expression was normalized to *cyclophilin A* as houskeeper. Data represent mean (n=4-7) ± SD.

Furthermore, VLDL secretion, representing hepatic lipoprotein assembly, was also identical between the genotypes. Four hours post injection, however, iDKO mice displayed slightly increased (1.2-fold) secretion of VLDL-TG (**Figure 17A**). Due to the slight impact of CGI-58/ATGL deficiency on VLDL secretion after 4 h, we repeated VLDL secretion up to 6 h post injection. Almost identlical plasma TG levels indicated no contribution of intestinal CGI-58/ATGL on hepatic lipoprotein metabolism (**Figure 17B**), which was in line with comparable hepatic *Mttp* expression between the genotypes (**Figure 17C**) (Korbelius et al., 2019).

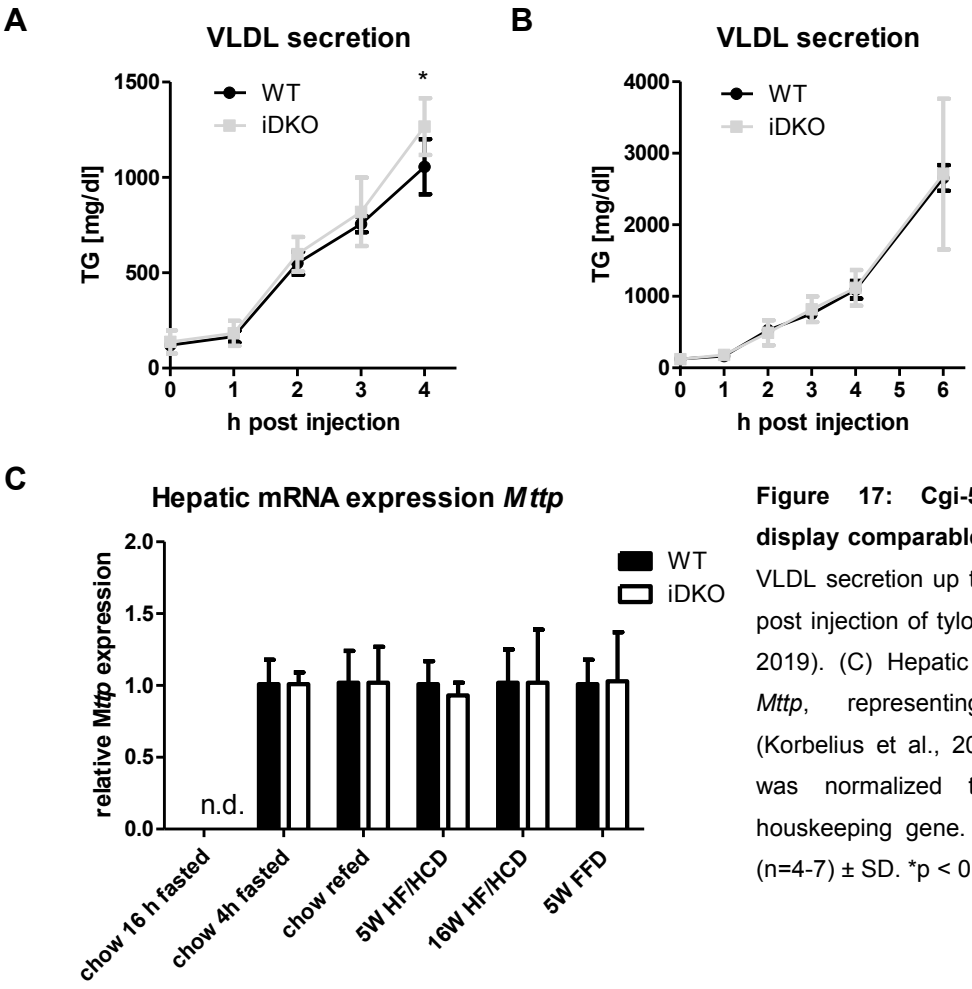

Figure 17: Cgi-58/Atgl iDKO mice display comparable VLDL secretion. (A) VLDL secretion up to 4 h or (B) up to 6 h post injection of tyloxapol (Korbelius et al., 2019). (C) Hepatic mRNA expression of *Mttp*, representing VLDL assembly (Korbelius et al., 2019). Gene expression was normalized to *cyclophilin A* as housekeeping gene. Data represent mean (n=4-7) ± SD. *p < 0.05.

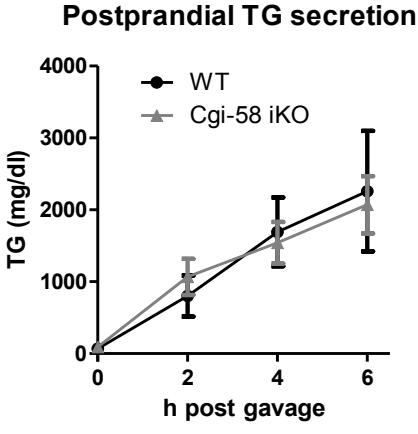

Figure 18: Comparable plasma TG concentrations up to 6 h post gavage. Postprandial TG secretion in HF/HCD-fed WT and Cgi-58 iKO mice was examined up to 6 h after administration of tyloxapol followed by an oral oil bolus. Data represent mean values (n=5). (Korbelius et al., 2019)

These results indicated that intestinal CGI-58 and ATGL are not essential for hepatic or intestinal lipoprotein synthesis and do not affect systemic lipid levels. Consistent with this, deletion of ATGL in the liver did not affect VLDL secretion (Wu et al., 2011), however, lack of intestinal (Xie et al., 2014) or hepatic (Brown et al., 2010) CGI-58 led to reduced plasma TG levels in the postprandial state. This indicated that CGI-58 is required for efficient postprandial lipoprotein secretion in an ATGL-independent manner. However, we

could not reproduce these data with our Cgi-58 iKO mice (**Figure 18**). Therefore, lack of CGI-58 and ATGL exclusively in the SI unlikely impacts the delivery of dietary lipids from the intestine into the periphery and consequently does not affect whole body lipid homeostasis.

2.2.6 Cgi-58/Atgl iDKO mice accumulate lipids from the first meal

Unchanged circulating lipid levels despite massive intracellular cLD accumulation further questioned the role of intestinal CGI-58 and ATGL in the hydrolysis of dietary lipids. In humans, it has been reported that lipids ingested with the first meal appear in the plasma after ingestion of the second meal (Fielding et al., 1996), indicating that dietary lipids are transiently stored in the SI. Therefore, we next studied the role of murine CGI-58 and ATGL in the hydrolysis of this transient lipid pool and their impact on secretion of these dietary lipids into the circulation. Organ weights remained comparable between the genotypes (

Figure 19) (Korbelius et al., 2019).

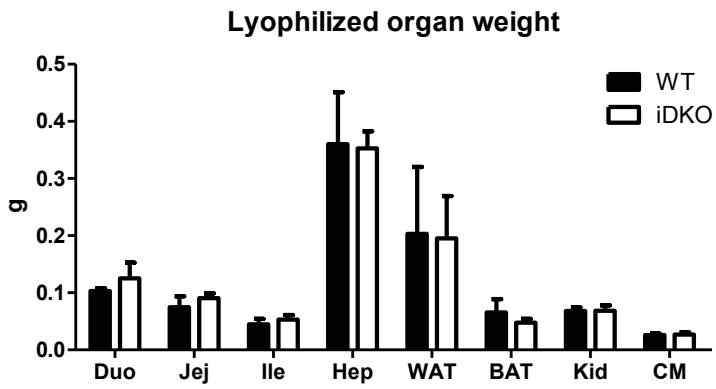

Figure 19: Comparable organ weights in WT and iDKO mice. Weight of lyophilized tissues 10 h post gavage of the first meal. Data represent mean (n=3) ± SD. Duo, duodenum; Jej, jejunum; Ile, ileum; Hep, hepar (liver); WAT/BAT, white/brown adipose tissue; Kid, kidney; CM, cardiac muscle. (Korbelius et al., 2019)

However, intestinal loss of CGI-58 and ATGL did not affect secretion of the first (^{14}C-triolein) or second (^{3}H-triolein) substrate into the circulation (**Figure 20A, B**). No effect on the release of primarily ingested lipids after ingestion of a sequential meal, neither in WT nor in iDKO mice, further indicated that the sequential meal effect occurs differently in mice and men. Interestingly, lipids from the first oil bolus were still accumulating in the proximal parts of the SI of Cgi-58/Atgl iDKO mice at the end of the experiment, which reflects 10 h post oral administration (**Figure 20C**). Levels of ^{14}C-triolein were increased 2-fold in the duodenum and 3-fold in the jejunum of Cgi-58/Atgl iDKO mice compared to control mice. Radioactive counts in other tissues like liver, white and brown adipose tissue, kidney and heart as well as the feces remained comparable between the genotypes (**Figure 20C**). Lipids ingested with the second oil bolus did not show any difference between the genotypes in any tissue, but Cgi-58/Atgl iDKO mice retained more ^{3}H-triolein in the stomach (**Figure 20D**) (Korbelius et al., 2019).

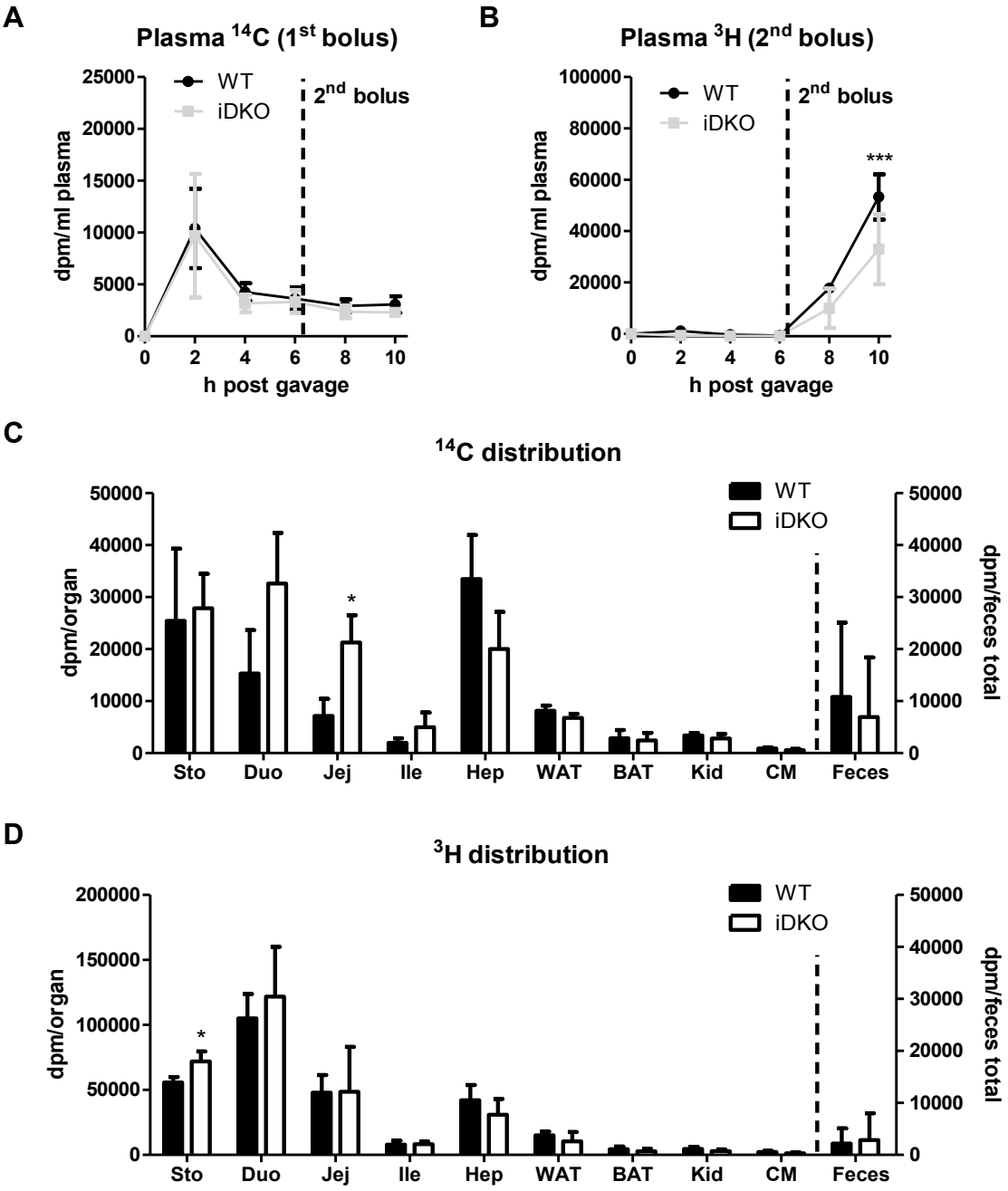

Figure 20: Cgi-58/Atgl iDKO mice accumulate lipids ingested with the first meal. (A) Secretion of the first ^{3}H-triolein-contraining bolus and (B) the second ^{14}C-labeled oil bolus into the circulation. (C) Distribution of the first oil bolus and (D) the second meal into tissues and feces. Data represent mean (n=3) ± SD. *p < 0.05; ***p ≤ 0.001. Sto, stomach; Duo, duodenum; Jej, jejunum; Ile, ileum; Hep, hepar (liver); WAT/BAT, white/brown adipose tissue; Kid, kidney; CM, cardiac muscle. (Korbelius et al., 2019)

Separation of the lipid classes via TLC revealed an accumulation of ^{14}C-labeled lipids in the TG fraction in duodenum and jejunum of Cgi-58/Atgl iDKO mice (**Figure 21A**), whereas distribution of the secondary ingested ^{3}H-labeled lipids was not altered between the genotypes (**Figure 21B**) (Korbelius et al., 2019).

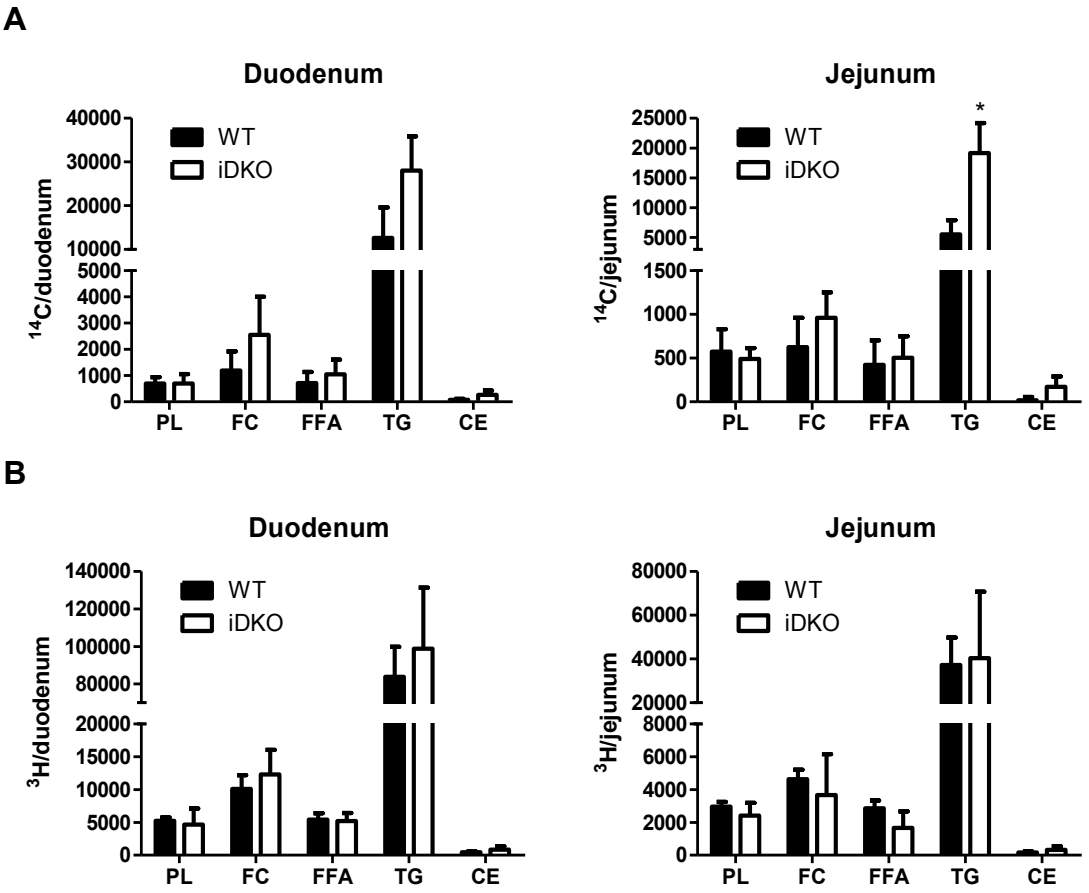

Figure 21: Lipids ingested with the primary meal accumulate in the SI of iDKO mice mainly in the TG fraction. (A) Distribution of ^{14}C into the various lipid classes, representing the first oil bolus. (B) Distribution of secondary ingested lipids, represented by ^{3}H counts in lipid fractions. Data represent mean (n=3) + SD; *p < 0.05. PL, phospholipid; FC, free cholesterol; FFA, free fatty acid; TG, triglyceride; CE, cholesteryl ester. (Korbelius et al., 2019)

Accumulation of primarily ingested lipids, but not those from the second meal might be attributable to i) an overload of intracellular lipid storage capacities, ii) direct secretion of secondary lipids into the circulation, bypassing intestinal storage and ATGL-mediated hydrolysis, or iii) delayed gastric emptying due to lipid-triggered delay in gut transit time (**Figure 22**).

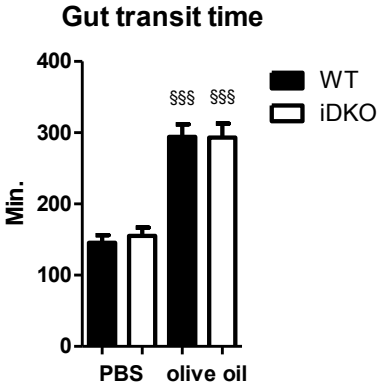

Figure 22: Preceding oil gavage causes drastically delayed gut transit.
Gut transit time was monitored in
WT and iDKO mice with or without an oral oil bolus prior to Evans Blue administration. Data represent mean (n=5-6) + SD. §§§p ≤ 0.001 between PBS and oil gavage.

2.2.7 CGI-58/ATGL deficiency in the SI does not affect dietary lipid absorption

Notwithstanding that the second meal effect does not exist in mice, the massive lipid accumulation within enterocytes in the absence of CGI-58 and ATGL indicated the existence of a transient intestinal lipid storage pool. However, the origin of these lipids still remained unclear. Therefore, we challenged mice orally with radioactively labeled lipids and sacrificed them in the early (30 min) and later (5 h) absorption phase.

Interestingly, although histological analysis of duodenal sections again revealed massive accumulation of neutral lipids within enterocytes (**Figure 23**), alimentary lipids administered with a radioactive label failed to accumulate in the SI of Cgi-58/Atgl iDKO mice in the early absorption phase (**Figure 24A**). This finding indicated that dietary lipids do not immediately accumulate within enterocytes and that cLDs stained by ORO rather contain previously formed lipids. (Korbelius et al., 2019)

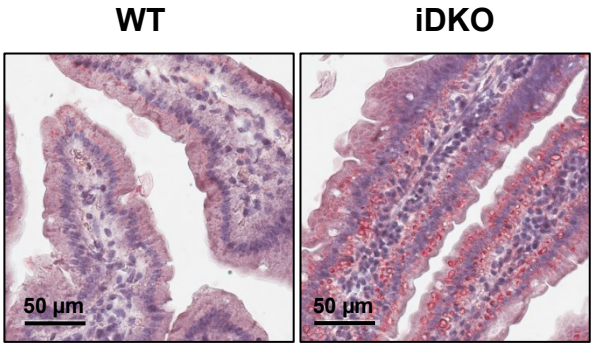

Figure 23: Increased cLD accumulation in duodena of iDKO mice 30 min post gavage. ORO staining of duodenal cryosections 30 min post gavage. Magnification, 40x; Scale bar, 50 µm. (Korbelius et al., 2019)

However, hepatic radioactivity was drastically reduced by 48% (**Figure 24A**). Histological analysis of livers by ORO staining confirmed the ameliorative effect of intestinal CGI-58/ATGL deficiency on fasting-induced hepatic steatosis (**Figure 24B**), which was attributable to 45% and 20% reductions in hepatic TG and CE concentrations, respectively (**Figure 24C**). Beside hepatic lipid levels, also circulating TG leves were drastically reduced by 48% (**Figure 24D**), which was attributable to impaired VLDL-TG secretion (**Figure 24E**). It is likely that slightly increased gastric retention of the radioactive substrate (**Figure 24A**) is responsible for delayed secretion into the circulation and subsequently impaired hepatic lipid uptake (Korbelius et al., 2019).

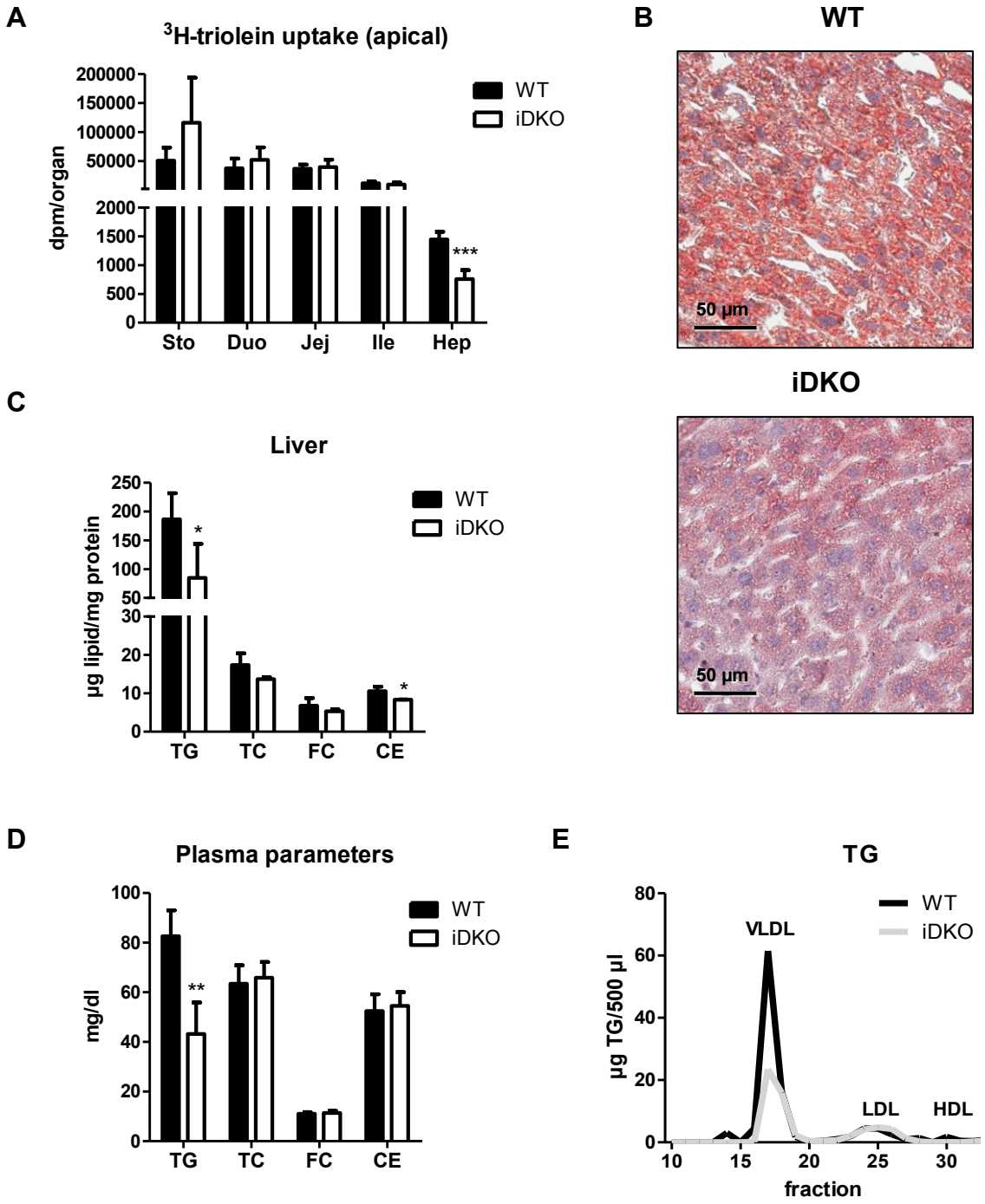

Figure 24: Cgi-58/Atgl iDKO mice display ameliorated hepatic steatosis 30 min post gavage. (A) Radioactivities in SI and liver of WT and iDKO mice 30 min post gavage of ^{3}H-triolein. (B) ORO staining of hepatic sections to visualize neutral lipids. (C) Intracellular lipid levels in the liver. (D) Plasma lipid parameters and (E) lipoprotein profile. Data represent mean (n=4-5) + SD. *p < 0.05; **p ≤ 0.01; ***p ≤ 0.001. Sto, stomach; Duo, duodenum; Jej, jejunum; Ile, ileum; Hep, hepar (liver). Magnification, 40x; Scale bar, 50 µm. (Korbelius et al., 2019)

To elucidate, whether impaired dietary lipid absorption or rather accelerated CM clearance is accountable for the decrease in plasma TG concentrations, we examined mRNA expression levels of apical as well as basolateral FA transporters. Surprisingly, mice lacking intestinal CGI-58 and ATGL displayed slightly increased mRNA levels of cluster of differentiation 36 (*Cd36*) and intestinal FA binding protein (*I-Fabp*), reflecting apical lipid uptake (**Figure 25A**). Similar intestinal lipid levels despite increased apical absorption might be due to increased lipoprotein secretion, as indicated by upregulation of jejunal *Mttp* mRNA (**Figure 25B**). Subsequent increases in mRNA levels of hepatic lipoprotein receptors (**Figure 25D**) and hepatic *Mttp* (**Figure 25E**) suggested rapid turnover of dietary lipids, with increased VLDL secretion being responsible for less lipid deposition in the liver. Decreased circulating TG levels despite elevated levels of intestinal and hepatic *Mttp* pointed toward changes in basolateral lipid uptake by the intestine. Beside passive diffusion of peripheral FA into the enterocyte, basolateral absorption of CM remnants is receptor dependent. Intestinal low density lipoprotein receptor (Ldl-R) accounts for 80% of the uptake, while LDL receptor-related protein 1 (Lrp1) takes over the rest (Soued and Mansbach, 1996). In the postprandial phase, Cgi-58/Atgl iDKO mice showed a slight increase in *Ldl-R* mRNA expression (**Figure 25C**), suggesting an accelerated basolateral uptake of lipoprotein particles, which might be more prominent at later time points.

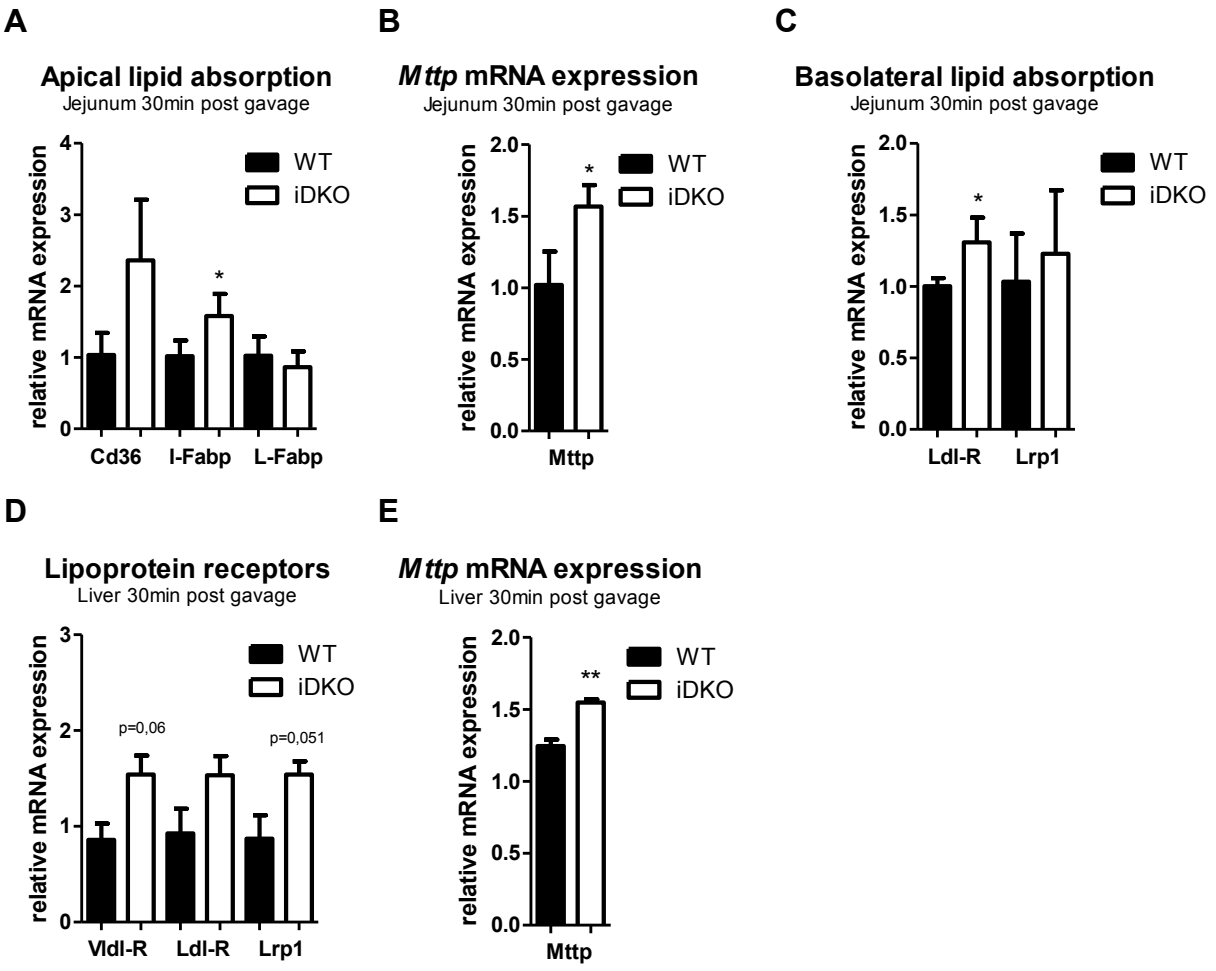

Figure 25: Increased intestinal and hepatic lipid uptake and secretion in Cgi-58/Atgl iDKO mice. Jejunal mRNA expression of genes involved in (A) apical lipid absorption, (B) intestinal lipoprotein secretion, and (C) basolateral lipid uptake 30 min post gavage. (D) mRNA expression of hepatic lipoprotein receptors and (E) hepatic *Mttp*. Gene expression was normalized to *cyclophilin A* as houskeeping gene. Data represent mean (n=3-7) ± SD. *p < 0.05; ** p ≤ 0.01.

To follow the fate of dietary lipids and to study the impact of intestinal CGI-58 and ATGL on alimentary lipid trafficking, we sacrificed mice in the intraprandial period, reflecting 5 h post administration of an oral lipid bolus. In line with comparable CM secretion (**Figure 16A**), circulating radioactivity remained comparable 2.5 h and 5 h post gavage of ^{3}H-triolein in Cgi-58 iKO (**Figure 26A**) and Cgi-58/Atgl iDKO mice (**Figure 26C**). In contrast to results obtained 30 min post gavage, mice lacking intestinal CGI-58 (and ATGL) displayed massive accumulation of the radioactive tracer in the proximal SI 5 h post gavage (**Figure 26B,D**). Mice carrying a single deletion of ATGL (Obrowsky et al., 2013) showed the same pattern, however, Cgi-58 iKO mice displayed the most pronounced phenotype with up to 9.7-fold increased radiaoctive counts in the duodenum.

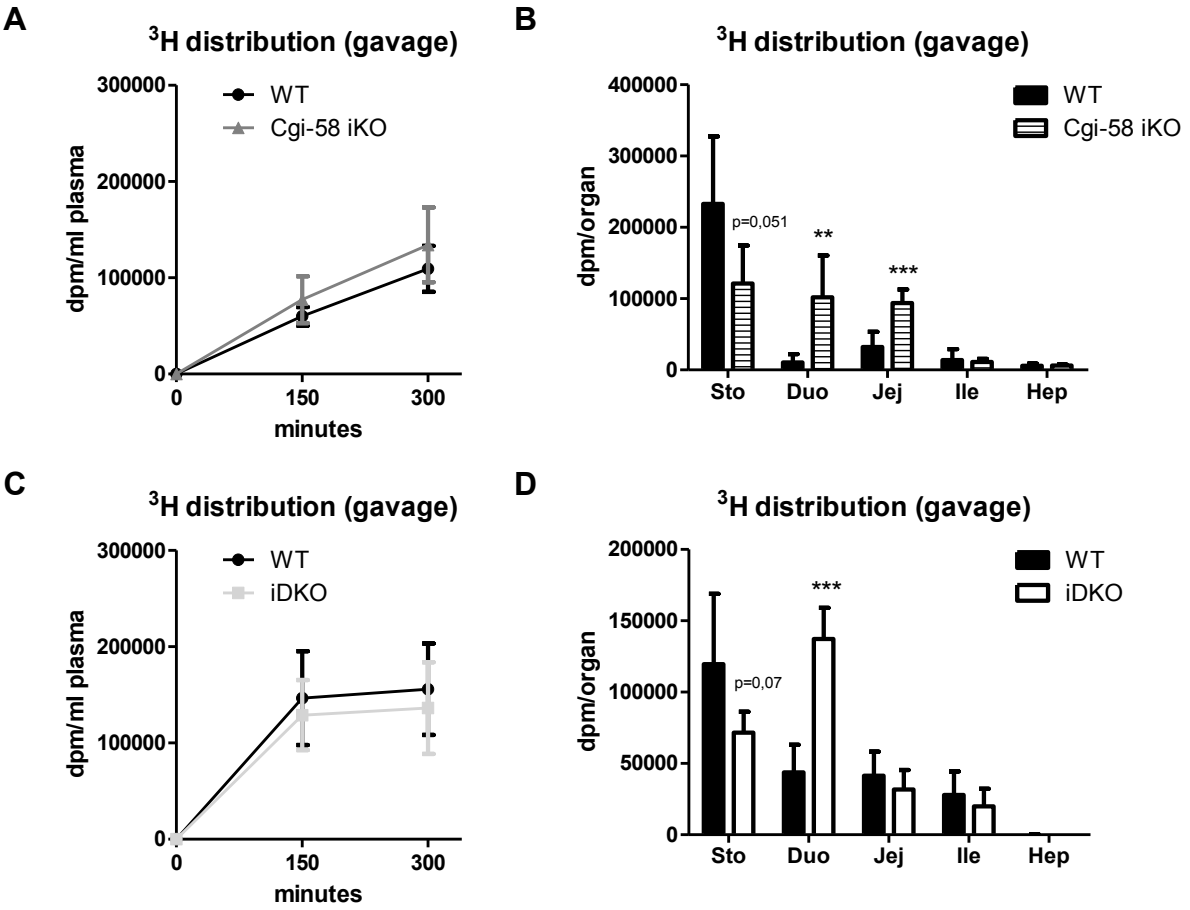

Figure 26: Accumulation of dietary lipids 5 h post gavage in proximal SI of Cgi-58 iKO and Cgi-58/Atgl iDKO mice. (A) Radioactivity in the plasma of WT and Cgi-58 iKO mice. (B) Intestinal and hepatic radioactivity 5 h post gavage in WT and Cgi-58 iKO mice. (C) Secretion of orally administered ^{3}H-triolein into the circulation of WT and iDKO mice. (D) Distribution of the radioactive tracer in intestinal and hepatic tissues of WT and iDKO mice. Data represent mean (n=4-6) ± SD. **p ≤ 0.01; ***p ≤ 0.001. Sto, stomach; Duo, duodenum; Jej, jejunum; Ile, ileum; Hep, hepar (liver).

Comparable intestinal radioactivity in the early absorption phase, unchanged secretion of the radioactive tracer into the circulation, and comparable fecal lipid excretion (**Figure 27A, B**) further indicated that intestinal CGI-58 and ATGL do not impact dietary lipid absorption *per se* (Korbelius et al., 2019). In line, mRNA expression levels of genes involved in apical FFA and cholesterol uptake (*Cd36*, *Npc1l1*) remained comparable between the genotypes (**Figure 27C**).

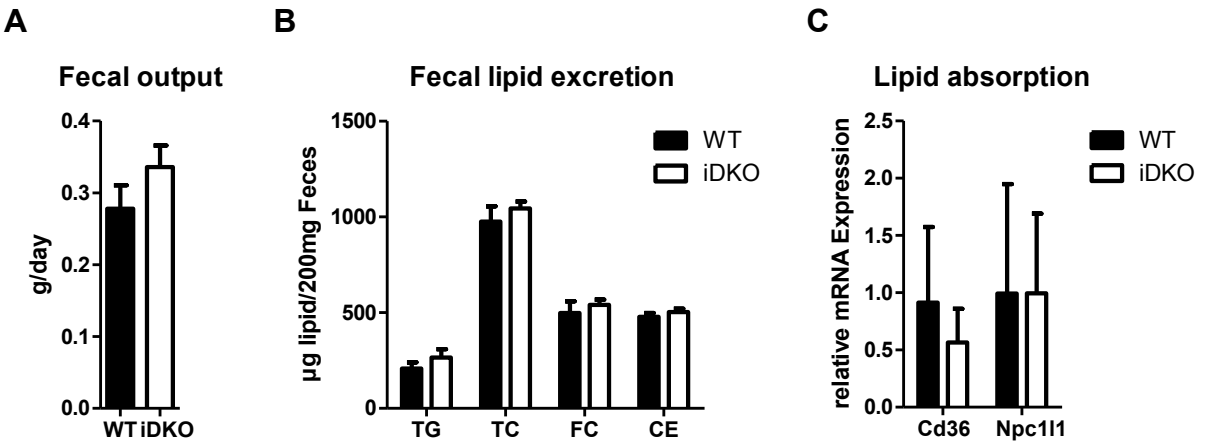

Figure 27: Unchanged dietary lipid absorption in Cgi-58/Atgl iDKO mice. (A) Daily fecal output and (B) fecal lipid excretion of HF/HCD-fed WT and iDKO mice (Korbelius et al., 2019). (C) Jejunal mRNA expression of *Cd36* and *Npc1l1* upon HF/HCD feeding. Expression levels were normalized to *cyclophilin A* as houskeeping gene. Data represent mean values (n=4-5) + SD.

2.2.8 Alimentary lipids start to accumulate 2 h post gavage in iDKO mice

As 30 min were not sufficient for dietary lipids to be incorporated into a cytoplasmic lipid storage pool, which acts as a substrate for intestinal CGI-58 and ATGL, we next aimed to study the time course of alimentary lipids. To visualize intestinal cLD formation, we gavaged mice with a BODIPY® labeled FA. Mice were sacrificed 30 min as well as 2 h post gavage, as suggested by previous studies (Vasquez et al., 2011). In both cohorts, body weights and plasma parameters remained comparable between the genotypes (**Table 7**).

Table 7: Body weight and plasma lipid parameters 30 min and 2 h post gavage.

	Chow 16 h fasted (30 min post gavage)		Chow 16 h fasted (2 h post gavage)	
	WT	**iDKO**	**WT**	**iDKO**
BW (g)	n.d.	n.d.	n.d.	n.d.
TG (mg/dl)	82.7±10.4	43.2±12.70**	174±59.3	222±103
TC (mg/dl)	63.5±7.41	65.9±6.32	79.4±5.87	82.2±11.8
FC (mg/dl)	11.0±0.72	11.4±0.82	18.5±2.91	20.2±6.09
CE (mg/dl)	52.5±6.75	54.5±5.51	60.9±4.22	62.1±7.94
FFA (mmol/l)	0.45±0.10	0.43±0.10	1.30±0.20	1.38±0.24
n	4	4	5	5

Body weights and plasma parameters of sex- and age-matched WT and Cgi-58/Atgl iDKO mice. Data represent mean ± SD. BW, body weight; TG, triglyceride; TC, total cholesterol; FC, free cholesterol; CE, cholesteryl ester; FFA, free fatty acid; n.d., not determined. **p ≤ 0.01. (Korbelius et al., 2019)

Lee et al. demonstrated that PLIN3 protein expression on intestinal cLDs is upregulated after an acute lipid load, highlighting a role of PLIN3 in the early phase of dietary lipid absorption (Lee et al., 2009). In line, *Plin3* mRNA expression was upregulated by 61-fold in WT jejuna 30 min post gavage (**Figure 13A**).

After 30 min, immunofluorescence staining for PLIN3 in BODIPY®-gavaged mice revealed major expression of PLIN3 at the apical border of the enterocyte in WT mice (**Figure 28A**), representing the uptake and early cLD formation phase of BODIPY®-labeled FA. However, mice lacking CGI-58 and ATGL mainly displayed an accumulation of endogenous cLDs, depicted as PLIN3-coated vesicles which did not contain BODIPY® (**Figure 28A**), indicating that 30 min are not sufficient for dietary lipids to accumulate in the SI of iDKO mice. In line with fluorescent images, *Plin3* mRNA levels were comparable in jejuna of iDKO mice (**Figure 28B**). "Empty" cLDs surrounded by PLIN3 but lacking BODIPY® therefore likely represent previously formed lipids, corresponding with ORO-positive cLDs found in the early absorption phase (**Figure 23**), although radioactivity remained comparable between the genotypes (**Figure 24A**) (Korbelius et al., 2019).

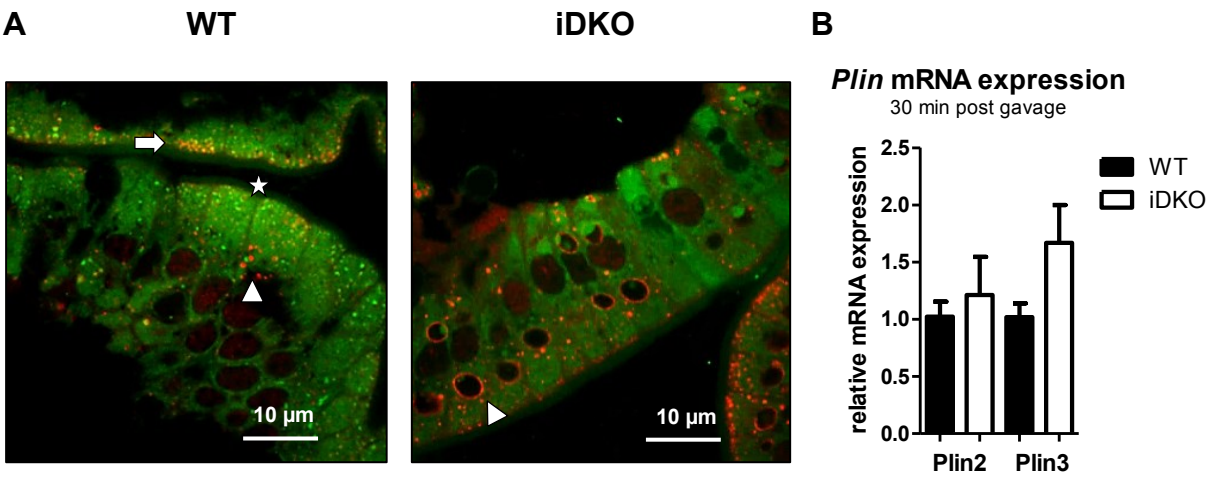

Figure 28: Thirty minutes are not sufficient for alimentary lipids to accumulate in the SI of iDKO mice. (A) PLIN3 immunofluorescence staining of jejunal cryosections 30 min post gavage of BODIPY®-palmitic acid (PA). Arrows indicate cLDs originating from BODIPY®-labeled PA colocalizing with PLIN3; arrowheads indicate endogenous cLDs coated with PLIN3; stars indicate BODIPY®-containing cLDs, which do not colocalize with PLIN3. Magnification, 100x; scale bar, 10 µm (Korbelius et al., 2019). (B) mRNA expression of *Plin2* and *Plin3* 30 min post gavage of 200 µl corn oil. Gene expression was normalized to *cyclophilin A* as housekeeping gene. Data represent mean values (n=4) + SD.

Two h post gavage, WT mice only marginally accumulated small cLDs in the jejunum, while Cgi-58/Atgl iDKO mice showed a massive increase in cLD number and size (**Figure 29A**). Interestingly, BODIPY®-labeled FAs were not only incorporated into cLDs coated with PLIN3,

but also into cLDs which were not colocalizing with PLIN3. One possibility might be that these BODIPY®-containing cLDs rather co-localize with PLIN2. WT mice only accumulated a few cLDs originating from BODIPY®-labeled FA, but displayed several bigger PLIN3-coated cLDs containing unlabeled, endogenous lipids. On the other hand, mice lacking CGI-58 and ATGL mainly displayed a co-localization of PLIN3 and BODIPY®-labeled lipids. Quantification of the three different cLDs (BODIPY®-labeled cLDs, PLIN3-coated vesicles and PLIN3-coated BODIPY®-containing cLDs) from multiple images revealed a significantly higher total cLD number in iDKO mice (**Figure 29B**). Furthermore, mice lacking intestinal CGI-58 and ATGL predominantly displayed BODIPY®-containing cLDs co-localizing with Plin3 (**Figure 29C**) (Korbelius et al., 2019).

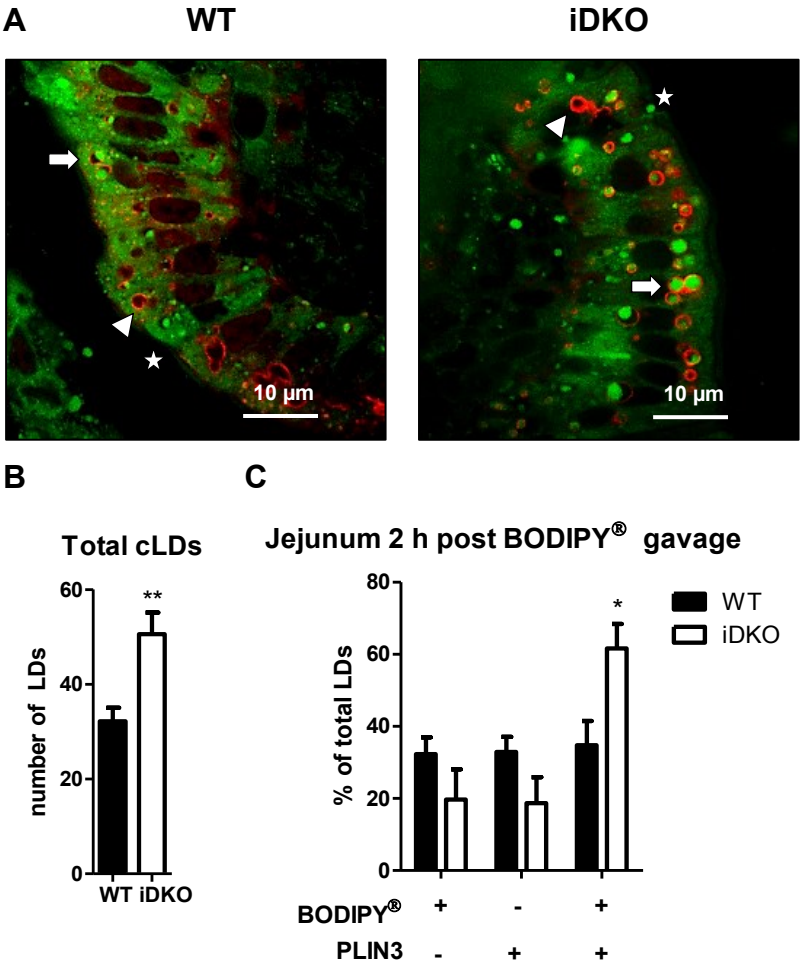

Figure 29: Cgi-58/Atgl iDKO mice display massive cLD accumulation 2 h post BODIPY® administration.

(A) PLIN3 immunofluorescence staining of jejunal cryosections 2 h post gavage of BODIPY®-FA. Arrows indicate cLDs originating from BODIPY®-labeled FA colocalizing with PLIN3; arrowheads indicate endogenous cLDs coated with PLIN3; stars indicate BODIPY®-containing cLDs, which do not colocalize with PLIN3. Magnification, 100x; scale bar, 10 µm. (B) Total number and (C) relative amount of cLDs containing BODIPY®, coated with PLIN3, and BODIPY®-containing PLIN3-coated vesicles 2 h post gavage. cLDs were quantitated by counting of multiple micrographs (n=5). Data represent mean + SEM. *p < 0.05; **p ≤ 0.01. (Korbelius et al., 2019)

Our results collectively suggest the existence of a secretion/reuptake cycle in the enterocyte, highlighting the role of intestinal CGI-58 and ATGL in the cleavage of basolateral absorbed lipids. This hypothesis is drawn from i) accumulation of radioactive lipids 5 h, but not 30 min post gavage and ii) incorporation of orally administered fluorescent lipids into cLDs 2 h, but

not 30 min post gavage, but iii) persistent cLD accumulation within enterocytes as visualized by ORO staining or “empty” PLIN3-coated vesicles.

2.2.9 Accumulation of basolaterally-derived lipids in Cgi-58/Atgl iDKO mice

Based on our secretion/reuptake hypothesis and the fact that enterocytes are also capable to take up small lipoprotein particles from the basolateral side (Soued and Mansbach, 1996), we injected Cgi-58 iKO and Cgi-58/Atgl iDKO mice i.p. with ^{3}H-oleate in Intralipid. As expected, circulating radioactivity remained comparable between the genotypes (**Figure 30A,C**). However, also i.p. applied lipids, mimicking the basolateral lipid uptake into the SI, accumulated in the proximal intestine of both iKO mouse models (**Figure 30B,D**), which was in line with results obtained in Atgl iKO mice (Obrowsky et al., 2013).

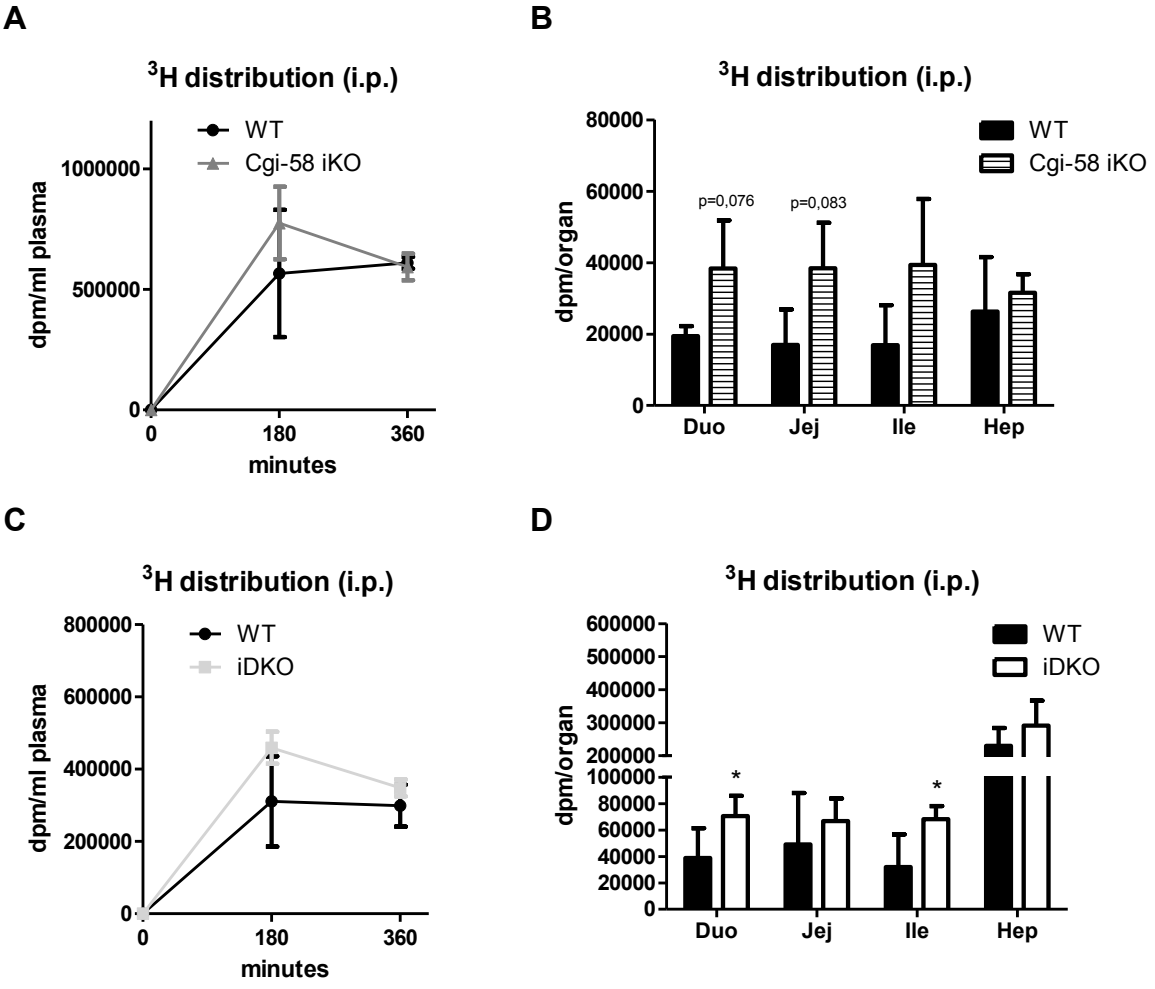

Figure 30: Accumulation of basolaterally lipids in proximal SI of Cgi-58 iKO and Cgi-58/Atgl iDKO mice. Radioactivity in (A) the plasma and (B) tissues of WT and Cgi-58 iKO mice. (C) Secretion of basolaterally administered ^{3}H-oleate into the circulation and (D) distribution of the tracer among tissues in WT and iDKO mice. Data represent mean (n=3-5) ± SD. *p < 0.05. Duo, duodenum; Jej, jejunum; Ile, ileum; Hep, hepar (liver).

As intravenous administration (i.v.) is the preferred route to study substrate uptake from the circulation, we next performed several i.v. experiments to further examine the role of intestinal CGI-58 and ATGL in the breakdown of basolaterally-derived lipids in a time- and substrate-dependent manner.

To primarily identify the source of basolaterally lipids accumulating within iDKO enterocytes, mice were injected i.v. either with ^{3}H-oleic acid (OA) complexed with BSA or ^{3}H-triolein (TO) incorporated into human VLDL. In line with all previous experiments, we could not observe any differences between the genotypes in circulating radioacitivty 1 h post injection (**Figure 31A,C**). As neiter ^{3}H-OA nor ^{3}H-TO accumulated to a greater extent in intestinal or hepatic tissues of iDKO mice, 1 h likely was not sufficient for the substrate to get stored as cLDs within enterocytes, raising the idea of initial substrate processing by the liver. Indeed, both tracers primarily targeted the liver (6-9% of total dose), shuttling < 1% to the enterocytes (**Figure 31B,D)**. These results were reconfirmed by hepatic cryosections of mice i.v. injected with BODIPY®-OA, which revealed a substantial deposition within hepatocytes, but less abundance in intestinal sections 30 min post injection, irrespective of the genotype (**Figure 31E,F**). In line with results obtained in BODIPY®-gavaged mice (**Figure 28A**), PLIN3 staining revealed an accumulation of BODIPY®-lacking “empty” cLDs 30 min after tracer administration, most likely containing endogenous lipids. (Korbelius et al., 2019)

Accumulation of radioactive and fluorescent tracers primarily in the liver suggested a pre-processing of i.v. applied lipids by hepatocytes before shuttling them to the intestine. To investigate the contribution of hepatocytes to basolateral lipid uptake by enterocytes, mice were again injected with the above mentioned substrates (^{3}H-OA bound to BSA or ^{3}H-TO incorporated into human VLDL). As both substrates failed to accumulate in the SI of iDKO mice within 30 min (**Figure 31F**) or 1 h (**Figure 31B,D**), mice were sacrificed 24 h post administration of the tracer. To elucidate the role of hepatic lipid processing and lipoprotein secretion on intestinal lipid uptake from the circulation, mice were fasted 12 h prior to organ harvesting. (Korbelius et al., 2019)

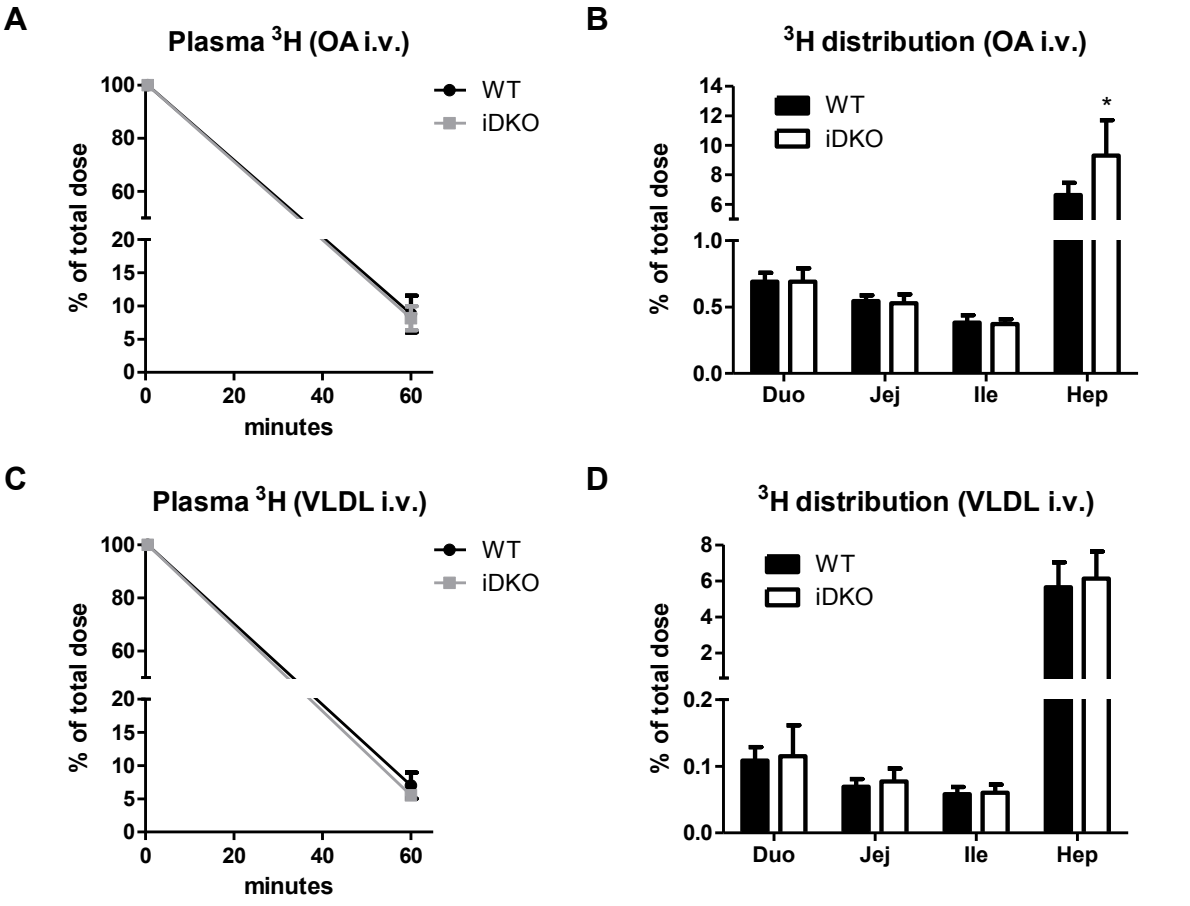

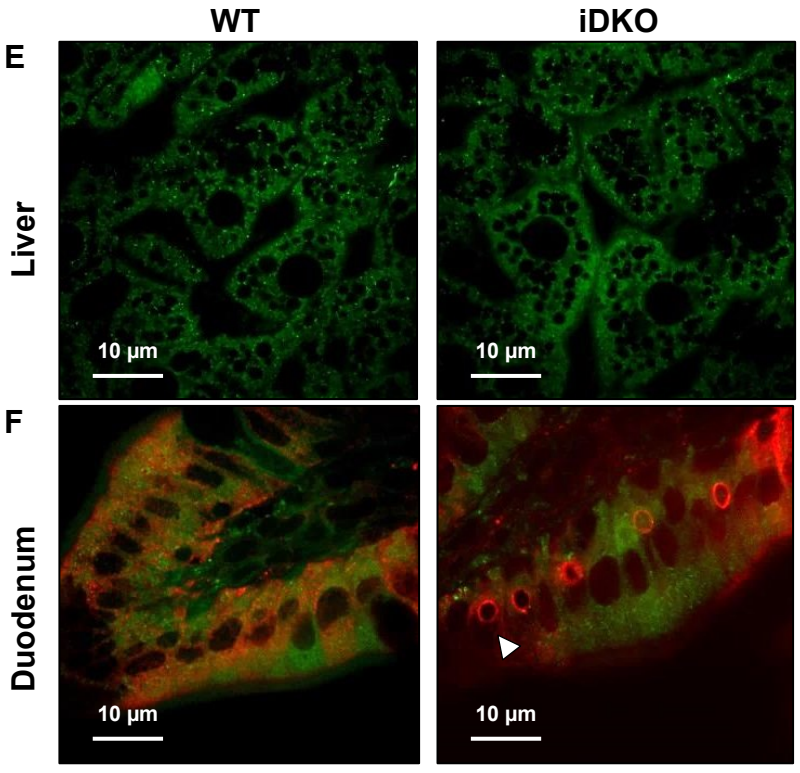

Figure 31: Intravenously applied lipids primarily target the liver 1 h post-injection. (A) Plasma and (B) tissue radioactivity 1 h post-administration of ^{3}H-OA. (C) Radioactivity in the plasma and (D) tissues 1 h after injection of human VLDL. (E) Hepatic and (F) intestinal cryosections 30 min after BODIPY®-OA (green) injection. Intestinal sections were co-stained with PLIN3 (red). Arrowheads indicate cLDs stained with PLIN3. Magnification, 100x; scale bar, 10 µm. Data represent mean (n=5-6) ± SD. *p < 0.05. Duo, duodenum; Jej, jejunum; Ile, ileum; Hep, hepar (liver). (Korbelius et al., 2019)

As expected, circulating radioactivities remained comparable between the genotypes in both experiments (**Figure 32A,C**). Both substrates accumulated to a higher extent in duodena of iDKO mice (2.0-fold for ^{3}H-OA and 2.3-fold for ^{3}H-VLDL) (**Figure 32B,D**). The increased deposition of VLDL-derived radioactivity in the intestine was accompanied by a 44% reduction in hepatic counts (**Figure 32D**), indicating a close interplay between hepatic and intestinal lipid metabolism. The contribution of hepatocytes in processing of the lipid substrate still remained elusive.

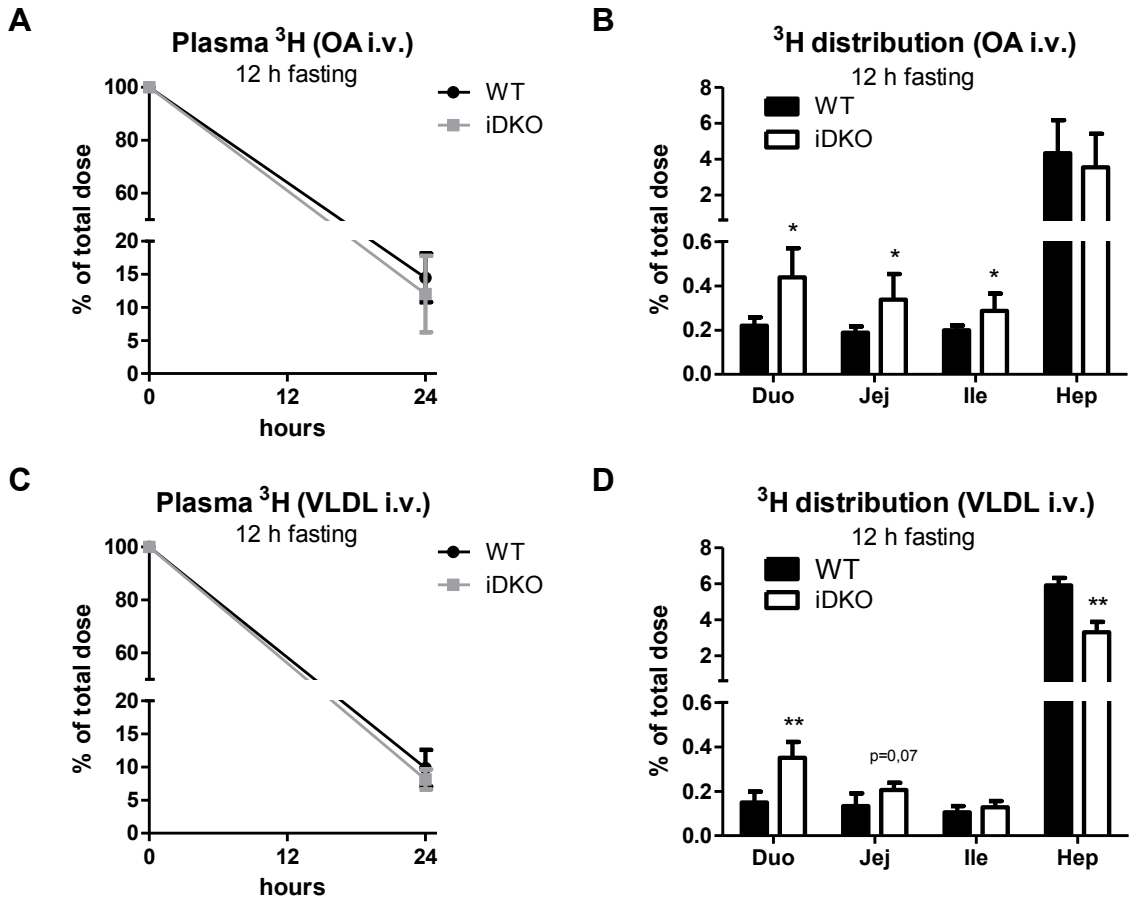

Figure 32: Cgi-58/Atgl iDKO mice accumulate basolaterally-derived lipids. (A) Circulating and (B) intracellular radioactivity 24 h post administration of ^{3}H-OA. (C) Plasma and (D) tissue tradioactivity 24 h post administration of ^{3}H-VLDL. Mice were fasted 12 h prior to sacrifice. Data represent mean (n=5-6) ± SD. Duo, duodenum; Jej, jejunum; Ile, ileum; Hep, hepar (liver). (Korbelius et al., 2019)

FPLC analysis of plasma samples 24 h post injection of ^{3}H-OA resulted in similar ^{3}H distribution between WT and Cgi-58/Atgl iDKO mice. The vast majority of circulating radioactivity was present in the albumin-bound FA fraction (**Figure 33**). Therefore, these findings argued against a pivotal role of hepatocytes in redistributing lipids back to the SI. However, increased accumulation of both tracers 24 h post injection affirmed an essential role of intestinal CGI-58/ATGL in the hydrolysis of a basolaterally-derived transient lipid storage pool. (Korbelius et al., 2019)

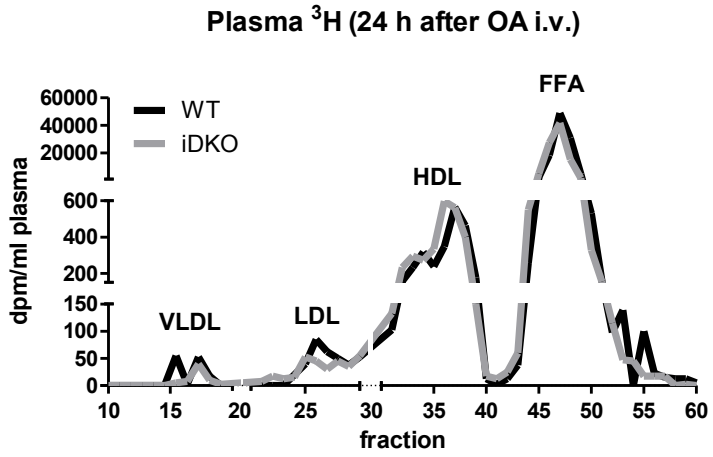

Figure 33: Distribution of intravenously applied oleic acid. FPLC profile of 200 µl pooled plasma 24 h post injection of ^{3}H-OA. (Data represent mean (n=5-6) (Korbelius et al., 2019).

2.2.10 Cgi-58/Atgl iDKO mice accumulate TG without lipids from dietary sources

Our results so far indicated a negligible contribution of intestinal CGI-58 and ATGL to dietary lipid turnover, but rather ascribed them an essential role in the hydrolysis of basolaterally-derived lipids. Therefore, we next restricted mice to endogenous lipids by fasting them for 16 h or challenging them with a FFD. After a prolonged fasting period, mice lacking solely Cgi-58 did not display any difference in plasma TG concentrations, however, circulating TG levels in Atgl iKO mice were decreased by 40% (**Figure 34**).

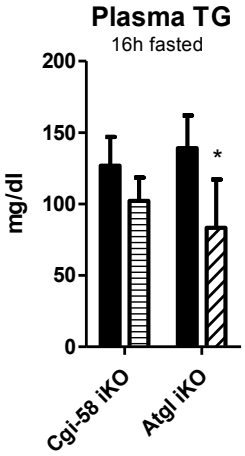

Figure 34: Plasma TG concentrations in Cgi-58 iKO and Atgl iKO mice. Data represent mean (n=3-7) + SD. * $p < 0.05$.

In mice lacking CGI-58 and ATGL, body weights and plasma lipid parameters remained comparabale between the genotypes after FFD-feeding. Interestingly, Cgi-58/Atgl iDKO mice sacrificed after a prolonged fasting period also displayed a significant 32% decrease in plasma TG concentrations (**Table 8, Figure 35A**). (Korbelius et al., 2019)

Table 8: Body weight and plasma lipid parameters of WT and Cgi-58/Atgl iDKO mice restricted to endogenous lipids.

	Chow (16 h fasted)		5 W FFD (refed)	
	WT	**iDKO**	**WT**	**iDKO**
BW (g)	19.4±1.74	19.2±0.89	22.1±1.07	22,5±0,93
TG (mg/dl)	119±30.4	81.5±26.02*	63.7±11.4	57,0±7,72
TC (mg/dl)	63.1±4.09	65.1±6.59	41.0±8.42	43,1±6,66
FC (mg/dl)	17.3±4.64	15.5±3.89	16.3±2.98	16,3±3,67
CE (mg/dl)	48. 5±9.51	49.6±7.56	24.7±6.49	26,8±3,35
FFA (mmol/l)	0.99± 0.31	1.02± 0.42	1.17±0.52	1,13±0,57
n	7	9	7	7

Body weights and plasma parameters of sex- and age-matched WT and Cgi-58/Atgl iDKO mice. Data represent mean ± SD. BW, body weight; TG, triglyceride; TC, total cholesterol; FC, free cholesterol; CE, cholesteryl ester; FFA, free fatty acid; n.d., not determined. *$p < 0.05$. (Korbelius et al., 2019)

Analysis of WT and iDKO plasma pools via FPLC revealed slight reduction of VLDL-TG levels in Cgi-58/Atgl iDKO mice whereas other lipoprotein fractions were not affected (**Figure 35B**). Unchanged VLDL secretion after tyloxapol injection (**Figure 17A,B**), inhibiting the uptake of circulating lipids into the tissues, underlined the hypothesis of accelerated basolateral lipid uptake being responsible for the decrease in plasma TG. Increased mRNA levels of *Lrp1* but not *Ldl*-R in the SI of Cgi-58/Atgl iDKO mice indicated a more rapid basolateral uptake of CM remnants (**Figure 35C**). As mice fasted for 16 h prior to oral administration of an oil bolus displayed ameliorated hepatic steatosis in the absence of intestinal CGI-58 and ATGL (**Figure 24B**), we next analyzed livers of 16 h fasted mice without a dietary trigger. Biochemical analysis of liver lipid content, as well as ORO staining of hepatic cryosections (**Figure 35D,E**) did not reveal significant differences between the genotypes. This might be due to a less pronounced effect on CM clearance without an oral lipid load (Korbelius et al., 2019).

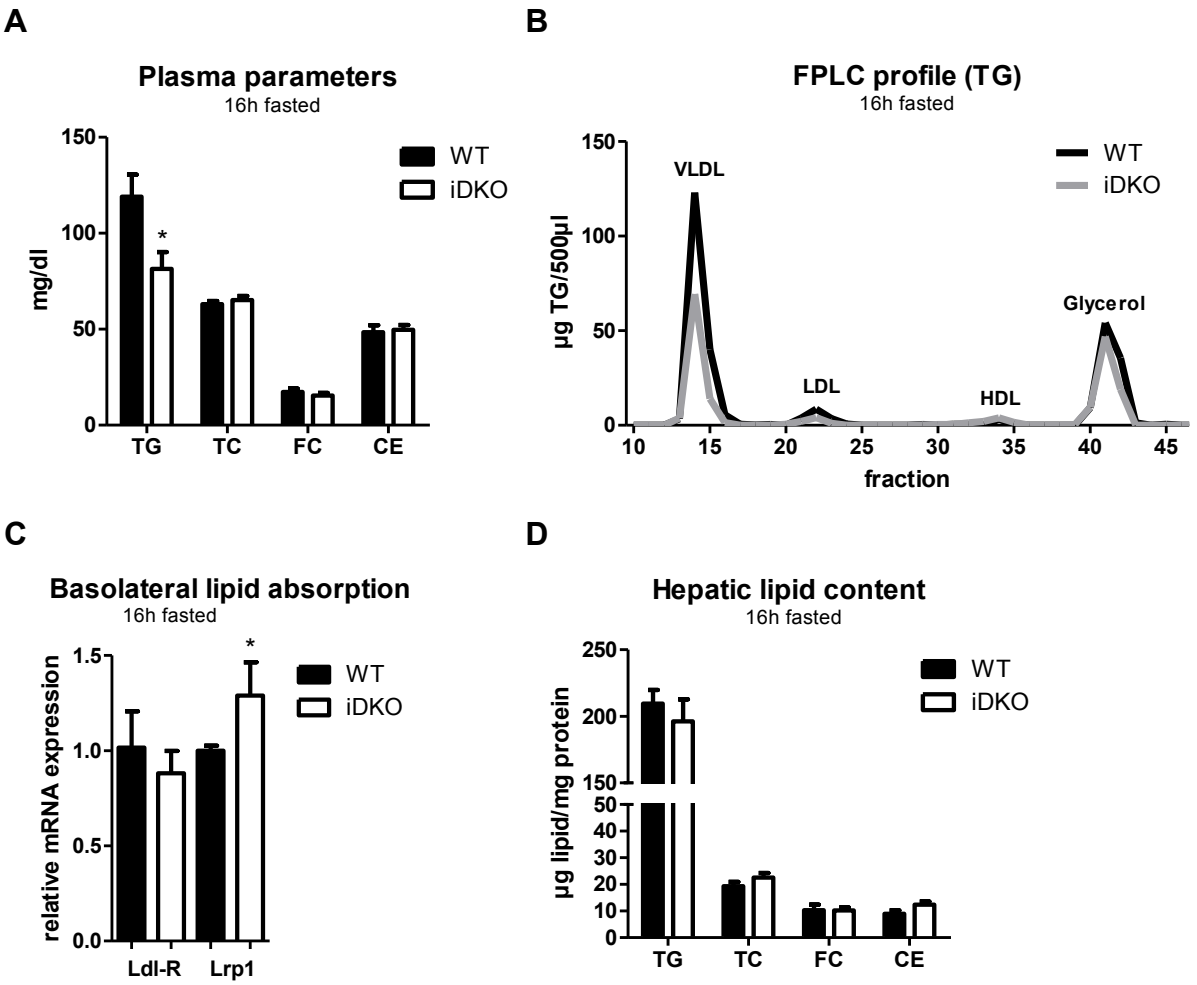

Figure 35: Decreased circulating VLGL-TG in 16 h-fasted iDKO mice. (A) Plasma lipid levels and (B) FPLC profile of 200 µl pooled plasma of WT and Cgi-58/Atgl iDKO mice (Korbelius et al., 2019). (C) mRNA expression of genes involved in basolateral lipid uptake. Expression was normalized to *cyclophilin A* as houskeeping gene. (D) Biochemical and (E) histological analysis of livers. Magnification, 40x; Scale bar, 50 µm. All mice were fasted 16 h prior to sacrifice. Data represent mean (n=6-9) + SD. *p < 0.05.

For other tissues, like the white adipose tissue, it has already been known for several decades that prolonged fasting leads to depletion of intracellular lipid storages (Williamson, 1964), although ATGL has not been discovered yet. Compared to fed conditions, intestinal lipids were also drastically reduced, as refed WT mice displayed duodenal TG levels around 65 µg TG/mg protein (**Figure 15A**), decreasing to 32 µg TG/mg protein already after 4 h of

fasting (**Figure 15B**). After 16 h of starvation, the intestinal TG content dropped to 7 µg/mg protein (**Figure 36A**), indicating that the SI has a major role in maintaining whole body lipid homeostasis in negative energy balance states. However, 16 h fasted Cgi-58/Atgl iDKO mice displayed 5.1-fold increased TG levels in the duodenum, which was also confirmed by ORO staining (**Figure 36A,B**). The persistent lipid accumulation again highlighted the importance of intestinal CGI-58 and ATGL in gut lipolysis. As mice gavaged with a fluorescently labeled FA were also fasted for 16 h, this finding further explained the accumulation of PLIN3-coated vesicles, filled with endogenous lipids 30 min post gavage (**Figure 28A**). (Korbelius et al., 2019)

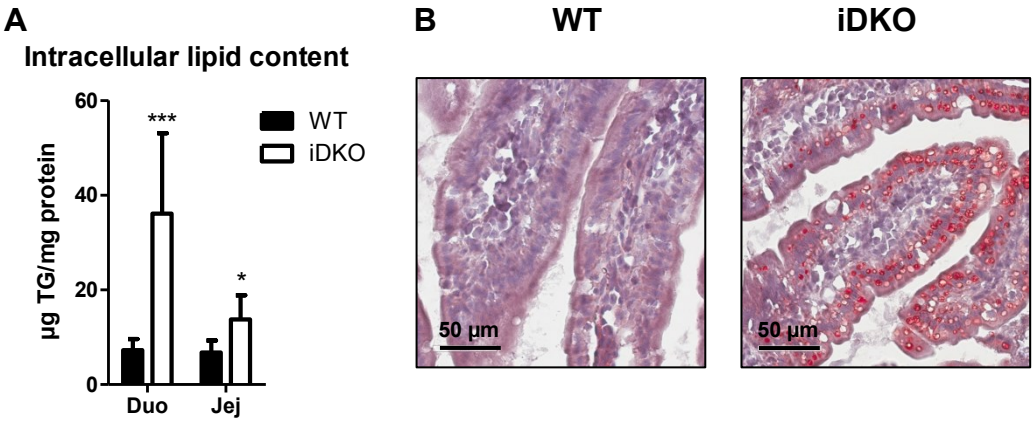

Figure 36: Persistent cLD accumulation in the proximal SI of 16 h-fasted iDKO mice. (A) Lipid extraction from duodena and jejuna of 16 h fasted mice. (B) ORO staining of duodenal cryosections. Magnification, 40x; Scale bar, 50 µm. Data represent mean values (n=7-9) + SD. *p < 0.05; ***p ≤ 0.001. Duo, duodenum; Jej, jejunum. (Korbelius et al., 2019)

Given that CGI-58 and ATGL in the SI seem to play a role in the hydrolysis of peripheral rather than dietary lipids, we restricted mice to endogenously produced fats by challenging them with a FFD. During five weeks of FFD feeding, body weight remained comparable between the genotypes (**Table 8**). Nevertheless, Cgi-58/Atgl iDKO mice still accumulated lipids in the proximal parts of the SI, with 2.8-fold and 2.5-fold increased TG concentrations in the duodenum and jejunum, respectively (**Figure 37A**). This lipid accumulation was verified by ORO staining of duodenal cryosections (**Figure 37B**). Plasma lipid levels did not reveal any differences in CGI-58/ATGL-deficient mice (**Table 8**) and also distribution of TG and cholesterol into lipoprotein classes was identical between the genotypes (**Figure 37C**). (Korbelius et al., 2019)

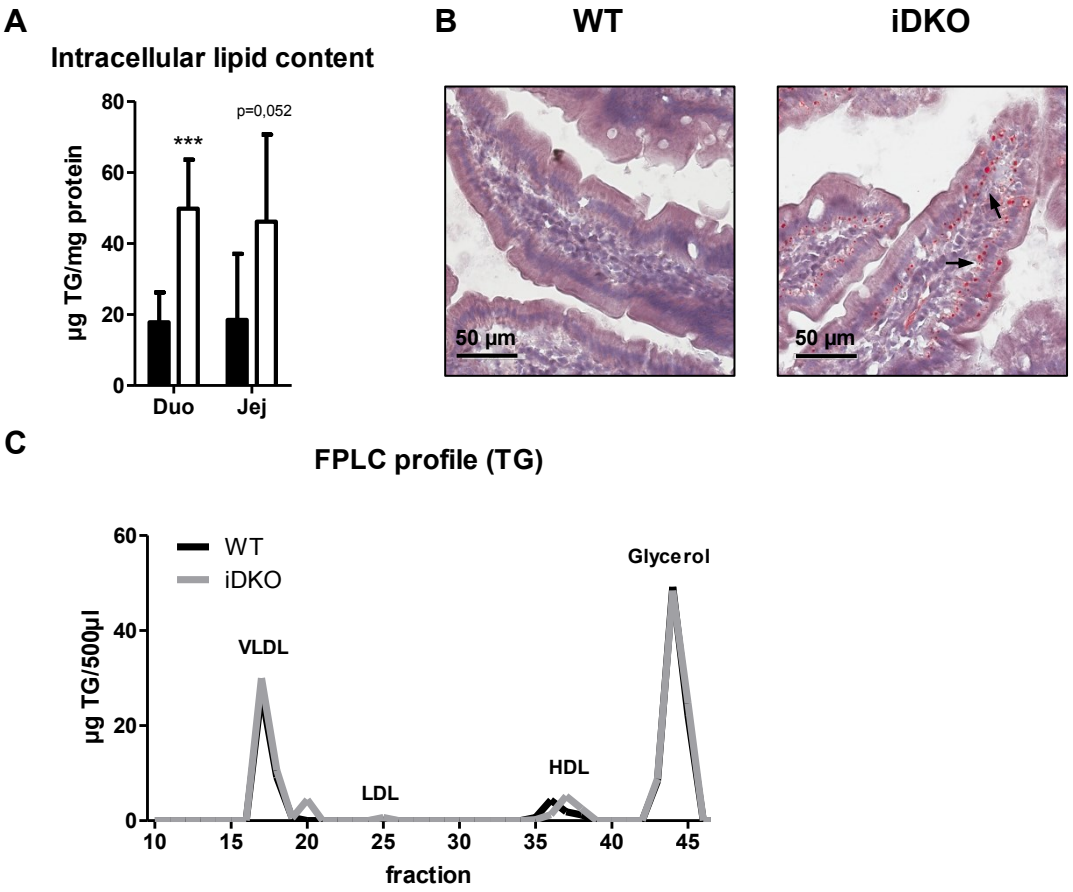

Figure 37: Cgi-58/Atgl iDKO mice display intestinal cLD accumulation despite deprivation of dietary lipids. (A) Biochemical and (B) histological analyses of FFD-fed WT and Cgi-58/Atgl iDKO mice. (C) Plasma lipoprotein profile of FFD-fed animals. Data represent mean values (n=7) + SD. ***p ≤ 0.001. Duo, duodenum; Jej, jejunum (Korbelius et al., 2019).

2.2.11 FFA released by intestinal CGI-58/ATGL are destined for FAO

By now, our results indicate a critical role of intestinal CGI-58/ATGL in the degradation of basolaterally-derived lipids, with a negligible role in dietary lipid absorption and lipoprotein formation. However, the destination of FFAs released via CGI-58/ATGL-mediated hydrolysis within enterocytes still remained elusive.

Previous publications showed that loss of ATGL impaired expression of peroxisome proliferator-activated receptor (PPAR) α and PPARδ target genes, leading to cardiac insufficiency, which could be restored by cardiac-specific overexpression of ATGL in ATGL KO mice or by treatment with PPARα agonists (Haemmerle et al., 2011). As ATGL was shown to be essential to provide FFAs for PPARα signaling also in the SI (Obrowsky et al., 2013), we examined the regulation of PPARα expression and some of its target genes. While we could not observe any effect in 4 h-fasted iDKO mice fed either chow or HF/HCD (data not shown), mRNA expression levels of PPARα target genes were altered in the refed state in Cgi-58/Atgl iDKO mice (**Figure 38**). Although *Pparα* expression itself was unchanged, all examined target genes involved in lipid metabolism (*Cd36*, *Abca1*) and oxidative stress (*Gstk1*, *Gstm3, Gstt*) were affected by the simultaneous lack of both proteins, pointing out a role of CGI-58 and ATGL in preventing oxidative stress under postprandial (refed) conditions. Despite an increase in *Acot2* mRNA levels, other genes involved in β-oxidation (*Cpt1α, Acox1*) were comparable between the genotypes (**Figure 38**).

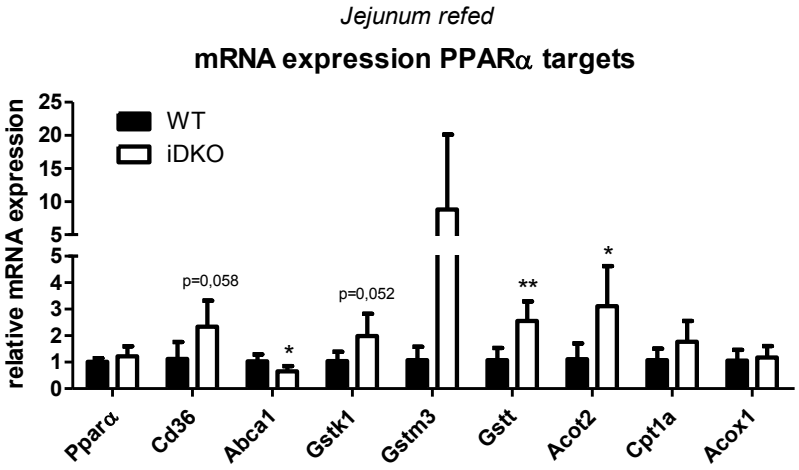

Figure 38: Intestinal CGI-58 and ATGL play a role in oxidative stress under refed conditions. mRNA expression of genes involved in dietary lipid absorption, oxidative stress and FA oxidation. Expression levels were normalized to *cyclophilin A* as housekeeping gene. Data represent mean values (n=4-5) + SD. *p < 0.05; **p ≤ 0.01.

However, despite unchanged mRNA expression of *Cpt1α* and *Acox1* we hypothesized a role of intestinal CGI-58/ATGL in the hydrolysis of basolaterally-derived lipids, which were shown to be preferentially shuttled to FAO or PL synthesis (Storch et al., 2008, Ho et al., 2002, Gangl and Ockner, 1975). Therefore, we measured intestinal FA oxidation in isolated enterocytes from jejuna of WT and Cgi-58/Atgl iDKO mice. We observed a 54% decrease in intestinal FAO rate in mice lacking CGI-58 and ATGL (**Figure 39**), suggesting that CGI-58/ATGL-mediated hydrolysis shuttles FFAs to mitochondria within the SI (Korbelius et al., 2019).

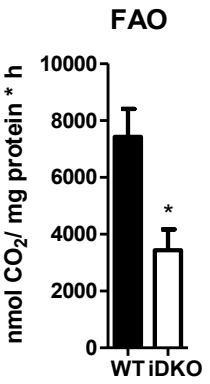

Figure 39: Impaired fatty acid oxidation in Cgi-58/Atgl iDKO enterocytes. Isolated jejunal enterocytes were incubated with ^{14}C-palmitic acid and CO_2 was trapped for 2 h. Data represent mean values (n=3) + SD. *p < 0.05. (Korbelius et al., 2019)

As basolaterally-derived lipids can also be shuttled to PL synthesis, we next examined the incorporation of i.p. applied OA into different lipid classes within enterocytes. TLC analysis revealed prominent incorporation of ^{3}H-OA into TG (and CE) fractions in the duodenum of Cgi-58 iKO (**Figure 40A**) and Cgi-58/Atgl iDKO mice (**Figure 40B**), with no significant differences in incorporation of the radioactive tracer into PLs. A similar pattern was observed in mice lacking solely intestinal ATGL (Obrowsky et al., 2013). These results indicated that it is unlikely that products generated by intestinal CGI-58 and ATGL are shuttled to the PL synthesis pathway. Therefore, upon re-esterification and subsequent storage in a basolaterally-derived lipid pool, ATGL-mediated hydrolysis rather releases FFA for FAO (Korbelius et al., 2019).

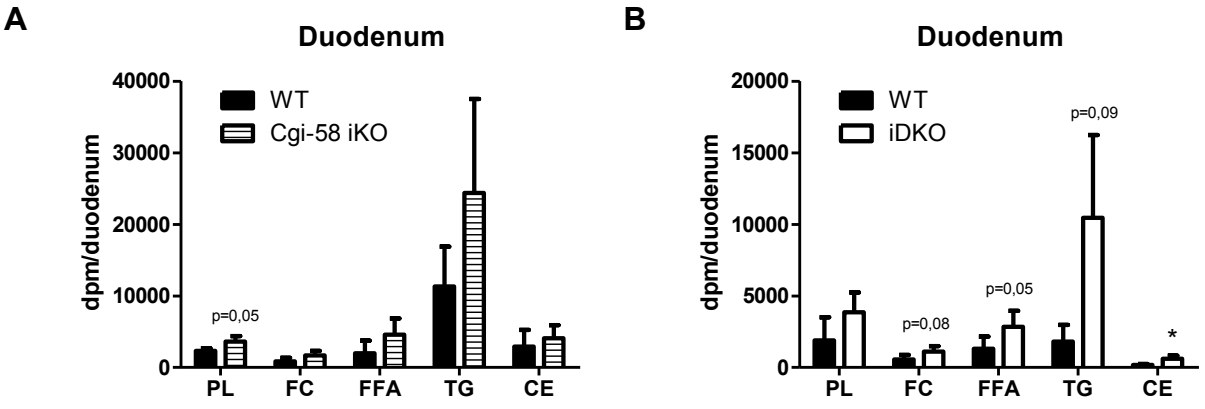

Figure 40: Basolaterally-derived ^{3}H-OA primarily gets incorporated into TGs. Incorporation of i.p. administered ^{3}H-OA in Intralipid into different lipid classes in the duodenum of (A) Cgi-58 iKO mice and (B) Cgi-58/Atgl iDKO iDKO mice. Data represent mean values (n=3-5) + SD. *p < 0.05. PL, phospholipid; FC, free cholesterol; FFA, free fatty acid; TG, triglyceride; CE, cholesteryl ester.

2.2.12 Intestinal CGI-58/ATGL deficiency affects expression of other potential lipases

In all cohorts, we observed the most prominent intracellular lipid accumulation in the proximal SI, indicating that uptake of circulating lipids, providing substrates for CGI-58/ATGL-mediated hydrolysis, primarily occurs in the duodenum rather than in the jejunum. Therefore, we next examined the consequences of intestinal CGI-58/ATGL deficiency on the expression of other lipases to elucidate if downregulation of other neutral lipases might add to the massive lipid deposition in iDKO duodena or whether upregulation of other enzymes might take over the function of ATGL in the jejunum, thereby attenuating lipid mass. Beside acidic and neutral lipolysis, which are mediated by lysosomal acid lipase (LAL) in the lysosome and ATGL in the cytosol, respectively [reviewed in (Zechner et al., 2017)], alkaline lipolysis exists and is mediated by PTL with tributyrin as preferred substrate (Sampugna et al., 1967). Whereas no effect was observed in expression levels of the cLD-associated lipases HSL and MGL as well as some ER-associated lipases of the carboxylesterases (Ces) family, duodenal expression of *Ptl* was significantly reduced by 70% in mice lacking CGI-58 and ATGL, presumably contributing to the massive increase in duodenal TG content (**Figure 41A**). In mice fed FFD for five weeks, *Ptl* expression was also significantly reduced (**Figure 41B**). Expression of *Ptl* was undetectable in the jejunum of WT and Cgi-58/Atgl iDKO mice, which is in line with previous data showing that in rat intestinal mucosa, PTL is expressed throughout the SI with a 3-fold higher expression in the first quarter than in the other three quarters combined (Mahan et al., 2001). Interestingly, while expression of neutral and acidic lipases did not differ between the genotypes in the jejunum, mRNA levels of *Ces1f* (Tgh2) and *Ces2g* were increased in mice lacking CGI-58 and ATGL more than 4- and 8-fold, respectively (**Figure 41C**). This maybe attenuated lipid accumulation in that part of the SI in the refed state. The same pattern could be observed in FFD-fed mice sacrificed in the refed state (**Figure 41D**). (Korbelius et al., 2019)

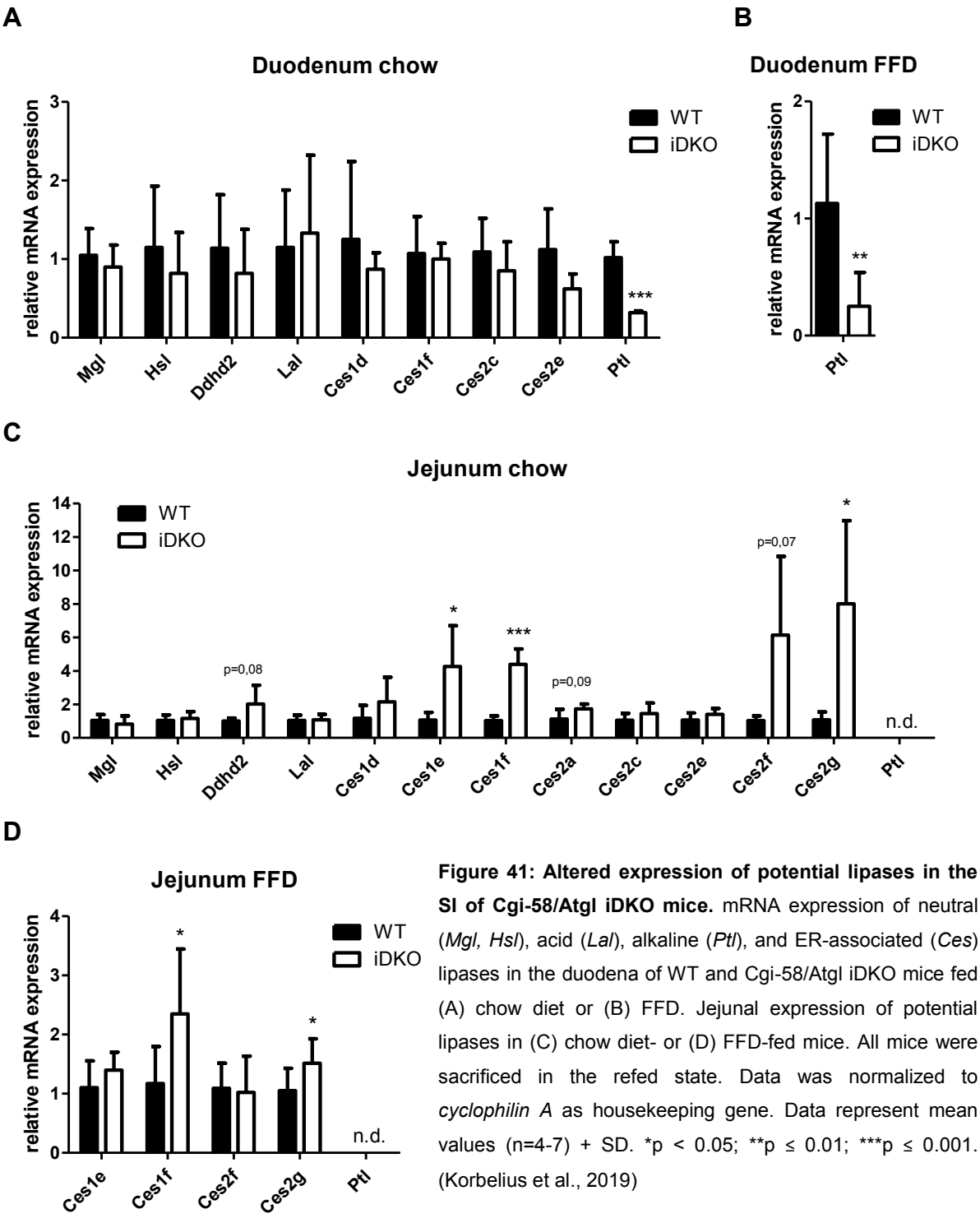

Figure 41: Altered expression of potential lipases in the SI of Cgi-58/Atgl iDKO mice. mRNA expression of neutral (*Mgl, Hsl*), acid (*Lal*), alkaline (*Ptl*), and ER-associated (*Ces*) lipases in the duodena of WT and Cgi-58/Atgl iDKO mice fed (A) chow diet or (B) FFD. Jejunal expression of potential lipases in (C) chow diet- or (D) FFD-fed mice. All mice were sacrificed in the refed state. Data was normalized to *cyclophilin A* as housekeeping gene. Data represent mean values (n=4-7) + SD. *p < 0.05; **p ≤ 0.01; ***p ≤ 0.001. (Korbelius et al., 2019)

2.2.13 CGI-58/ATGL deficiency does not influence autophagy

So far, our results highlighted a role of CGI-58/ATGL in the breakdown of a cytoplasmic lipid pool rather derived from the basolateral side, raising the question which enzyme accounts for hydrolysis of alimentary cLDs within the enterocyte. Previous studies have shown that autophagy plays an important role in intestinal lipid homeostasis, especially after an oral lipid load (Khaldoun et al., 2014). As autophagy was found to be triggered by an alimentary lipid supply, we stained intestines of BODIPY®-gavaged mice with CathD to elucidate if dietary lipids are also channeled to lysosomes. As the majority of alimentary lipids is absorbed in the jejunum, leading to apically-derived cLD formation within enterocytes in this part of the SI [reviewed in (D'Aquila et al., 2016)], we used jejunal sections for CathD immunofluorescence.

Thirty min post gavage, only WT mice displayed small cLDs at the apical membrane of the enterocyte, which partly co-localized with CathD, indicating an immediate trapping of dietary lipids by lysosomes (**Figure 42A**). After 2 h, iDKO mice accumulated BODIPY-containing cLDs to a greater extent than WT mice as observed in the jejunal sections stained with PLIN3 (**Figure 29**). Neither WT nor iDKO mice showed co-staining of BODIPY® and CathD, but CathD-positive circular structures were observed in the jejunum of Cgi-58/Atgl iDKO mice within the enterocyte (**Figure 42B**). This suggested channeling of previously formed lipids to the lysosome, 2 h post oral administration of an oil bolus. In both genotypes, CathD expression was predominantly found in the lamina propria, presumably staining macrophages.

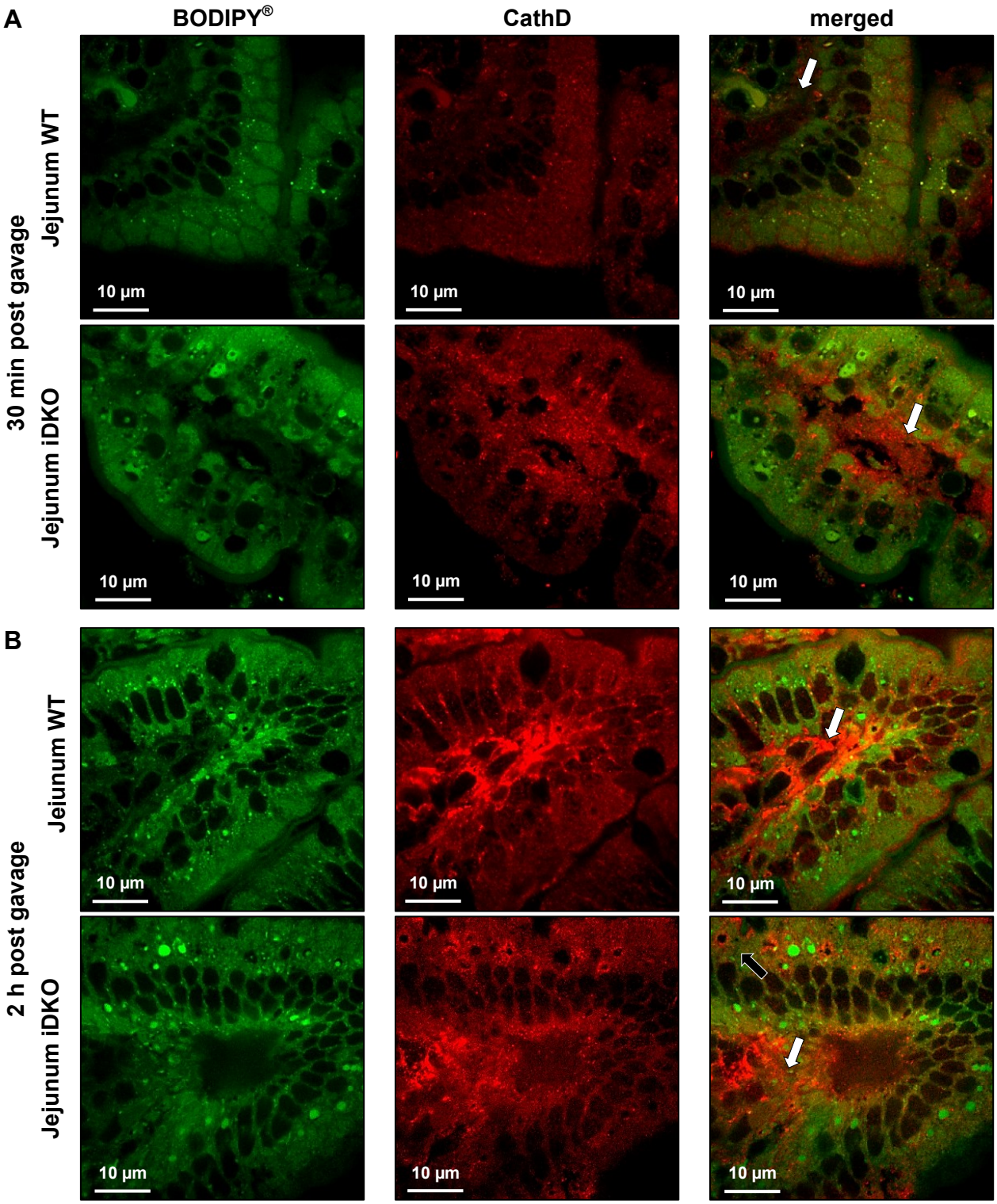

Figure 42: Cgi-58/Atgl iDKO mice display cathepsinD (CathD)-positive structures within the enterocyte 2 h post BODIPY® gavage. Jejunal sections of WT and Cgi-58/Atgl iDKO mice (A) 30 min and (B) 2 h post gavage of BODIPY®-FA. Sections were co-stained with CathD (red). Beside macrophages in the lamina propria (white arrows), CathD-positive circular structures within the enterocyte (black arrows) are visible in the jejunum of Cgi-58/Atgl iDKO mice 2 h post gavage. Magnification, 100x; scale bar, 10 µm.

Despite differences observed 30 min as well as 2 h post gavage, mRNA expression of *Lal*, the sole enzyme known to be involved in acid lipolysis within the lysosome, remained comparable between the genotypes (**Figure 43A**). However, *Lal* mRNA levels were drastically increased by 2.9- and 5.1-fold 30 min and 2 h post gavage, respectively (**Figure 43B**). Therefore, LAL might be a possible candidate for hydrolysis of an alimentary lipid pool within enterocytes, however, loss of intestinal CGI-58 and ATGL does not greatly influence this pathway.

A

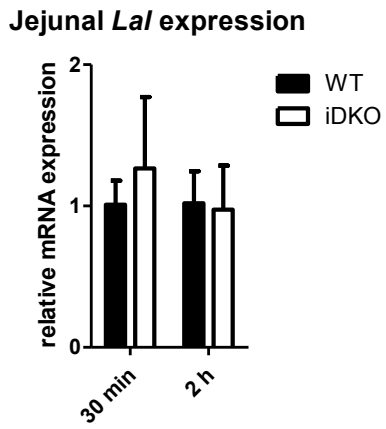

B

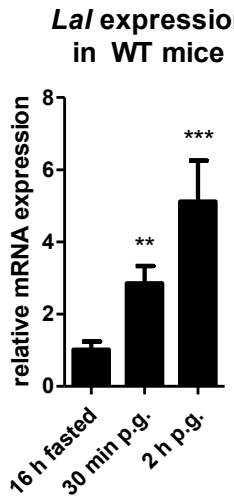

Figure 43: *Lal* mRNA expression levels 30 min and 2 h post gavage.

(A) Jejunal *Lal* expression in WT and Cgi-58/Atgl iDKO mice 30 min and 2 h post gavage. (B) Nutritional regulation of *Lal* expression in jejuna of WT mice. Gene expression was normalized to *cyclophilin A* as housekeeping gene. Data represent mean (n=3-5) + SD.

2.3 Discussion

Under postprandial conditions, alimentary TGs are transiently stored in LDs of enterocytes and provide substrates for CM assembly within the interprandial period. In humans, it was shown that CMs secreted after a second meal contained TG ingested in the first meal (Jackson et al., 2002, Evans et al., 1998, Fielding et al., 1996), indicating that resynthesized TG are not immediately available for CM synthesis, but meanwhile get incorporated into cLDs. During absorption, cLDs become smaller (Zhu et al., 2009), suggesting that stored TG are mobilized by lipases. In adipocytes, cLDs are hydrolyzed to FFA and free glycerol by the action of ATGL, HSL, and MGL [reviewed in (Zechner et al., 2012)]. Compared to WAT, *Cgi-58* and *Atgl* expressions throughout the SI are around 35% to 50%, respectively. We hypothesized that ATGL and its coactivator CGI-58 are possible candidates for the hydrolysis of a cytoplasmic TG storage pool in the SI.

Abolished mRNA and protein expression of both proteins specifically in enterocytes led to 62% (4 h fasted) and 49% (refed) reduced TGH activity in the jejunum, the major side of dietary lipid absorption. This already highlighted a role of CGI-58 and ATGL in the degradation of a cytoplasmic lipid storage pool in the SI. (Korbelius et al., 2019)

2.3.1 Effects on intracellular lipid homeostasis

Beside co-activation of ATGL by CGI-58, its lipolytic activity is strongly regulated by PLIN proteins. In the basal state, CGI-58 is associated with PLIN on the surface of the LD and is not able to activate ATGL. Stimulation of lipolysis via catecholamines activates a signal cascade leading to the phosphorylation of PLIN, allows CGI-58 to dissociate from PLIN and bind to ATGL (Granneman et al., 2007). Regarding this regulatory function of PLINs on lipolysis, we wondered how intestinal PLIN expression might be influenced in the absence of CGI-58 and ATGL. Recent publications indicate distinct roles for PLIN2 and PLIN3 in the SI with varying expression levels after chronic and acute high-fat challenge (Lee et al., 2009). We could show that PLIN2 and PLIN3 are nutritionally regulated in WT mice, with drastically increased mRNA expressions of both genes after prolonged fasting (16 h) or 30 min post gavage of an oil bolus. The functions of PLINs in the jejunum have not been investigated so far. Some data indicate that PLIN2 is necessary to stabilize long-term stored TGs by limiting the interaction of lipid hydrolases with the LD, whereas PLIN3 is primarily located on nascent LDs (Lee et al., 2009). We could not observe relevant differences in PLIN expression levels between WT and Cgi-58/Atgl iDKO mice, except slightly decreased Plin3 mRNA after

refeeding. However, drastic variances in cLD size and localization within enterocytes render the idea of different cLD pools featuring different proteomes likely.

Disruption of intestinal CGI-58 and ATGL resulted in massive accumulation of neutral lipids in the SI, especially in the refed state and after HF/HCD feeding, with a predominant increase of TG levels in the proximal parts of the SI. Concentrations of TC or CE remained unchanged between the genotypes (Korbelius et al., 2019), indicating a specific degradation of TGs by intestinal CGI-58/ATGL. However, liver-specific (Guo et al., 2013) and intestine-specific (Xie et al., 2014) CGI-58 KO mice displayed increased cholesterol levels in the respective tissues, while ATGL KO livers did not accumulate cholesterol (Haemmerle et al., 2006, Wu et al., 2011). These findings indicated that intestinal and hepatic CGI-58 might function as a coactivator of a cholesterol esterase, but unchanged CE hydrolase activity in hepatocyte-specific CGI-58 KO mice suggested that CGI-58 might rather influence the sequestration of CE and FC on the LDs (Guo et al., 2013). (Korbelius et al., 2019)

In chow diet-fed mice in the refed state, lipid accumulation shifted from the jejunum to the very proximal part of the SI, the duodenum, which was surprising as dietary lipids predominantly accumulate in the jejunum after an oral lipid load [reviewed in (D'Aquila et al., 2016)]. This discrepancy raised the question if downregulation of other lipases may contribute to the duodenal lipid accumulation or upregulation of other lipases may take over TG hydrolysis and attenuate lipid mass in the jejunum. After lipolytic stimulation in the WAT, the vast majority of CGI-58 disperses from the LD into the cytoplasm (Yamaguchi et al., 2007), while just a small amount remains at the LD surface to interact and activate ATGL (Granneman et al., 2007). These findings together with the ATGL-independent skin-barrier defect observed in NLSDI patients and the impact on cholesterol metabolism indicates that CGI-58 has some functions independent from activating ATGL. There might exist another lipid hydrolase, which is regulated by CGI-58 (Radner et al., 2010, Guo et al., 2013). Therefore, we analyzed mRNA expression levels of other potential lipases. In line with observations in adipocytes, where CGI-58 failed to activate lipolysis in the absence of ATGL, but was able to stimulate TG hydrolase activity in HSL-deficient WAT (Schweiger et al., 2006), HSL expression remained unaffected in our mice. Also expression levels of DDHD2, which has been shown to act as a TG hydrolase in the brain (Inloes et al., 2014), were not altered in mice lacking CGI-58/ATGL (Korbelius et al., 2019).

Beside acidic and neutral lipolysis, which are mediated by LAL in the lysosome and ATGL in the cytosol, respectively [reviewed in (Zechner, 2017)], there exists an alkaline lipolysis mediated by pancreatic lipase (PTL) with tributyrin as preferred substrate (Sampugna et al., 1967). We found that mRNA expression of Ptl was reduced by 70% in the duodenum of iDKO mice, presumably contributing to the massive increase in duodenal TG content (Korbelius et al., 2019). In rat intestinal mucosa, PTL is expressed throughout the SI with a 3-fold higher expression in the first quarter than in the other three quarters combined. Zhu et al. already suspected PTL to be a possible candidate for LD degradation in the enterocyte (Zhu et al., 2009), as synthesis of PTL was shown to be restricted to villus enterocytes and crypt cells in the rat intestine (Mahan et al., 2001). In contrast to pancreatic PTL (pPTL), which is responsible for the TG breakdown in the intestinal lumen, enterocytes are not able to secrete intestinal PTL (iPTL) (Mahan et al., 2001). This again emphasizes the importance of iPTL in lipid metabolism within the enterocyte. Further studies on iPTL might help to identify the yet unknown lipase accountable for the degradation of dietary lipids, which are further used for CM synthesis. However, with expression levels of iPTL being highest in the duodenum, a role of iPTL in the synthesis of CMs, which occurs in the jejunum, is questionable.

It still remained elusive, why lipids did not accumulate in the jejunum of refed Cgi-58/Atgl iDKO mice despite significantly reduced TGH activity. Jejunal mRNA expression profiling of other TG lipases revealed a remarkable increase in expression of several carboxylesterases (Ces), mainly Ces1e, Ces1f, Ces2f, and Ces2g (Korbelius et al., 2019). Carboxylesterases are believed to catalyze neutral lipid hydrolysis and are uniquely expressed among tissues (Jones et al., 2013). Ces1f, also known as TGH2, was shown to hydrolyze p-nitophenyl butyrate, triolein and monoolein in adipocytes with a preference for short-chain FA TGs, but *in vivo* evidence for a role of this enzyme in lipolysis or intestinal lipid metabolism is still missing (Okazaki et al., 2006). In WAT, subcellular fractionation revealed the presence of Ces1f in the fat cake fraction together with Ces3 (TGH-1) and HSL, suggesting that Ces3 and Ces1f mediate the breakdown of neutral lipids stored in cLDs where PLIN1 co-localizes. Further, unlike Ces3, Ces1f is highly expressed in the SI and, in contrast to WAT, intestinal mRNA levels are increased upon refeeding (Okazaki et al., 2006). As only refed Cgi-58/Atgl iDKO mice show this drastic increase in Ces1f mRNA levels, it is likely that upregulation of *Ces1f* by refeeding takes over the role of ATGL, whose intestinal expression is - in contrast to WAT - induced upon feeding/gavage (Li et al., 2019). Therefore, upregulation of *Ces1f* might be a compensatory mechanism for prevention of jejunal TG accumulation. In addition, Ces2g, which was found to be 8-fold increased in the jejunum of refed Cgi-58/Atgl iDKO

mice, possesses TGH activity (Robert Zimmermann, personal communication). Together with massively increased mRNA expression of *Ces2g* in steatotic livers of C57BL/6 mice (Jones et al., 2013), these data suggest an important role of this enzyme in intestinal and hepatic lipid metabolism. (Korbelius et al., 2019)

2.3.2 Effects on systemic lipid homeostasis

Although the most pronounced differences were observed in the duodenum and not in the jejunum, which represents the major site for dietary lipid absorption and lipoprotein synthesis, we further investigated the contribution of intestinal CGI-58/ATGL deficiency on circulating lipid parameters. Considering that the SI plays a crucial role in sustaining lipid supply in interprandial periods, together with the massive increase in intestinal cLD content in Cgi-58/Atgl iDKO mice, ATGL and its coactivator CGI-58 might still be involved in the hydrolysis of lipids to provide FFAs for CM synthesis. (Korbelius et al., 2019)

Interestingly, plasma parameters did not differ between the genotypes in any feeding state and CM secretion was not affected by the loss of CGI-58 and ATGL. These observations coincide with previously published data from liver-specific ATGL KO mice, in which VLDL production and plasma TG concentrations were comparable to WT mice, suggesting that ATGL is not required to provide substrates for intestinal or hepatic lipoprotein assembly (Wu et al., 2011). Thus, the observed decrease in hepatic lipoprotein secretion in whole-body ATGL KO mice (Haemmerle et al., 2006) was due to decreased FFA delivery from the WAT to the liver. In line, mice lacking solely intestinal ATGL did not show any differences in intestinal lipoprotein assembly (Obrowsky et al., 2013). In contrast, ASO-mediated knockdown of CGI-58 in the liver led to significantly reduced VLDL secretion but unaltered plasma TG levels in chow diet-fed mice (Brown et al., 2010). This finding was corroborated by gain-of-function and loss-of-function experiments in hepatoma cells, indicating a role of CGI-58 in coupling cytoplasmic TG hydrolysis to packaging into TG-rich lipoproteins (Brown et al., 2007). Impaired postprandial lipid secretion in intestine-specific CGI-58 KO mice indicated that CGI-58 is required for efficient postprandial lipoprotein secretion in an ATGL-independent manner (Xie et al., 2014). Although we used sex- and age-matched Cgi-58 iKO mice, we failed to reproduce this finding, This contradictory observation might result from the different diets used, as Xie et al. fed mice a western-type HFD [40% energy from fat; 20.7%(w/w) lard, 0.2% (w/w) cholesterol] instead of HF/HCD [60% energy from fat; 34% (w/w) crude fat, 1% (w/w) cholesterol]. (Korbelius et al., 2019)

Although our results so far evidenced a negligible role of intestinal CGI-58/ATGL in intestinal lipoprotein metabolism, we further aimed to investigate the fate of dietary lipids within the SI of Cgi-58/Atgl iDKO mice. In humans, it has been reported that lipids ingested with the first meal appear in the plasma after ingestion of a second meal, supporting the existence of transient lipid storage (Fielding et al., 1996). The authors suggested that the rapidity of the early peak in plasma TG after ingestion of a second meal is rather attributable to the release of preformed CMs than complete processing of the lipid in the intestinal lumen. The second meal might stimulate the secretion of these transiently stored lipids by an increase in small intestinal blood flow or by displacement by the newly arriving dietary fat (Fielding et al., 1996). If ATGL and CGI-58 were involved in the hydrolysis of this lipid pool, secretion of primary ingested lipids would be diminished in iDKO mice after ingestion of the subsequent meal. Plasma levels of primary ingested lipids, however, were not altered between the genotypes upon administration of the secondary oil bolus. This again indicates that intestinal CGI-58 and ATGL do not affect secretion of dietary fats into the periphery. Nevertheless, also WT mice failed to display the proposed “sequential meal effect”, questioning this phenomenon in rodents. Suprisingly, secretion of the second oil bolus into the circulation was drastically diminished, most likely due to increased gastric retention of the substrate. Comparable intestinal radioactivities implied delayed gastric emptying being responsible for delayed secretion of the substrate into the bloodstream. However, fecal exretion of the radioactive tracer and water- and oil-based gut transit time remained comparable between the genotypes. Interestingly, 10 h post gavage of the first meal, these lipids still accumulated in the SI of CGI-58/ATGL-deficient mice, but secondary gavaged fat got stuck in the SI to the same extent as in WT mice. This might be due to i) an overload of lipids, leading to saturation of the intestinal storage capacity, ii) secondary lipids bypassing cytosolic storage/hydrolysis and direct secretion into the circulation without involvement of ATGL, or iii), potentiated lipid-triggered delay in gut transit with insufficient time for the lipids to get reabsorbed basolaterally and accumulate as LDs, which are the supposed substrates for intestinal CGI-58 and ATGL. In sum, these experiments suggest that intestinal CGI-58 and ATGL are rather involved in the hydrolysis of an intestinal lipid pool comprising of peripheral lipids than in the hydrolysis of the transient dietary lipid storage used for CM synthesis. (Korbelius et al., 2019)

Nevertheless, results obtained with Cgi-58 iKO and Cgi-58/Atgl iDKO mice once more highlighted the existence of a yet unknown enzyme responsible for intracellular TG catabolism to provide FFAs as substrates for lipoprotein production in the SI. As mentioned above, one possible candidate might be PTL, however, also LAL could account for the

degradation of dietary-derived cLDs, which are destined for CM synthesis. Impaired VLDL synthesis in livers of LAL KO mice (Radovic et al., 2016) together with rapid capture of newly synthesized LDs by autophagosomal structures within enterocytes (Khaldoun et al., 2014) renders a lipophagic pathway responsible for dietary-derived TGs likely (Korbelius et al., 2019). Staining of intestinal sections from BODIPY®-gavaged WT mice indicated an immediate trapping of dietary lipids by lysosomal structures, as indicated by co-localization of BODIPY®-contraining cLDs with CathD 30 min post gavage. In addition, *Lal* gene expression was induced by a dietary trigger in WT mice, indicating an essential role of LAL in the catabolism of dietary cLDs within the enterocyte. However, deficiency of intestinal CGI-58/ATGL did not affect this pathway.

2.3.3 Origin of accumulating cLDs

Comparable lipoprotein secretion together with results obtained from the sequential meal study raised the question whether CGI-58 and ATGL are involved in the breakdown of another lipid pool, which is not destined for CM synthesis. As the SI is also capable to take up FFAs or small lipoprotein particles from the circulation (Soued and Mansbach, 1996), the idea of a second transient lipid storage pool beside dietary-derived cLDs gained attention.

2.3.3.1 Dietary sources (apical)

Primarily, we aimed to completely understand the role of CGI-58/ATGL in dietary lipid absorption. Therefore, we sacrificed mice either in the early (30 min post gavage), late (2 h post gavage), or later (5 h post gavage) absorption phase. Results from these experiments should shed some light on the fate of dietary lipids as well as the role of intestinal CGI-58/ATGL deficiency in cLD formation and catabolism within enterocytes.

Surprisingly, experiments with radioactive or fluorescent tracers revealed no accumulation or cLD formation in Cgi-58/Atgl iDKO enterocytes 30 min post gavage, indicating that lipid absorption from the apical side *per se* is not affected by the loss of intestinal CGI-58/ATGL. In line, we observed comparable daily fecal excretion and fecal lipid content, arguing against disturbances in dietary lipid uptake. However, similar to results obtained by the sequential meal study, we observed increased gastric retention and decreased circulating plasma lipid concentrations. Circulating as well as hepatic lipid levels were affected in these mice, leading to decreased VLDL-TG concentrations and ameliorated hepatic steatosis. (Korbelius et al., 2019) Increased expression levels of intestinal *I-Fabp* and *Mttp* together with elevated mRNA expression of hepatic lipoprotein receptors indicated an accelerated intracellular lipid trafficking in the SI, subsequent increased secretion of CMs, and higher uptake of CM

remnants by the liver. Further upregulation of hepatic *Mttp* might result in less hepatic steatosis in Cgi-58/Atgl iDKO mice, however, the decrease in VLDL-TG might origin from subsequent increased basolateral uptake of lipids by an upregulation of *Ldl-R* expression, which accounts for 80% of basolateral uptake into enterocytes (Soued and Mansbach, 1996). We used tyloxapol to study CM secretion over a period of 4 h to prevent the basolateral uptake of lipids back into the enterocyte. This explains comparable TG secretion 1 h post gavage when using tyloxapol, but decreased circulating TG levels in iDKO mice when sacrificed 30 min post gavage. As CM clearance occurs quite fast in mice, with almost complete degradation after 15 min (Quiroga et al., 2012), it became more likely that the SI takes up CM remnants from the basolateral side already 30 min post gavage. However, the increase in *Ldl-R* expression indicates rather uptake of CM remnants than native CMs, as lipoprotein binding occurs via ApoE in this case (Soued and Mansbach, 1996), further excluding the possibility of CM reabsorption directly from the lymphatic system. Upregulation of intestinal *Ldl-R* 30 min post gavage might therefore add to lipid accumulation within enterocytes at later time points.

Indeed, already 2 h post gavage we observed massive cLD accumulation in Cgi-58/Atgl-deficient enterocytes, predominantly colocalizing with PLIN3. About 20% of BODIPY®-containing cLDs did not colocalize with PLIN3, suggesting i) slower PLIN3 production than BODIPY® incorporation into cLDs or ii) colocalization with PLIN2, as basolaterally-derived cLDs might possess a different proteome. However, PLIN2 is usually upregulated upon chronic HFD feeding (Lee et al., 2009), arguing against the presence of PLIN2 in our chow diet-fed mice. (Korbelius et al., 2019) When mice were sacrificed 5 h post gavage of a radioactive tracer, we saw a massive deposition of lipids in the very proximal parts of the SI. In line, cLDs originating from the diet rather accumulate within jejunal enterocytes [reviewed in (D'Aquila et al., 2016)], highlighting the specific role of duodenal cells for basolateral reabsorption. Massive increase of cLDs in the SI of Atgl iKO (Obrowsky et al., 2013), Cgi-58 iKO, and Cgi-58/Atgl iDKO mice indicated an essential role of both proteins in the degradation of a reabsorbed basolateral lipid pool.

2.3.3.2 Endogenous sources (basolateral)

Hence, we hypothesized that alimentary lipids, which are taken up apically, undergo a re-esterification in the ER and are either directly secreted into the circulation, bypassing the transient storage pool, or are stored within cLDs, hydrolyzed, and packed into CM without involvement of intestinal CGI-58 and ATGL. The observed lipid pools then would rather derive from lipids reabsorbed from the blood (basolateral uptake) and get stuck in the enterocyte because of CGI-58/ATGL deficiency. (Korbelius et al., 2019)

We could show that also basolaterally supplied lipids accumulated in the SI of Cgi-58/Atgl iDKO mice 6 h post injection, emphasizing the possibility that the accumulation of orally administered lipids in the SI might be due to lipids secreted and reabsorbed from the circulation within this time period. Soued et al. have shown that the intestine is capable to take up lipids basolaterally, as FAs of TGs stored in rat intestinal mucosa consist of only 71% exogenous oleate (Soued and Mansbach, 1996). This receptor-mediated uptake was highest in the villus tips of the proximal SI, fitting to the observed increase in radiolabeled lipids in the duodenum of iDKO mice. Beside receptor-dependent absorption of lipoprotein particles, CM remnants are internalized by endocytosis. In 1992, Mansbach and Dowell already proposed the existence of a basolateral-derived lipid pool within the enterocyte (Mansbach and Dowell, 1992), later showing that the SI competes with the liver for the uptake of CM remnant TG (Mansbach and Dowell, 1995). As stated previously, we demonstrated that lack of intestinal CGI-58 and ATGL did not lead to lipid accumulation in the early phase of absorption, supporting the theory that lipids accumulating 2 h post gavage origin from the periphery. (Korbelius et al., 2019)

To further investigate the origin of basolaterally-derived lipids, which likely serve as substrates for CGI-58/ATGL-mediated lipolysis, and to elucidate the contribution of hepatocytes in sustaining intestinal lipid homeostasis, we injected mice i.v. either with radioactively labelled lipoproteins or FA. When mice were sacrificed 1 h post injection of a radioactive tracer, ^{3}H-OA but not ^{3}H-VLDL accumulated in the liver of Cgi-58/Atgl iDKO mice without affecting intestinal or circulating lipid concentrations, indicating an essential role of hepatocytes in sustaining whole-body lipid hoemostasis. Substrates administered at the retroorbital plexus are either directly delivered to the liver via the hepatic artery or bypass the SI via mesenteric arteries and reach the liver via the portal vein (Encapsula-NanoSciences-LLC, 2012). Assuming that the substrate primarily targets the liver via the hepatic artery, hepatocytes take up circulating FAs rather than VLDL particles [reviewed in (Choi and Ginsberg, 2011)]. However, WT mice displayed comparable uptake rates of both

substrates (6.6% of OA vs. 5.7% of VLDL). Supposing that i.v.-administered substrates initially get processed by the SI before being shuttled to the liver, it is likely that 1 h was not sufficient time for intracellular processing of lipoprotein particles (^{3}H-VLDL) within the enterocyte. This highlights a role of intestinal CGI-58 and ATGL on processing of basolaterally-applied FAs, thereby affecting hepatic lipid homeostasis by a yet unknown mechanism. However, these results highlighted the close interplay between enterocytes and hepatocytes in systemic lipid turnover. (Korbelius et al., 2019)

Therefore, we next sacrificed mice 24 h post i.v. administration of ^{3}H-OA and ^{3}H-VLDL. Before sacrifice, mice were fasted for 12 h to trigger VLDL release from the liver. Both tracers accumulated in the proximal parts of CGI-58/ATGL-deficient intestines, primarily indicating a hepatic contribution in delivering substrates for intestinal CGI-58/ATGL. Interestingly, application of ^{3}H-VLDL, but not ^{3}H-OA, led to significantly decreased radioactivities in livers of Cgi-58/Atgl iDKO mice, suggesting a competition of lipoprotein uptake between the SI and the liver, as suggested previously (Mansbach and Dowell, 1995). However, it remains enigmatic in which form the tracer is delivered to the tissues 24 h post i.v. administration of ^{3}H-VLDL. We could show that ^{3}H-OA does not get processed and incorporated into lipoproteins 24 h post-injection after a 12 h fasting period, but rather circulates in form of FFAs in the plasma. However, it is worth mentioning that active lipoprotein lipase (LPL) in the plasma might have already degraded plasma TGs until the time of analysis, thereby falsifying the distribution of the radioactive tracer. Clearance of 95% of the injected tracer within 1 h and shuttling of < 10% to the liver and intestine suggest a dynamic distribution among organs besides the enterohepatic system. Although our study highlights the close connection between gut and liver lipid metabolism, further studies are required to completely understand the interplay between small intestine, lipoprotein metabolism, and hepatocytes. Detailed flux analyses tracing lipids and their distribution among metabolically active organs are needed to elucidate their role in whole body lipid homeostasis. (Korbelius et al., 2019)

Again, all results pointed toward the involvement of intestinal CGI-58/ATGL in the catabolism of basolaterally absorbed lipids. Additionally, Cgi-58/Atgl iDKO mice restricted to endogenously produced lipids by prolonged fasting or feeding a FFD displayed sustained cLD accumulation, rendering a role of intestinal CGI-58/ATGL in the hydrolysis of a dietary lipid pool unlikely. (Korbelius et al., 2019)

2.3.4 Fate of FFA generated by intestinal CGI-58/ATGL-mediated lipolysis

As we could identify CGI-58 and ATGL as essential players in the degradation of a basolateral lipid pool and basolaterally-derived lipids were shown to be used rather for PL synthesis and energy purposes than for CM assembly (Storch et al., 2008, Ho et al., 2002, Gangl and Ockner, 1975), we next investigated the fate of CGI-58/ATGL-released FFAs within the enterocyte. (Korbelius et al., 2019)

In line with previous studies on hepatic CGI-58 (Brown et al., 2010) as well as hepatic (Ong et al., 2011) and intestinal (Obrowsky et al., 2013) ATGL, we could show that also simultaneous lack of intestinal CGI-58/ATGL leads to impaired FAO. It is likely that TG-rich lipoproteins are cleaved by endothelial LPL to release FAs, which are then taken up by enterocytes, re-esterified into TGs, hydrolyzed by ATGL/CGI-58, and utilized for FA oxidation (Korbelius et al., 2019). The importance of LPL cleavage was highlighted in previous publications showing that only CM remnants but not CMs can be absorbed basolaterally (Soued and Mansbach, 1996). It is therefore difficult to distinguish the origin of FFA used for FAO in isolated enterocytes, however, exposure of isolated cells with VLDL particles would not reflect physiological conditions. In addition, impaired release of CO_2 despite unchanged mRNA levels of PPARα and genes involved in FAO point toward non-transcriptional effects of the respective proteins, as observed in LFABP KO mice (Lagakos et al., 2013). However, glutamine and ketone bodies represent the major carbon source for the SI (accounting for 35% and 50% of CO_2 produced by the SI, respectively and only 3% of CO_2 production results from FAO (Windmueller and Spaeth, 1978). Degradation of a basolaterally-derived lipid pool within enterocytes might provide energy for dietary lipid absorption from the apical side, highlighting the importance of both distinct intracellular lipid pools in sustaining intestinal lipid homeostasis.

FFAs released by intestinal CGI-58/ATGL-mediated hydrolysis might also be destined for PL synthesis. However, basolaterally or apically applied lipid tracers did not get incorporated into PL in a different manner between the genotypes. This might be due to the stereoselectivity of ATGL. *Sn*1,3-DG and *sn*2,3-DG, the lipolytic products generated by ATGL alone or upon stimulation by CGI-58, respectively, rather get hydrolyzed by HSL (*sn*1,3-DG) or re-esterified into TGs by DGAT enzymes (*sn*2,3-DG), but cannot directly enter the PL synthesis pathway (Eichmann et al., 2012). Thus, upon re-esterification, storage in a basolaterally-derived lipid pool, and ATGL hydrolysis, FFAs are rather used for β-oxidation. (Korbelius et al., 2019)

Ultimately, as lack of solely intestinal ATGL was associated with impaired PPARα signaling in the SI (Obrowsky et al., 2013), we next investigated the consequences of intestinal CGI-58/ATGL deficiency on this pathway. We found that simultaneous lack of CGI-58 and ATGL causes alterations in PPARα target gene expression only in the refed state. This finding indicated that under postprandial conditions, CGI-58 and ATGL play a role in phase II biotransformation, as shown by upregulation of various glutathione-S-transferases (GST) in Cgi-58/Atgl iDKO mice. In enterocytes, numerous metabolic reactions occur, yielding hydrophilic molecules by conjugation e.g. with glutathione via GSTs (de Vogel-van den Bosch et al., 2008). This conjugation is important to increase the water solubility of lipophilic metabolites to facilitate their excretion. TG-rich lipoprotein lipolysis mediated by LPL caused production of preformed mediators of oxidative stress (Wang et al., 2009). Our data therefore suggest that the same might be true for intracellular neutral lipolysis mediated by CGI-58 and ATGL.

In summary, our study demonstrates that intestinal ATGL and CGI-58 are not involved in the catabolism of alimentary lipids absorbed at the apical side. In contrast, these two proteins contribute to the hydrolysis of re-absorbed TGs originating from basolateral absorption in enterocytes, which are not destined for CM synthesis. This hypothesis was confirmed by i) accumulation of dietary lipids 2 h, but not 30 min post oral lipid load, ii) increased deposition of basolaterally-applied tracers, iii) persistent cLD accumulation after prolonged fasting, and iv) massively elevated lipid concentrations despite restriction of dietary fat. Future studies elucidating this process, the close interplay between the SI and hepatocytes, and identifying the yet unknown enzyme responsible for degradation of the apically-derived lipid pool are needed to fully understand intestinal lipid metabolism. (Korbelius et al., 2019)

Figure 44 represents a revised model of intestinal lipid metabolism. (Korbelius et al., 2019)

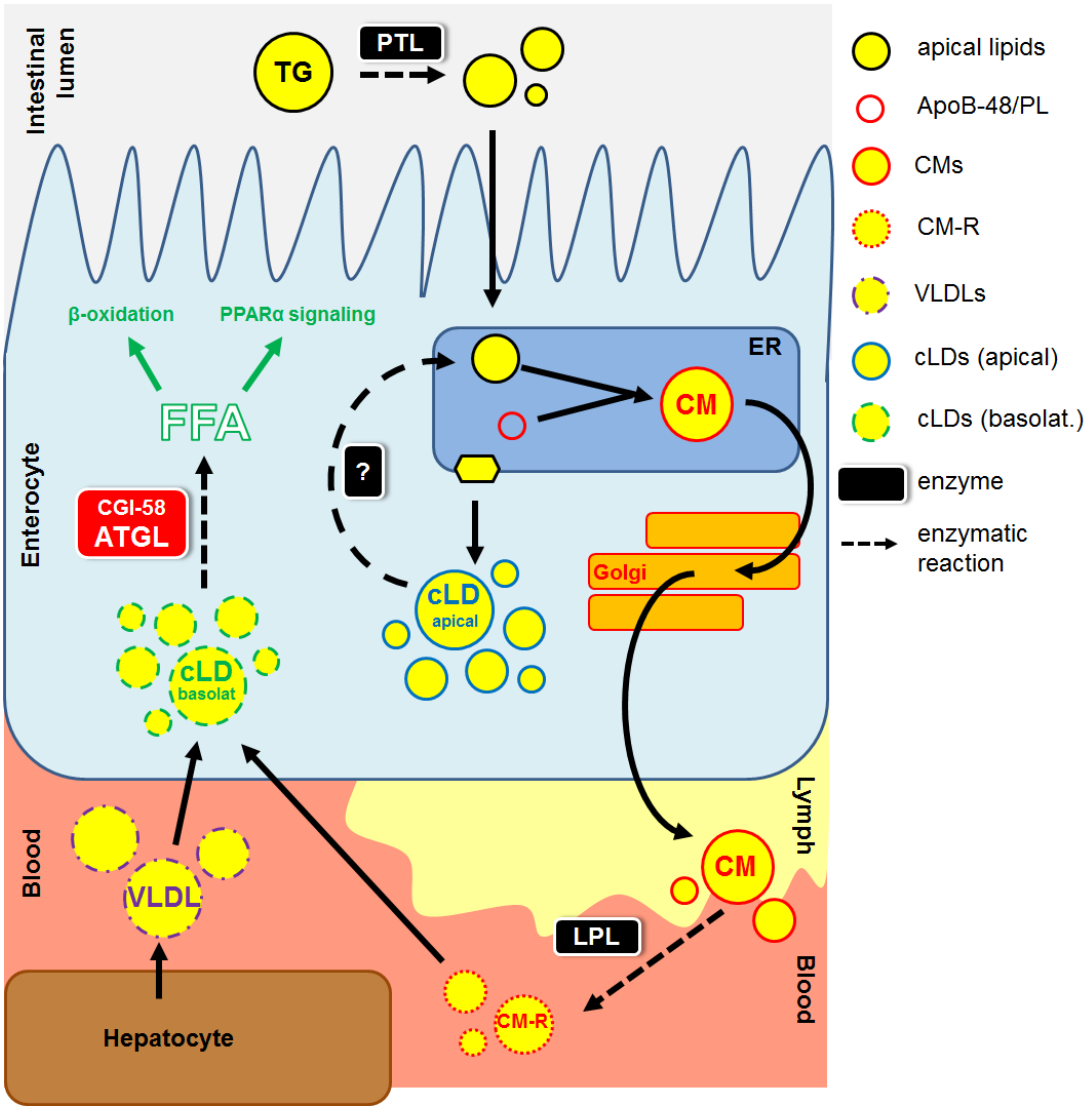

Figure 44: Proposed model for the role of CGI-58 and ATGL in intestinal lipid metabolism. CGI-58/ATGL are not involved in providing substrates for chylomicron (CM) synthesis. The responsible enzyme is still elusive. Cytosolic lipid droplets (cLD) containing lipids reabsorbed from the circulation accumulate in enterocytes lacking CGI-58/ATGL independent of dietary lipids and without affecting circulating lipid concentrations. (Korbelius et al., 2019)

3 Characterization of intestine-specific ATGL transgenic mice

3.1 Materials and Methods

3.1.1 Cloning, transformation, and plasmid DNA isolation

Intestinal-specific overexpression of murine ATGL is driven by the 12.4 kb Villin promoter (http://www.addgene.org/19358). The corresponding plasmid has already been used in previous studies (Madison et al., 2002). The murine Atgl CDS was amplified and restriction enzyme cleavage sites for XhoI (CTCGAG) and AgeI (ACCGGT), start (ATG) and stop (TCA) codons as well as the Flag-Tag (CTTGTCATCGTCT) were added via PCR using the following primers: forward, 5'-GGTAACTCGAGACC-ATGTTCCCGAGGGAGA-3'; reverse, 5'-TGGTACCGGT-TCACTTGTCATCGTCT-3' (restriction enzyme cleavage sites are underlined). The ATGL amplicon and the Villin plasmid were digested with XhoI and AgeI. After dephosphorylation of the vector to avoid re-ligation, gel electrophoresis was performed (1.5% agarose gel, 90 V, 30 min) (**Figure 45**).

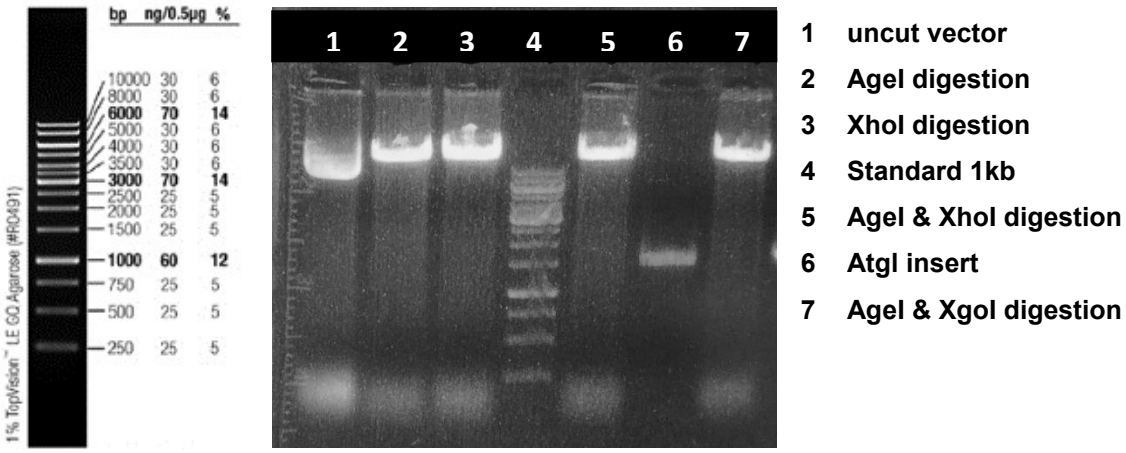

Figure 45: Gel electrophoresis of vector and insert.

Bands from slots 5, 6, 7, and 8 were cut out and DNA was eluted according to manufacturers manual (MicroElute® Gel Extraction Kit, Omega Bio-Tek; Norcross, GA). To estimate the amount of DNA, we ran a concentration gel, resulting in 2-fold higher intensity of the vector. Considering that the Atgl insert is approximately ten times smaller than the vector (1,540 bp vs. 16,686 bp), the amount of eluted Atgl DNA was 5-fold higher. Next, ATGL was ligated downstream of the 12.4 kb villin promotor using T4 ligase and a ligation mix containg insert

and vector in a 3:1 ratio. After incubation for 2 h at 25°C, the enzyme was heat inactivated for 10 min at 70°C. After transformation of the ligated products into *E.Coli* C2987 cells, plasmid DNA was isolated (QIAprep® Miniprep, Quiagen; Hilden, Germany). Control digestion with AgeI and XhoI revealed efficient incorporation of the insert into the plasmid (**Figure 46**).

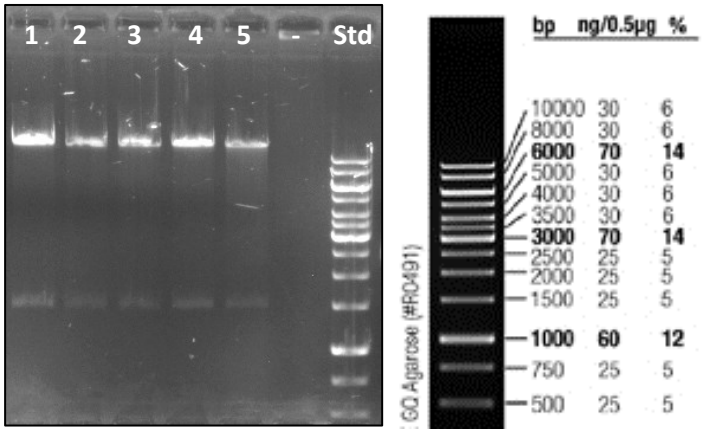

Figure 46: Control digestion with AgeI and XhoI. Isolated DNA from *E.coli* was digested with AgeI and XhoI and loaded on an agarose gel. The upper band represents the vector, while the lower band reflects the ATGL insert.

Sample 4, yielding a DNA concentration of 130.6 ng/µl was used for further analysis. As sequencing of sample 4 did not work out, we performed a MaxiPrep (Marchery Nagel; Düren, Germany) of one positive clone from the MiniPrep. After successful equencing, the isolated plasmid from the MaxiPrep was digested with PmeI to eliminate the vector backbone and to linearize the construct (**Figure 47**).

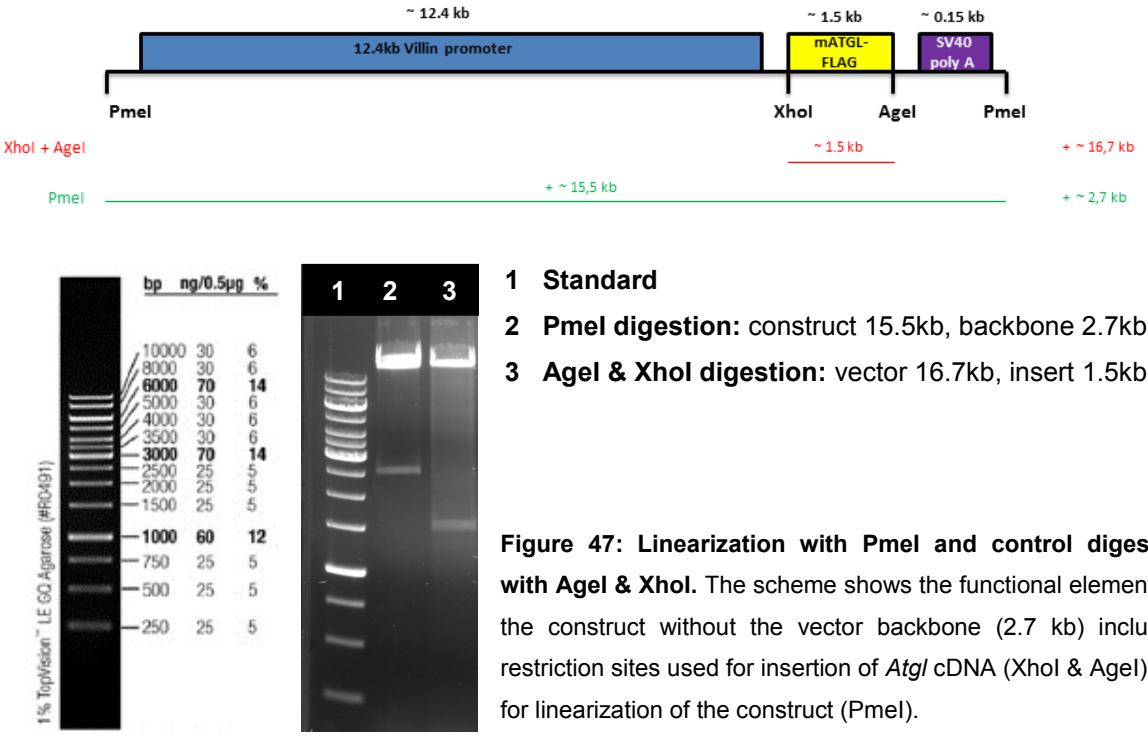

1 **Standard**

2 **PmeI digestion:** construct 15.5kb, backbone 2.7kb

3 **AgeI & XhoI digestion:** vector 16.7kb, insert 1.5kb

Figure 47: Linearization with PmeI and control digestion with AgeI & XhoI. The scheme shows the functional elements of the construct without the vector backbone (2.7 kb) including restriction sites used for insertion of *Atgl* cDNA (XhoI & AgeI) and for linearization of the construct (PmeI).

To avoid spontaneous mutations due to UV stress, no picture from the purified, linearized construct was taken. The final transgene (c = 38.4 ng/µl) was injected into mouse pronuclei and then transplanted into surrogate females to produce potential transgenic founders. Microinjection into C57BL/6J mice was performed in cooperation with Thomas Ruelicke (Institute of Laboratory Animal Science, University of Veterinary Medicine, Vienna, Austria).

3.1.2 Animals

Age- and sex-matched Atgl iTg and WT littermates were maintained in a temperature-controlled environment with unlimited access to food and water in a regular light-dark cycle (12 h/12 h). All experiments were performed using female mice from high-expressing breedings, unless stated otherwise. Mice were fed a standard chow diet (11.9% caloric intake from fat; Altromin, Lage, Germany) or challenged with HF/HCD (34% crude fat, 1% cholesterol; Ssniff®, Soest, Germany).

All experiments were performed in accordance with the European Directive 2010/63/EU, approved by the Division of Genetic Engineering and Animal Experiments, Austrian Federal Ministry of Education, Science and Research (Vienna, Austria; BMWFW-66.010/0154-WF/V/3b/2015).

3.1.3 Lipid analyses

Plasma lipid analysis (2.1.2 *Plasma lipid analysis*, tissue lipid analysis (2.1.5 *Tissue lipid analysis*), and histology and ORO staining (2.1.6 *Histology and ORO staining*) were performed as described earlier.

3.1.4 Lipoprotein secretion

CM and VLDL secretion were determined in chow-diet fed mice fasted for 16 h and injected with tyloxapol (500 mg/kg body weight; Merck KGaA; Darmstadt, Germany) to inhibit peripheral lipolysis. For CM secretion, mice were gavaged with 200 µl olive oil 30 min later. Blood was taken prior to the injection, as well as 1, 2, and 4 h post gavage. For VLDL secretion, plasma was collected 2, 4, and 6 h post injection. Plasma TG and cholesterol concentrations were measured as described in 2.1.2 *Plasma lipid analysis*.

3.1.5 Western Blotting

Sample preparation was done as described in 2.1.8 *Western Blotting*. To prove the efficient intestine-specific overexpression, 80 µg of protein were separated by SDS-PAGE and transferred onto a nitrocellulose membrane, followed by incubation with an anti-FLAG

antibody (Sigma, Vienna, Austria; 1:2000). Monoclonal anti-mouse β-actin (Santa Cruz Biotechnology, Heidelberg, Germany) was used as loading control. Secondary anti-mouse (1:500) antibody, conjugated with HRP (Dako, Glostrup, Denmark) was visualized using the Clarity™ Western ECL Substrate Kit (Bio Rad Laboratories; Hercules, CA) on a ChemiDoc™ MP imaging system (Bio Rad Laboratories; Hercules, CA).

3.1.6 RNA isolation and quantitative real-time PCR

RNA extraction, cDNA synthesis, and quanitative real-time PCR were performed as described in 2.1.9 *RNA isolation and quantitative real-time PCR*.

3.1.7 Triglyceride hydrolase activity

TG hydrolase activity in jejunal samples was assayed as described in

2.1.10 Triglyceride hydrolase activity.

3.1.8 Apical lipid absorption

Mice fed HF/HCD for 5 weeks were fasted for 4 h, injected with 500 mg/kg body weight tyloxapol (Merck KGaA; Darmstadt, Germany) and gavaged with 200 µl oil containing 2 µCi [9,10-^{3}H(N)]-triolein (Perkin Elmer, Waltham, MA) and 0.5 µCi [1-^{14}C]-cholesterol (Perkin Elmer, Waltham, MA).

Blood was collected 150 and 300 min post gavage and mice were sacrificed 5 h after administration of the oil bolus. Duodenum, jejunum, ileum, stomach, and liver were collected and radioactivities were measured in lyophilized tissues by liquid scintillation counting.
To study the early absorption phase, overnight fasted mice were gavaged with 200 µl corn oil containing 2 µCi [9,10-^{3}H(N)]-triolein (Perkin Elmer, Waltham, MA) and sacrificed 30 min post gavage. Samples were processed as described in 2.1.12 *Apical lipid absorption*.

3.1.9 Statistical analyses

Statistical analyses were performed using GraphPad Prism 5.0 software. Significance was calculated by unpaired Student's *t*-test or ANOVA followed by Bonferroni post-tests. Data are shown as mean ± SD. For statistical analysis of mRNA expression, values were calculated using the $2^{-\Delta\Delta CT}$ method and represented as mean + SD. The following levels of statistical significance were used: *, $p < 0.05$; **, $p \leq 0.01$; ***, $p \leq 0.001$. All diagrams are sorted by a uniform color code: black bars represent WT mice, white bars high-expressing Atgl iTg mice, and grey bars low-expressing Atgl iTg mice.

3.2 Results

3.2.1 Efficient overexpression of ATGL in the SI

To confirm the intestine-specific overexpression ATGL in the SI, mRNA expression in the SI of different breedings was analyzed. Breeding 02, showing an 81-fold increase in duodenal *Atgl* mRNA expression was kept as the high-expressing breeding, while breeding 04 with only a 27-fold increase of *Atgl* in the duodenum was used to maintain a low-expressing transgenic line (**Figure 48**).

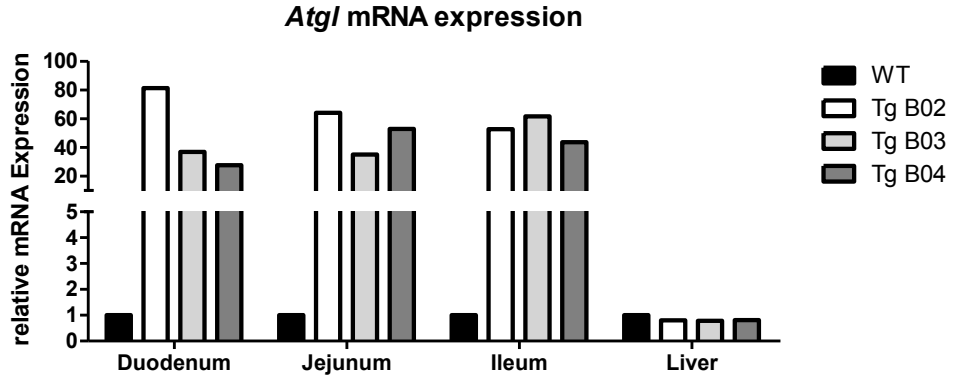

Figure 48: Expression of *Atgl* in offsprings of different breedings. Gene expression levels of *Atgl* normalized to *cyclophilin A* as internal control was analyzed in the SI and liver of 4 h-fasted WT and Atgl iTg mice. Transgenic breedings B02 and B04 were kept to establish one high-expressing and one low-expressing mouse strain, respectively.

Western blot analysis of jejunal and hepatic tissue lysates revealed expression of the ATGL FLAG-Tag solely in the jejunum of transgenic mice (**Figure 49A**). The FLAG-Tag on the ATGL construct (1.5 kb) resulted in the expression of a 55.5 kDa protein. Jejunal *Atgl* mRNA levels were 39-fold increased in low-expressing Atgl iTg mice (**Figure 49B**). Neutral TG hydrolase activity was slightly increased in the jejunum of high-expressing Atgl iTg mice (**Figure 49C**), indicating that enzymatic activity of ATGL is not upregulated in the same manner as *Atgl* mRNA expression.

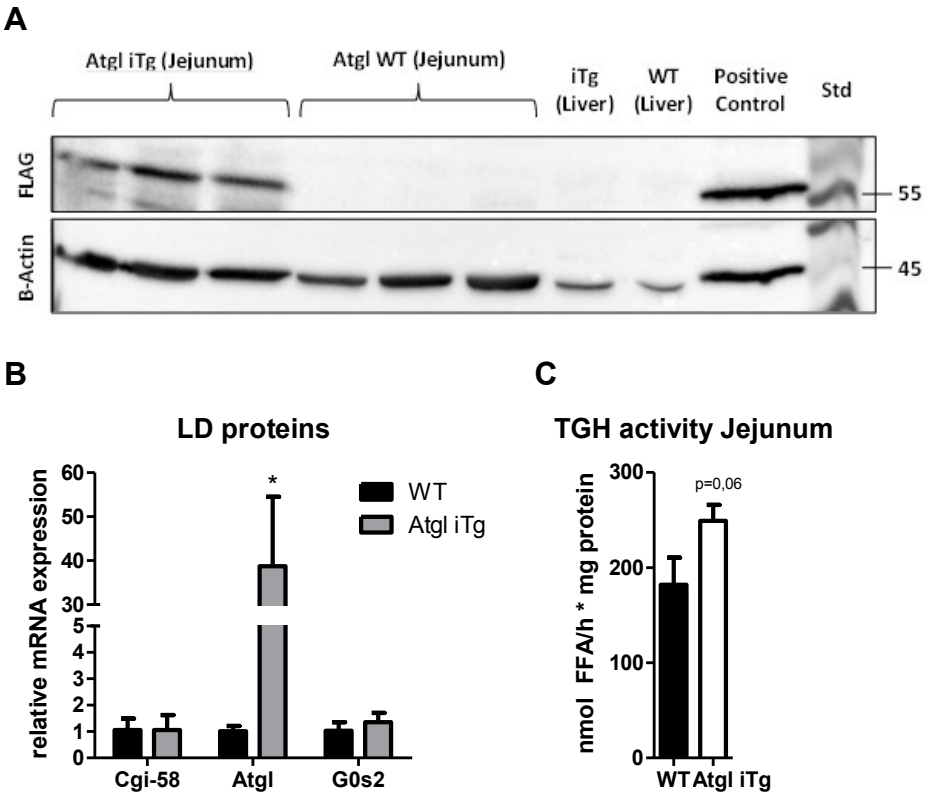

Figure 49: Flag-Tag Western blot analysis and mRNA expression profile of Atgl in WT and Atgl iTg mice. (A) Mucosal scrapings of the jejunum and liver lysates were incubated with the anti-FLAG antibody. A FLAG-tagged Ces2c construct, provided by Guenter Haemmerle, served as a positive control. Monoclonal anti-mouse β-actin was used as loading control. (B) mRNA expression of *Atgl* in the jejunum of low-expressing transgenic mice. Expression levels were normalized to *cyclophilin A* as houskeeping gene. (C) TGH activity in chow-fed Atgl iTg mice (high-expressing) and their corresponding littermates. All mice were fasted 4 h prior to organ collection. Data represent mean values (n=3-6) + SD. *p < 0.05.

3.2.2 Unchanged body weights and plasma lipid content in Atgl iTg mice

To investigate the effect of intestinal ATGL overexpression on whole body lipid homestasis, we recorded systemic lipid levels as well as body weights in mice fed chow and HF/HCD. Body weight remained comparable between chow diet-fed WT and Atgl iTg mice from both high- and low-expressing strains, as well as after HF/HCD feeding for five weeks (**Table 9**). After 4 h of fasting, no differences were observed in circulating lipid concentrations on chow or HF/HCD (**Table 9**).

Table 9: Body weights and plasma lipid parameters of WT and Atgl iTg mice under various nutritional conditions.

	Chow (16 h fasted)		Chow (4 h fasted)	
	WT	**iTg**	**WT**	**iTg**
BW (g)	15.2±1.31	15.5±1.43	17.9±0.52	19.2±1.65
TG (mg/dl)	53.1±8.08	59.0±10.3	65.9±6.28	63.3±14.0
TC (mg/dl)	58.7±4.72	56.6±11.5	66.7±5.64	63.3±4.82
FC (mg/dl)	16.8±2.97	19.0±4.65	9.77±2.15	10.4±1.87
CE (mg/dl)	41.9±2.91	40.3±9.30	56.9±5.13	53.0±4.69
FFA (mmol/l)	1.70±0.37	1.66±0.30	0.48±0.18	0.47±0.10
n	6	7	6	6
	Chow 16 h fasted (30 min post gavage)		**5 W HF/HCD (4 h fasted)**	
	WT	**iTg**	**WT**	**iTg**
BW (g)	n.d.	n.d.	20.1±1.63	21.2±1.82
TG (mg/dl)	31.1±3.27	40.4±5.08**	41.1±5.73	40.7±5.89
TC (mg/dl)	50.7±3.14	59.0±4.64**	81.8±15.1	93.2±17.9
FC (mg/dl)	22.1±2.65	24.8±2.93	17.6±2.47	15.8±2.23
CE (mg/dl)	28.6±2.03	34.2±4.51*	64.2±14.8	77.4±16.3
FFA (mmol/l)	1.03±0.10	1.12±0.15	0.28±0.08	0.29±0.08
n	6	6	10	10

Body weights and plasma parameters of sex- and age-matched WT and Atgl iTg mice. Data represent mean ± SD. BW, body weight; TG, triglyceride; TC, total cholesterol; FC, free cholesterol; CE, cholesteryl ester; FFA, free fatty acid; n.d., not determined. *$p < 0.05$; **$p \leq 0.01$.

Although circulating lipid levels remained comparable between WT and Atgl iTg mice, we next investigated the role of intestinal ATGL in providing FFA for lipoprotein secretion. CM secretion was found to be identical in mice lacking intestinal ATGL and CGI-58 (**Figure 16**), however, overexpression of ATGL resulted in a slight decrease in CM-TG (10%) (**Figure 50A**) and -TC levels (23%) (**Figure 50B**) on chow diet. In line, secretion of TGs within VLDL particles was drastically reduced by 29% in Atgl iTg mice 6 h post injection of tyloxapol (**Figure 50C**), accompanied by a slight decrease (14%) in VLDL-TC levels (**Figure 50D**).

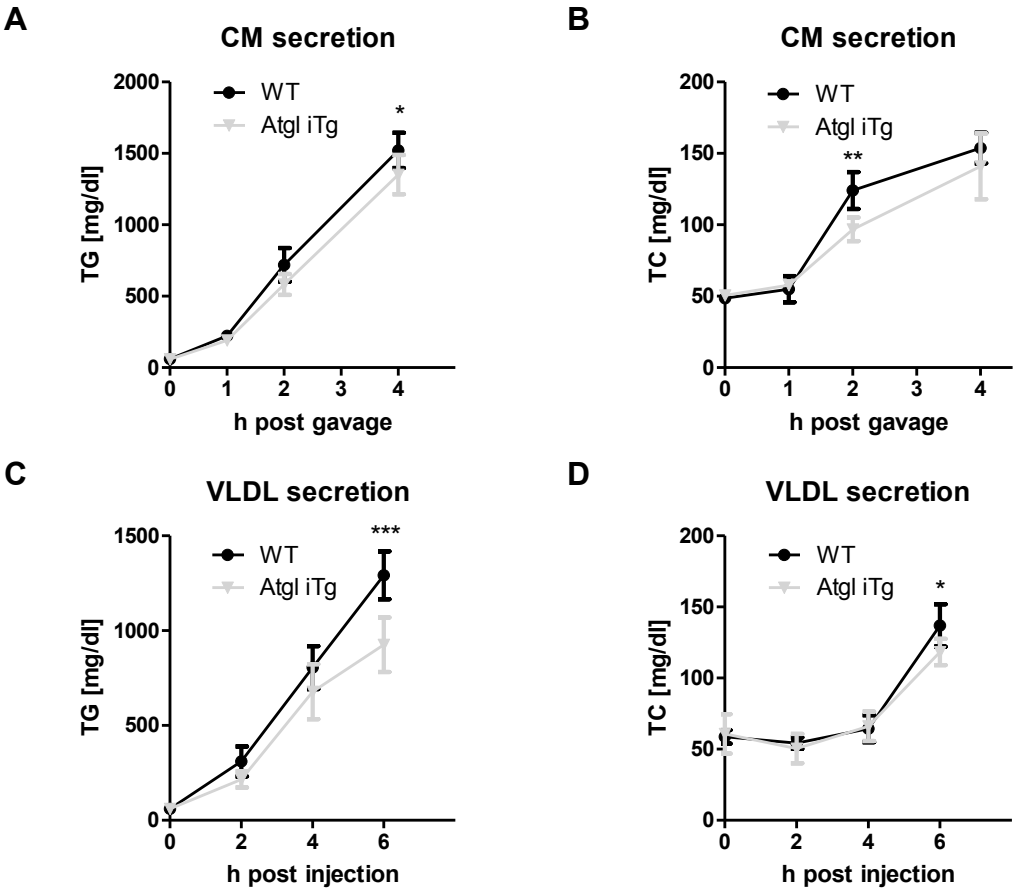

Figure 50: CM and VLDL secretion in chow diet-fed WT and Atgl iTg mice. High-expressing Atgl iTg and control mice were fasted 16 h prior to i.p. administration of tyloxapol. (A) Secretion of CM-TG and (B) CM-TC 1, 2, and 4 h after an oral lipid load. (C) VLDL-TG and (D) VLDL-TC concentrations 2, 4, and 6 h after the administration of tyloxapol. Data represent mean values (n=5-6) ± SD. *p < 0.05; **p ≤ 0.01; ***p ≤ 0.001.

3.2.3 Atgl iTg display accelerated dietary cholesterol absorption

Although comparable CM secretion suggested a negligible role of intestinal ATGL on dietary lipoprotein metabolism, we investigated if ATGL directly impacts TG and cholesterol absorption from the diet *per se*. Therefore, HF/HCD-fed mice were gavaged with ^{3}H-triolein and ^{14}C-cholesterol and sacrificed 5 h post gavage. We observed unchanged secretion of ^{3}H-triolein into the circulation (**Figure 51A**), in line with unchanged circulating TG levels in previous cohorts. Radioactive counts were comparable in intestines and livers of WT and Atgl iTg mice (**Figure 51B**). This finding corroborated the results from Atgl iKO (Obrowsky et al., 2013) and Cgi-58/Atgl iDKO mice (Korbelius et al., 2019) that intestinal ATGL does not have a direct impact on the absorption and degradation of luminally absorbed lipids.

As Atgl iKO mice showed impaired cholesterol absorption from the diet (Obrowsky et al., 2013), we investigated the effect of intestinal ATGL overexpression on dietary cholesterol absorption. Oral administration of ^{14}C-cholesterol revealed a 1.6-fold increase in plasma radioactivity in HF/HCD-fed Atgl iTg mice (**Figure 51C**). Furthermore, while Atgl iKO mice also accumulated less radioactivity in the liver (Obrowsky et al., 2013), mice overexpressing ATGL in the SI displayed slightly more hepatic ^{14}C-cholesterol (**Figure 51D**). Although absorption of ^{14}C-cholesterol into the intestine remained comparable between WT and Atgl iTg mice, jejunal organ weight was slightly decreased in ATGL overexpressing mice (**Figure 51F**). Fecal excretion of the radioactive tracer was reduced by 40% in Atgl iTg mice (**Figure 51E**), indicating accelerated cholesterol absorption from the intestinal lumen.

These *in vivo* studies indicated that intestinal ATGL is a main regulator of dietary cholesterol absorption.

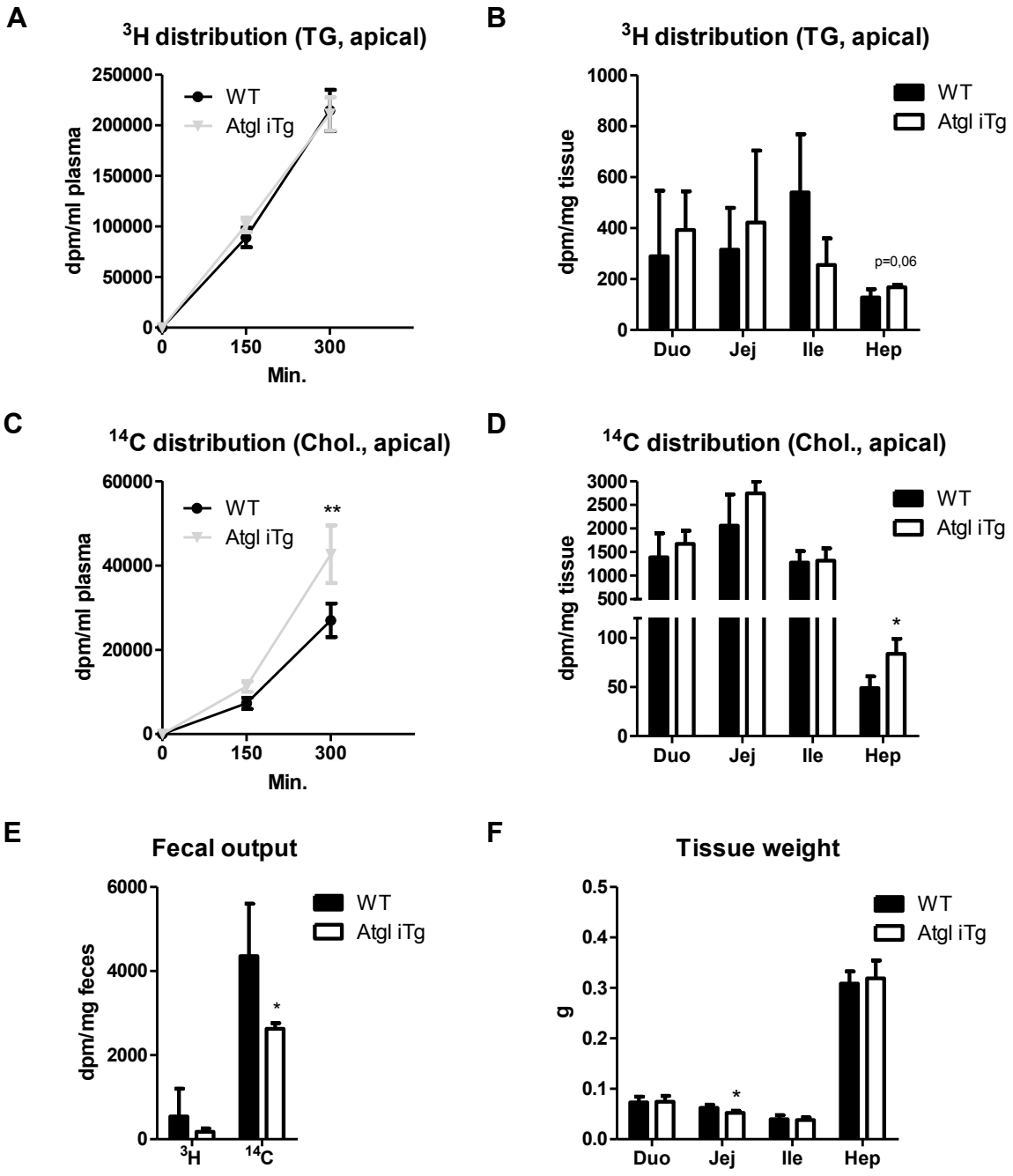

Figure 51: Overexpression of intestinal ATGL affects dietary cholesterol absorption. HF/HCD-fed mice were gavaged with corn oil containing ^{3}H-triolein and ^{14}C-cholesterol. (A) Secretion of ^{3}H-triolein into the circulation. (B) Distribution of ^{3}H into intestinal and hepatic tissues. (C) ^{14}C counts in the circulation 150 and 300 min post gavage. (D) ^{14}C-cholesterol levels in the SI and liver of Atgl iTg and WT mice. (E) Fecal excretion of the radioactive tracers. (F) Lyophilized organ weights used for normalization. Data represent mean values (n=4-5) ± SD. *$p < 0.05$; **$p \leq 0.01$.

3.2.4 ATGL affects intestinal PPARα signaling upon HF/HCD feeding

Previous studies identified ATGL as an important player in the regulation of PPARα target genes. It is known that intestinal PPARα regulates genes involved in lipid absorption, FAO, defense against oxidative stress, and inflammation. Intestinal *Atgl* overexpression (87-fold increase in *Atgl* mRNA) was accompanied by a slight increase of the endogenous coactivator *Cgi-58* and a slight decrease of the endogenous inhibitor *G0s2* (**Figure 52**). *Pparα* mRNA expression was 1.5-fold elevated in Atgl iTg mice upon HF/HCD feeding, consequently leading to an upregulation of several PPARα target genes (*Npc1l1, Abcg5, Abcg8*). Upregulation of *Npc1l1*, the main cholesterol importer, and additional upregulation of the cholesterol exporters *Abcg5* and *Abcg8* might explain the observed increase in plasma ^{14}C-cholesterol (**Figure 51C**).

Even though the cholesterol transporters NPC1L1 and ABCG5/8 were significantly increased in Atgl iTg mice, their expression levels were not affected in mice lacking intestinal ATGL (Obrowsky et al., 2013). However, disturbances in intestinal cholesterol homeostasis in ATGL KO mice were suggested to be caused by decreased *Cd36* expression and downregulation of *Abca1* (Obrowsky et al., 2013). Intestinal CD36 is not only responsible for luminal absorption of FA, but also of free cholesterol. In the gut, both CD36 and ABCA1 are regulated by PPARα. Transgenic mice fed a HF/HC diet also displayed slightly elevated mRNA expression levels of *Cd36* and *Abca1*, indicating that FAs released via the action of intestinal ATGL are primarily used to modulate intestinal cholesterol homeostasis via activation of PPARα. Interestingly, other PPARα-regulated genes involved in oxidative stress defense (gluthation-S-transferases *Gstk1, Gstm3*) or lipoprotein assembly (*Mttp*) remained comparable between the genotypes (**Figure 52**).

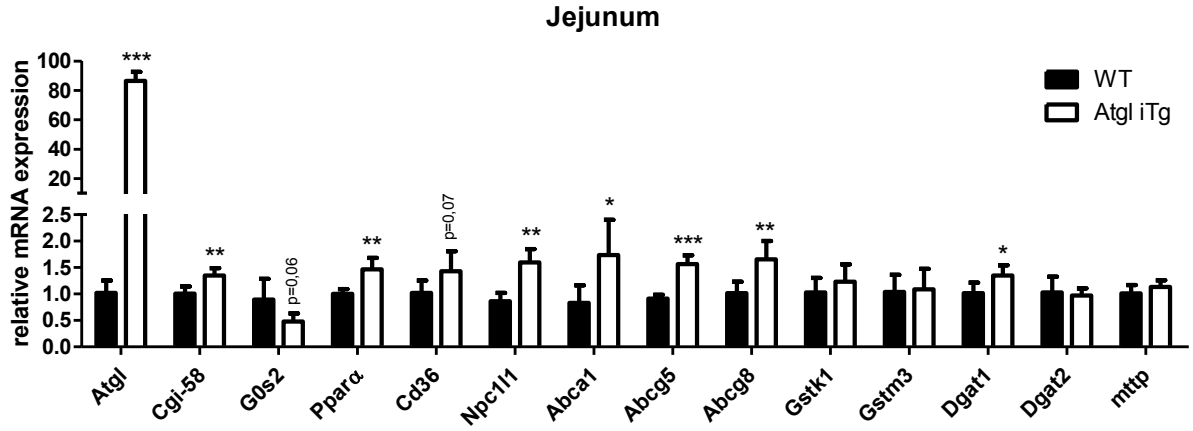

Figure 52: Jejunal mRNA profile in HF/HCD-fed WT and Atgl iTg mice. Expression levels of genes involved in PPARα signaling, cholesterol metabolism, and oxidative stress. Expression levels were normalized to *cyclophilin A* as houskeeping gene. Data represent mean values (n=4-5) + SD. *p < 0.05; **p ≤ 0.01; ***p ≤ 0.001.

Although mRNA expression of genes involved in FAO (*Acox1, Acot2, Pgc1α, Mcad, Cpt1α*) were comparable between both genotypes (**Figure 53A**), FAO in isolated jejunal enterocytes slightly increased in mice overexpressing ATGL (**Figure 53B**).

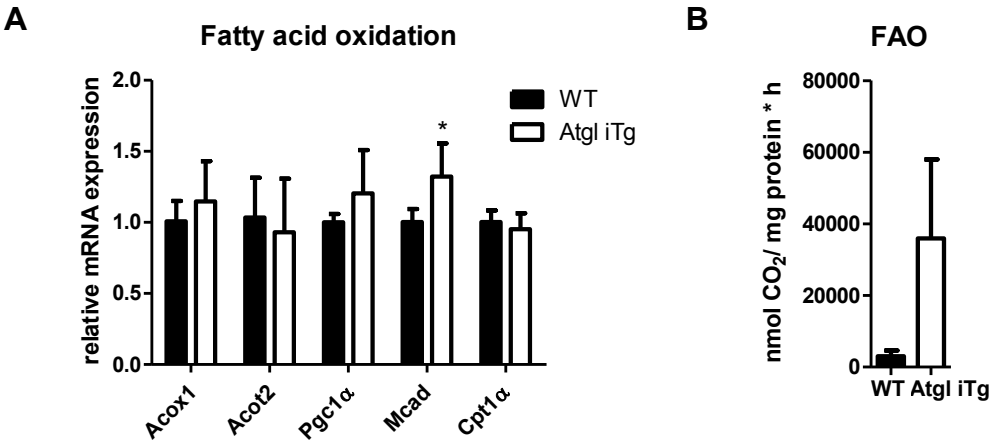

Figure 53: Overexpression of intestinal ATGL leads to increased FAO. (A) Expression levels of genes involved in FAO. Expression levels were normalized to *cyclophilin A* as houskeeping gene. (B) FAO in isolated jejunal enterocytes. Data represent mean values (n=2-5) + SD. *p < 0.05.

Due to the slight effect on intestinal and hepatic lipoprotein secretion, we next wondered if Atgl iTg mice showed differences in intracellular lipid levels. It was previously reported that lack of intestinal ATGL led to massive lipid accumulation in the SI (Obrowsky et al., 2013), therefore intestine-specific overexpression of ATGL was expected to have an ameliorative effect on HF/HCD-induced intestinal steatosis. Organ weights of WT and Atgl iTg (high-expressing) mice remained comparable after 5 weeks of HF/HCD feeding (**Figure 54A**). Biochemical estimation of intestinal and hepatic lipid contents revealed no significant differences between the genotypes, however, in line with trends observed in organ weights, duodenal TG concentrations were reduced by 20% (**Figure 54B**) and hepatic TG content was increased by 22% in Atgl iTg mice (**Figure 54C**). This already suggested an ameliorative effect of intestinal ATGL overexpression on intestinal lipid depostition and highighted once more its role in the degradation of an intestinal lipid storage pool.

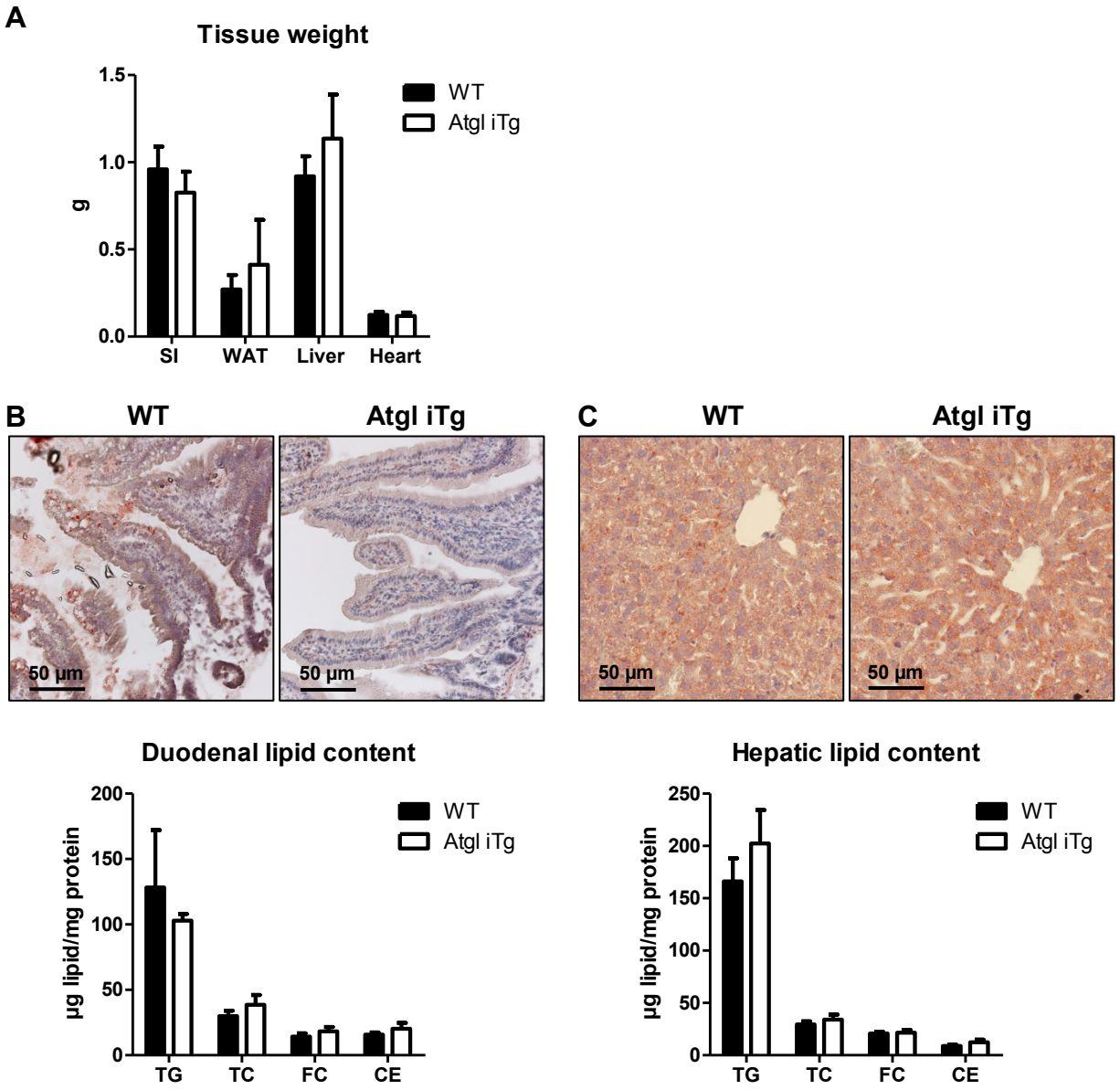

Figure 54: Organ weights, intestinal and hepatic lipid levels in HF/HCD-fed WT and Atgl iTg mice. (A) Organ weights of WT and Atgl iTg mice 5 weeks after HF/HCD feeding. Histological and biochemical analysis of (B) duodena and (C) livers. Mice were fasted 4 h prior to sacrifice. Data represent mean values (n=4-5) + SD. Magnification, 40x; Scale bar, 50 µm.

3.2.5 Overexpression of ATGL affects circulating lipid levels 30 min post gavage

To investigate the role of intestinal ATGL not only after a chronic lipid challenge, but also after an acute lipid load, we sacrificed mice 30 min post gavage of an oil bolus. In contrast to mice chronically challenged with HF/HCD, acute lipid administration did not affect gene expression levels of FA and cholesterol importers (*Cd36*), intracellular FA transporters (*I-Fabp*, *L-Fabp*) or cholesterol exporters (*Abcg5/8*) in the jejunum, indicating that intestinal ATGL does not directly affect dietary lipid absorption (**Figure 55**).

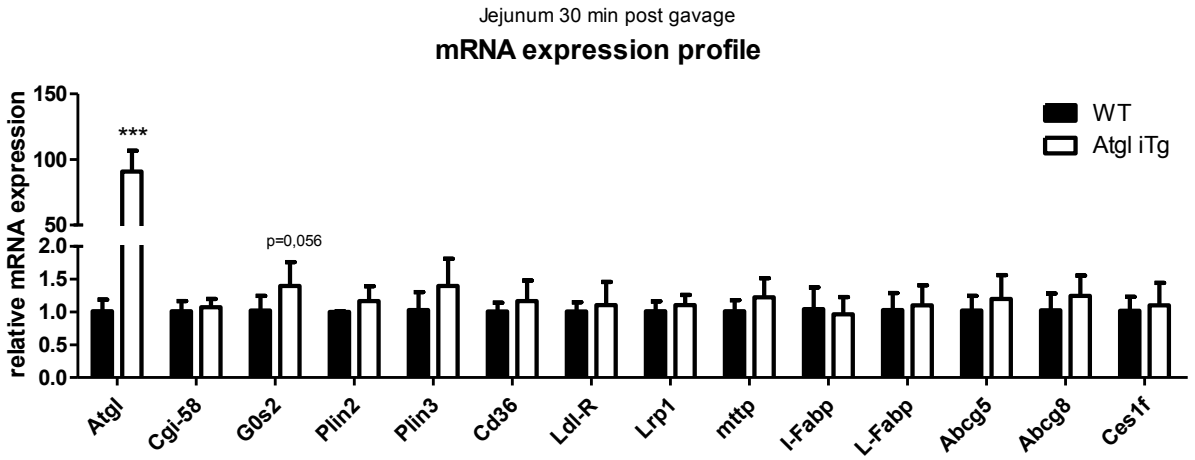

Figure 55: Jejunal mRNA profile 30 min post gavage. Expression profile of genes involved in lipid absorption and FA transport in enterocytes. Expression levels were normalized to *cyclophilin A* as houskeeping gene. Data represent mean values (n=5-6) + SD. ***p ≤ 0.001.

Furthermore, oppositional to mice lacking ATGL and CGI-58 (**Figure 24D**), Atgl iTg mice displayed significantly increased circulating plasma parameters with 29% and 16% elevated TG and cholesterol concentrations, respectively (**Figure 56A**). Intracellular TG levels in the jejunum, the side of lipoprotein secretion, were reduced by 40%, but did not reach statistical significance (**Figure 56B**), again questioning the role of intestinal ATGL in dietary TG absorption. Interestingly, ORO staining revealed localization of cLDs in the epithelial layer of the SI in same extent in WT and Atgl iTg mice (**Figure 56B**). Biochemical and histological anaysis of hepatic tissues did not show any differences between the genotypes, beside slightly elevated CE levels in Atgl iTg mice (**Figure 56C**).

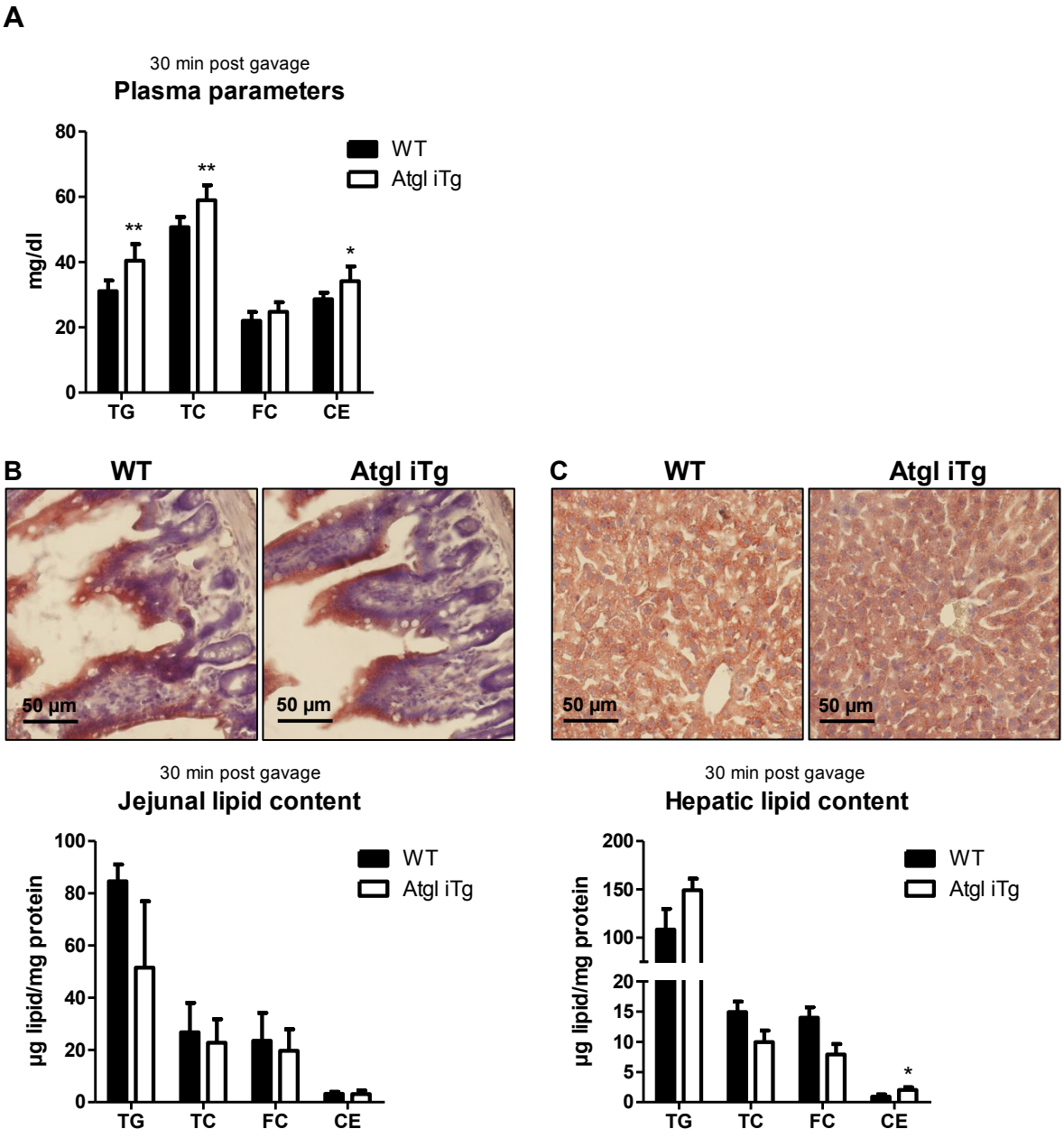

Figure 56: Intestinal and hepatic lipid levels in Atgl iTg mice 30 min post gavage. (A) Plasma lipid levels in WT and Atgl iTg mice 30 min after administration of an oil bolus. ORO staining and intracellular lipid levels in (B) jejuna and (C) livers. Data represent mean values (n=4-6) + SD. Magnification, 40x; scale bar, 50 µm. *p < 0.05; **p ≤ 0.01.

Taken together, intestine-specific overexpression of ATGL mildly ameliorates HF/HCD-induced intestinal steatosis, thus identifying ATGL as an important hydrolase within enterocytes. Comparable lipoprotein secretion, however, indicates that ATGL does not provide FFAs as substrates for CM assembly. With regard to dietary lipid absorption, our *in vivo* studies so far evidence that ATGL rather regulates cholesterol homeostasis via activation of PPARα.

3.3 Discussion

To investigate potential beneficial effects of intestinal ATGL overexpression, we generated mice expressing a FLAG-tagged Atgl coding sequence under the control of the enterocyte-specific villin promotor (Atgl iTg). Injection of the transgenic construct into mouse pronuclei and transplantation into surrogate females resulted in transgenic founders with approximately 80-fold increased *Atgl* mRNA expression levels. Despite drastically elevated *Atgl* mRNA levels, enzymatic activity of ATGL in the jejunum of Atgl iTg mice was only mildly induced.

Mice specifically overexpressing ATGL in the small intestine did not show any differences in their phenotypic appearance. Even after challenging mice for 5 weeks with a HF/HCD, WT and Atgl iTg mice gained body weight in a comparable manner. We could not observe any effect on plasma parameters in any feeding state, which is in line with results obtained from intestine-specific ATGL KO mice (Obrowsky et al., 2013). Interestingly, secretion of lipids as CMs or VLDLs was slightly impaired in Atgl iTg mice, presumably due to increased burning of cellular lipids as indicated by increased FAO. However, deletion of intestinal (Obrowsky et al., 2013, Korbelius et al., 2019) or hepatic ATGL (Wu et al., 2011) in previous studies suggested that ATGL is not required for providing FAs for lipoprotein assembly, therefore the observed slight decrease might is unlikely of biological relevance.

When Atgl iTg mice were challenged with a HF/HCD, organ weights remained comparable, with a tendency toward reduced intestinal, but increased liver weight. Biochemical estimation of intestinal and hepatic lipid levels revealed no significant differences between the genotypes, however, duodenal TG concentrations were reduced in Atgl iTg mice by 60%. This already indicated an ameliorative effect of intestinal ATGL overexpression on intestinal lipid deposition and highlighted its role in the degradation of an intestinal TG storage pool. However, the effects of ATGL overexpression on intracellular TG levels were not as pronounced as expected. This might be due to the fact that although *Atgl* expression is massively upregulated, its activity is not increased to the same extent. This might be the consequence of limited availability of CGI-58 as overexpression of ATGL did not affect expression levels of *Cgi-58.* Thus, complete neutral lipolysis, involving stimulation of ATGL by CGI-58, occurs at the same level as in WT mice.

To elucidate if overexpression of ATGL somehow impacts dietary TG absorption, HF/HCD-fed mice were gavaged with ^{3}H-TO. In line with results obtained in mice lacking ATGL in the SI (Obrowsky et al., 2013, Korbelius et al., 2019), we observed unchanged secretion of the tracer into the circulation. Radioactivity in intestines and livers also remained comparable

between the genotypes. As tyloxapol was used in this study to prevent peripheral lipolysis, thus avoiding uptake of lipids from the basolateral side, this finding is in line with our revised model for intestinal lipid metabolism. Therefore, ATGL indeed is rather involved in the cleavage of basolaterally-derived lipids rather than in dietary lipid uptake.

However, mice lacking ATGL specifically in the SI displayed impaired cholesterol absorption from the diet. Oral administration of ^{14}C-cholesterol to HF/HCD-fed Atgl iTg mice revealed a 1.6-fold increase in plasma radioactivity. This finding was in line with data obtained from intestine-specific ATGL KO mice, in which oral gavage of cholesterol resulted in significantly decreased plasma cholesterol concentrations. Furthermore, while ATGL iKO mice also accumulated less radioactivity in the liver, Atgl iTg mice displayed slightly more hepatic ^{14}C-cholesterol. (Obrowsky et al., 2013)

Although absorption of ^{14}C-cholesterol into the intestine remained comparable between WT and Atgl iTg mice, jejunal organ weight was slightly decreased. Fecal excretion of the radioactive tracer was reduced by 40% in Atgl iTg mice, indicating accelerated cholesterol absorption from the intestinal lumen. This coincided with significantly elevated mRNA expression levels of *Npc1l1*, the main cholesterol importer. Additional upregulation of the cholesterol exporters *Abcg5* and *Abcg8* further explained the observed increase in plasma radioactivity. These *in vivo* studies primarily indicated that intestinal ATGL is a main regulator of dietary cholesterol absorption, most likely through activation of PPARα, whose mRNA expression levels were also significantly increased in the jejunum of Atgl iTg mice.

Previous studies identified ATGL as an important player in the regulation of PPARα target genes (Haemmerle et al., 2011, Obrowsky et al., 2013). It is known that intestinal PPARα regulates genes involved in lipid absorption, FAO, defense against oxidative stress, and inflammation (de Vogel-van den Bosch et al., 2008). Even though the cholesterol transporters *Npc1l1* and *Abcg5/8* were significantly increased in Atgl iTg mice, their expression levels were not affected in mice lacking intestinal ATGL. However, disturbances in intestinal cholesterol homeostasis in ATGL KO mice were suggested to be caused by decreased *Cd36* expression and downregulation of *Abca1*. Intestinal CD36 is not only responsible for luminal absorption of FAs, but also of free cholesterol. In the gut, both CD36 and ABCA1 are regulated by PPARα. Transgenic mice fed a HF/HCD also displayed slightly elevated mRNA expression levels of *Cd36* and *Abca1*, further strengthening the role of intestinal ATGL in PPARα signaling. The observed increase in circulating ^{14}C-cholesterol levels might therefore also be accountable to an upregulation of intestinal *Abca1*. Interestingly, other PPARα-regulated genes involved in oxidative stress defense (gluthation-

S-transferases) or FAO remained comparable between the genotypes, indicating that FAs released by the action of intestinal ATGL are primarily used to modulate intestinal cholesterol homeostasis via activation of PPARα.

To further investigate the role of ATGL on intestinal TG metabolism, we sacrificed mice 30 min post an oral lipid load to mimic the early phase of alimentary lipid absorption. In contrast to results obtained in mice lacking intestinal CGI-58/ATGL (Korbelius et al., 2019), we found significantly increased concentrations of plasma TGs and total cholesterol, which was attributable to an increase in CE levels. Concordant with results obtained in Cgi-58/Atgl iDKO mice, intestinal lipid levels remained comparable in these mice. While lack of both CGI-58 and ATGL also ameliorated hepatic steatosis, overexpression of solely ATGL resulted in slightly increased hepatic CE levels and a tendency toward increased TG concentrations. However, the effect was more pronounced in mice lacking both proteins necessary for the first step of neutral lipolysis, indicating that CGI-58 also contributes to the hepatic phenotype.

Taken together, intestine-specific overexpression of ATGL mildly ameliorates HF/HCD-induced intestinal steatosis, thus identifying ATGL as an important hydrolase within enterocytes. The effect of ATGL overexpression on intracellular TG metabolism is less pronounced than expected, which might be due to limited availability of CGI-58 to excute complete lipolysis. Instead, Atgl iTg mice display more pronounced changes in cholesterol concentrations, suggesting that intestinal ATGL plays an important role in regulating cholesterol homeostasis in a CGI-58-independent manner. Comparable lipoprotein secretion, however, indicates that ATGL does not provide FFAs as substrates for CM assembly. With regard to dietary lipid absorption, our *in vivo* studies evidence that ATGL rather regulates cholesterol homeostasis via activation of PPARα than TG metabolism.

4 Bibliography

ABUMRAD, N. A. & DAVIDSON, N. O. 2012. Role of the gut in lipid homeostasis. *Physiol Rev,* 92**,** 1061-85.

ALPERS, D. H., BASS, N. M., ENGLE, M. J. & DESCHRYVER-KECSKEMETI, K. 2000. Intestinal fatty acid binding protein may favor differential apical fatty acid binding in the intestine. *Biochim Biophys Acta,* 1483**,** 352-62.

BEILSTEIN, F., CARRIERE, V., LETURQUE, A. & DEMIGNOT, S. 2016. Characteristics and functions of lipid droplets and associated proteins in enterocytes. *Exp Cell Res,* 340**,** 172-9.

BORGSTROEM, B. 1964. INFLUENCE OF BILE SALT, PH, AND TIME ON THE ACTION OF PANCREATIC LIPASE; PHYSIOLOGICAL IMPLICATIONS. *J Lipid Res,* 5**,** 522-31.

BROWN, J. M., BETTERS, J. L., LORD, C., MA, Y., HAN, X., YANG, K., ALGER, H. M., MELCHIOR, J., SAWYER, J., SHAH, R., WILSON, M. D., LIU, X., GRAHAM, M. J., LEE, R., CROOKE, R., SHULMAN, G. I., XUE, B., SHI, H. & YU, L. 2010. CGI-58 knockdown in mice causes hepatic steatosis but prevents diet-induced obesity and glucose intolerance. *J Lipid Res,* 51**,** 3306-15.

BROWN, J. M., CHUNG, S., DAS, A., SHELNESS, G. S., RUDEL, L. L. & YU, L. 2007. CGI-58 facilitates the mobilization of cytoplasmic triglyceride for lipoprotein secretion in hepatoma cells. *J Lipid Res,* 48**,** 2295-305.

BUHMAN, K. K., SMITH, S. J., STONE, S. J., REPA, J. J., WONG, J. S., KNAPP, F. F., JR., BURRI, B. J., HAMILTON, R. L., ABUMRAD, N. A. & FARESE, R. V., JR. 2002. DGAT1 is not essential for intestinal triacylglycerol absorption or chylomicron synthesis. *J Biol Chem,* 277**,** 25474-9.

CASPARY, W. F. 1992. Physiology and pathophysiology of intestinal absorption. *Am J Clin Nutr,* 55**,** 299S-308S.

CHOI, S. H. & GINSBERG, H. N. 2011. Increased very low density lipoprotein (VLDL) secretion, hepatic steatosis, and insulin resistance. *Trends Endocrinol Metab,* 22**,** 353-63.

COOPER, A. D. 1997. Hepatic uptake of chylomicron remnants. *J Lipid Res,* 38**,** 2173-92.

D'AQUILA, T., HUNG, Y. H., CARREIRO, A. & BUHMAN, K. K. 2016. Recent discoveries on absorption of dietary fat: Presence, synthesis, and metabolism of cytoplasmic lipid droplets within enterocytes. *Biochim Biophys Acta,* 1861**,** 730-47.

DE VOGEL-VAN DEN BOSCH, H. M., BUNGER, M., DE GROOT, P. J., BOSCH-VERMEULEN, H., HOOIVELD, G. J. & MULLER, M. 2008. PPARalpha-mediated effects of dietary lipids on intestinal barrier gene expression. *BMC Genomics,* 9**,** 231.

DEMIGNOT, S., BEILSTEIN, F. & MOREL, E. 2014. Triglyceride-rich lipoproteins and cytosolic lipid droplets in enterocytes: key players in intestinal physiology and metabolic disorders. *Biochimie,* 96**,** 48-55.

DIJK, W., MATTIJSSEN, F., DE LA ROSA RODRIGUEZ, M., LOZA VALDES, A., LOFT, A., MANDRUP, S., KALKHOVEN, E., QI, L., BORST, J. W. & KERSTEN, S. 2017. Hypoxia-Inducible Lipid Droplet-Associated Is Not a Direct Physiological Regulator of Lipolysis in Adipose Tissue. *Endocrinology,* 158**,** 1231-1251.

DISTEFANO, M. T., DANAI, L. V., ROTH FLACH, R. J., CHAWLA, A., PEDERSEN, D. J., GUILHERME, A. & CZECH, M. P. 2015. The Lipid Droplet Protein Hypoxia-inducible Gene 2 Promotes Hepatic Triglyceride Deposition by Inhibiting Lipolysis. *J Biol Chem,* 290**,** 15175-84.

DUNCAN, R. E., AHMADIAN, M., JAWORSKI, K., SARKADI-NAGY, E. & SUL, H. S. 2007. Regulation of lipolysis in adipocytes. *Annu Rev Nutr,* 27**,** 79-101.

EICHMANN, T. O., GRUMET, L., TASCHLER, U., HARTLER, J., HEIER, C., WOBLISTIN, A., PAJED, L., KOLLROSER, M., RECHBERGER, G., THALLINGER, G. G., ZECHNER, R., HAEMMERLE, G., ZIMMERMANN, R. & LASS, A. 2015. ATGL and CGI-58 are lipid droplet proteins of the hepatic stellate cell line HSC-T6. *J Lipid Res,* 56**,** 1972-84.

ENCAPSULA-NANOSCIENCES-LLC. 2012. *Systemic Administration of Clodronate Liposomes via Intravenous Injection* [Online]. Available: https://www.clodrosome.com/routes-of-administration/intravenous/.

ESTRADA-LUNA, D., ORTIZ-RODRIGUEZ, M. A., MEDINA-BRISEÑO, L., CARREÓN-TORRES, E., IZQUIERDO-VEGA, J. A., SHARMA, A., CANCINO-DÍAZ, J. C., PÉREZ-MÉNDEZ, O., BELEFANT-MILLER, H. & BETANZOS-CABRERA, G. 2018. Current Therapies Focused on High-Density Lipoproteins Associated with Cardiovascular Disease. *Molecules,* 23**,** 2730.

EVANS, K., KUUSELA, P. J., CRUZ, M. L., WILHELMOVA, I., FIELDING, B. A. & FRAYN, K. N. 1998. Rapid chylomicron appearance following sequential meals: effects of second meal composition. *Br J Nutr,* 79**,** 425-9.

FIELDING, B. A., CALLOW, J., OWEN, R. M., SAMRA, J. S., MATTHEWS, D. R. & FRAYN, K. N. 1996. Postprandial lipemia: the origin of an early peak studied by specific dietary fatty acid intake during sequential meals. *Am J Clin Nutr,* 63**,** 36-41.

FOLCH, J., LEES, M. & SLOANE STANLEY, G. H. 1957. A simple method for the isolation and purification of total lipides from animal tissues. *J Biol Chem,* 226**,** 497-509.

GAJDA, A. M. & STORCH, J. 2015. Enterocyte fatty acid-binding proteins (FABPs): different functions of liver and intestinal FABPs in the intestine. *Prostaglandins Leukot Essent Fatty Acids,* 93**,** 9-16.

GANGL, A. & OCKNER, R. K. 1975. Intestinal metabolism of plasma free fatty acids. Intracellular compartmentation and mechanisms of control. *J Clin Invest,* 55**,** 803-13.

GAO, Y., NELSON, D. W., BANH, T., YEN, M. I. & YEN, C. L. 2013. Intestine-specific expression of MOGAT2 partially restores metabolic efficiency in Mogat2-deficient mice. *J Lipid Res,* 54**,** 1644-52.

GLATZ, J. F. & LUIKEN, J. J. 2017. From fat to FAT (CD36/SR-B2): Understanding the regulation of cellular fatty acid uptake. *Biochimie,* 136**,** 21-26.

GRANNEMAN, J. G., MOORE, H. P., GRANNEMAN, R. L., GREENBERG, A. S., OBIN, M. S. & ZHU, Z. 2007. Analysis of lipolytic protein trafficking and interactions in adipocytes. *J Biol Chem,* 282**,** 5726-35.

GREVENGOED, T. J., KLETT, E. L. & COLEMAN, R. A. 2014. Acyl-CoA metabolism and partitioning. *Annu Rev Nutr,* 34**,** 1-30.

GROND, S., RADNER, F. P. W., EICHMANN, T. O., KOLB, D., GRABNER, G. F., WOLINSKI, H., GRUBER, R., HOFER, P., HEIER, C., SCHAUER, S., RULICKE, T., HOEFLER, G., SCHMUTH, M., ELIAS, P. M., LASS, A., ZECHNER, R. & HAEMMERLE, G. 2017. Skin Barrier Development Depends on CGI-58 Protein Expression during Late-Stage Keratinocyte Differentiation. *J Invest Dermatol,* 137**,** 403-413.

GUO, F., MA, Y., KADEGOWDA, A. K., BETTERS, J. L., XIE, P., LIU, G., LIU, X., MIAO, H., OU, J., SU, X., ZHENG, Z., XUE, B., SHI, H. & YU, L. 2013. Deficiency of liver Comparative Gene Identification-58 causes steatohepatitis and fibrosis in mice. *J Lipid Res,* 54**,** 2109-20.

HAEMMERLE, G., LASS, A., ZIMMERMANN, R., GORKIEWICZ, G., MEYER, C., ROZMAN, J., HELDMAIER, G., MAIER, R., THEUSSL, C., EDER, S., KRATKY, D., WAGNER, E. F., KLINGENSPOR, M., HOEFLER, G. & ZECHNER, R. 2006. Defective lipolysis and altered energy metabolism in mice lacking adipose triglyceride lipase. *Science,* 312**,** 734-7.

HAEMMERLE, G., MOUSTAFA, T., WOELKART, G., BUTTNER, S., SCHMIDT, A., VAN DE WEIJER, T., HESSELINK, M., JAEGER, D., KIENESBERGER, P. C., ZIERLER, K., SCHREIBER, R., EICHMANN, T., KOLB, D., KOTZBECK, P., SCHWEIGER, M., KUMARI, M., EDER, S., SCHOISWOHL, G., WONGSIRIROJ, N., POLLAK, N. M., RADNER, F. P., PREISS-LANDL, K., KOLBE, T., RULICKE, T., PIESKE, B., TRAUNER, M., LASS, A., ZIMMERMANN, R., HOEFLER, G., CINTI, S., KERSHAW, E. E., SCHRAUWEN, P., MADEO, F., MAYER, B. & ZECHNER, R. 2011. ATGL-mediated fat catabolism regulates cardiac mitochondrial function via PPAR-alpha and PGC-1. *Nat Med,* 17**,** 1076-85.

HAEMMERLE, G., ZIMMERMANN, R., HAYN, M., THEUSSL, C., WAEG, G., WAGNER, E., SATTLER, W., MAGIN, T. M., WAGNER, E. F. & ZECHNER, R. 2002. Hormone-sensitive lipase deficiency in mice causes diglyceride accumulation in adipose tissue, muscle, and testis. *J Biol Chem,* 277**,** 4806-15.

HO, S. Y., DELGADO, L. & STORCH, J. 2002. Monoacylglycerol metabolism in human intestinal Caco-2 cells: evidence for metabolic compartmentation and hydrolysis. *J Biol Chem,* 277**,** 1816-23.

HOFER, P., BOESZOERMENYI, A., JAEGER, D., FEILER, U., ARTHANARI, H., MAYER, N., ZEHENDER, F., RECHBERGER, G., OBERER, M., ZIMMERMANN, R., LASS, A., HAEMMERLE, G., BREINBAUER, R., ZECHNER, R. & PREISS-LANDL, K. 2015. Fatty Acid-binding Proteins Interact with Comparative Gene Identification-58 Linking Lipolysis with Lipid Ligand Shuttling. *J Biol Chem,* 290**,** 18438-53.

HUSSAIN, M. M. 2014. Intestinal lipid absorption and lipoprotein formation. *Curr Opin Lipidol,* 25**,** 200-6.

INLOES, J. M., HSU, K. L., DIX, M. M., VIADER, A., MASUDA, K., TAKEI, T., WOOD, M. R. & CRAVATT, B. F. 2014. The hereditary spastic paraplegia-related enzyme DDHD2 is a principal brain triglyceride lipase. *Proc Natl Acad Sci U S A,* 111**,** 14924-9.

IQBAL, J. & HUSSAIN, M. M. 2009. Intestinal lipid absorption. *Am J Physiol Endocrinol Metab,* 296**,** E1183-94.

JACKSON, K. G., ROBERTSON, M. D., FIELDING, B. A., FRAYN, K. N. & WILLIAMS, C. M. 2002. Olive oil increases the number of triacylglycerol-rich chylomicron particles compared with other oils: an effect retained when a second standard meal is fed. *Am J Clin Nutr,* 76**,** 942-9.

JENKINS, C. M., MANCUSO, D. J., YAN, W., SIMS, H. F., GIBSON, B. & GROSS, R. W. 2004. Identification, cloning, expression, and purification of three novel human calcium-independent phospholipase A2 family members possessing triacylglycerol lipase and acylglycerol transacylase activities. *J Biol Chem,* 279**,** 48968-75.

JONES, R. D., TAYLOR, A. M., TONG, E. Y. & REPA, J. J. 2013. Carboxylesterases Are Uniquely Expressed among Tissues and Regulated by Nuclear Hormone Receptors in the Mouse. *Drug Metab Dispos,* 41**,** 40-9.

KHALDOUN, S. A., EMOND-BOISJOLY, M. A., CHATEAU, D., CARRIERE, V., LACASA, M., ROUSSET, M., DEMIGNOT, S. & MOREL, E. 2014. Autophagosomes contribute to intracellular lipid distribution in enterocytes. *Mol Biol Cell,* 25**,** 118-32.

KHALIFEH-SOLTANI, A., GUPTA, D., HA, A., IQBAL, J., HUSSAIN, M., PODOLSKY, M. J. & ATABAI, K. 2016. Mfge8 regulates enterocyte lipid storage by promoting enterocyte triglyceride hydrolase activity. *JCI Insight,* 1**,** e87418.

KORBELIUS, M., VUJIC, N., SACHDEV, V., OBROWSKY, S., RAINER, S., GOTTSCHALK, B., GRAIER, W. & KRATKY, D. 2019. ATGL/CGI-58-dependent hydrolysis of a lipid storage pool in murine enterocytes. *Cell Reports,* 28, 1923-34.

LAGAKOS, W. S., GUAN, X., HO, S. Y., SAWICKI, L. R., CORSICO, B., KODUKULA, S., MUROTA, K., STARK, R. E. & STORCH, J. 2013. Liver fatty acid-binding protein binds monoacylglycerol in vitro and in mouse liver cytosol. *J Biol Chem,* 288**,** 19805-15.

LASS, A., ZIMMERMANN, R., HAEMMERLE, G., RIEDERER, M., SCHOISWOHL, G., SCHWEIGER, M., KIENESBERGER, P., STRAUSS, J. G., GORKIEWICZ, G. & ZECHNER, R. 2006. Adipose triglyceride lipase-mediated lipolysis of cellular fat stores is activated by CGI-58 and defective in Chanarin-Dorfman Syndrome. *Cell Metab,* 3**,** 309-19.

LEE, B., ZHU, J., WOLINS, N. E., CHENG, J. X. & BUHMAN, K. K. 2009. Differential association of adipophilin and TIP47 proteins with cytoplasmic lipid droplets in mouse enterocytes during dietary fat absorption. *Biochim Biophys Acta,* 1791**,** 1173-80.

LI, D., RODIA, C. N., JOHNSON, Z. K., BAE, M., MUTER, A., HUESSINGER, A. E., TAMBINI, N., LONGO, A. M., DONG, H., LEE, J.-Y. & KOHAN, A. B. 2019. Intestinal basolateral lipid substrate transport (BLST) is linked to chylomicron secretion and is regulated by apoC-III. *Journal of Lipid Research*.

LI, H., SONG, Y., ZHANG, L. J., GU, Y., LI, F. F., PAN, S. Y., JIANG, L. N., LIU, F., YE, J. & LI, Q. 2012. LSDP5 enhances triglyceride storage in hepatocytes by influencing lipolysis and fatty acid beta-oxidation of lipid droplets. *PLoS One,* 7**,** e36712.

LÖFFLER, G., PETRIDES, P. & HEINRICH, P. 2009. *Biochemie & Pathobiochemie,* Heidelberg, Germany, Springer Verlag.

LORD, C. C. & BROWN, J. M. 2012. Distinct roles for alpha-beta hydrolase domain 5 (ABHD5/CGI-58) and adipose triglyceride lipase (ATGL/PNPLA2) in lipid metabolism and signaling. *Adipocyte,* 1**,** 123-131.

MACPHERSON, R. E., RAMOS, S. V., VANDENBOOM, R., ROY, B. D. & PETERS, S. J. 2013. Skeletal muscle PLIN proteins, ATGL and CGI-58, interactions at rest and following stimulated contraction. *Am J Physiol Regul Integr Comp Physiol,* 304**,** R644-50.

MADISON, B. B., DUNBAR, L., QIAO, X. T., BRAUNSTEIN, K., BRAUNSTEIN, E. & GUMUCIO, D. L. 2002. Cis elements of the villin gene control expression in restricted domains of the vertical (crypt) and horizontal (duodenum, cecum) axes of the intestine. *J Biol Chem,* 277**,** 33275-83.

MAHAN, J. T., HEDA, G. D., RAO, R. H. & MANSBACH, C. M., 2ND 2001. The intestine expresses pancreatic triacylglycerol lipase: regulation by dietary lipid. *Am J Physiol Gastrointest Liver Physiol,* 280**,** G1187-96.

MANSBACH, C. M., 2ND & DOWELL, R. F. 1992. Uptake and metabolism of circulating fatty acids by rat intestine. *Am J Physiol,* 263**,** G927-33.

MANSBACH, C. M., 2ND & DOWELL, R. F. 1995. Role of the intestine in chylomicron remnant clearance. *Am J Physiol,* 269**,** G144-52.

MASSON, C. J., PLAT, J., MENSINK, R. P., NAMIOT, A., KISIELEWSKI, W., NAMIOT, Z., FULLEKRUG, J., EHEHALT, R., GLATZ, J. F. & PELSERS, M. M. 2010. Fatty acid- and cholesterol transporter protein expression along the human intestinal tract. *PLoS One,* 5**,** e10380.

MCMAHON, D., DINH, A., KURZ, D., SHAH, D., HAN, G. S., CARMAN, G. M. & BRASAEMLE, D. L. 2014. Comparative gene identification 58/alpha/beta hydrolase domain 5 lacks lysophosphatidic acid acyltransferase activity. *J Lipid Res,* 55**,** 1750-1761.

MISSAGLIA, S., COLEMAN, R. A., MORDENTE, A. & TAVIAN, D. 2019. Neutral Lipid Storage Diseases as Cellular Model to Study Lipid Droplet Function. *Cells,* 8.

MONTERO-MORAN, G., CAVIGLIA, J. M., MCMAHON, D., ROTHENBERG, A., SUBRAMANIAN, V., XU, Z., LARA-GONZALEZ, S., STORCH, J., CARMAN, G. M. & BRASAEMLE, D. L. 2010. CGI-58/ABHD5 is a coenzyme A-dependent lysophosphatidic acid acyltransferase. *J Lipid Res,* 51**,** 709-19.

MU, H. & HOY, C. E. 2004. The digestion of dietary triacylglycerols. *Prog Lipid Res,* 43**,** 105-33.

NELSON, D. W., GAO, Y., YEN, M. I. & YEN, C. L. 2014. Intestine-specific deletion of acyl-CoA:monoacylglycerol acyltransferase (MGAT) 2 protects mice from diet-induced obesity and glucose intolerance. *J Biol Chem,* 289**,** 17338-49.

NEWBERRY, E. P., XIE, Y., KENNEDY, S., HAN, X., BUHMAN, K. K., LUO, J., GROSS, R. W. & DAVIDSON, N. O. 2003. Decreased hepatic triglyceride accumulation and altered fatty acid uptake in mice with deletion of the liver fatty acid-binding protein gene. *J Biol Chem,* 278**,** 51664-72.

NIOT, I., POIRIER, H., TRAN, T. T. & BESNARD, P. 2009. Intestinal absorption of long-chain fatty acids: evidence and uncertainties. *Prog Lipid Res,* 48**,** 101-15.

OBROWSKY, S., CHANDAK, P. G., PATANKAR, J. V., PFEIFER, T., POVODEN, S., SCHREIBER, R., HAEMMERLE, G., LEVAK-FRANK, S. & KRATKY, D. 2012. Cholesteryl ester accumulation and accelerated cholesterol absorption in intestine-specific hormone sensitive lipase-null mice. *Biochim Biophys Acta,* 1821**,** 1406-14.

OBROWSKY, S., CHANDAK, P. G., PATANKAR, J. V., POVODEN, S., SCHLAGER, S., KERSHAW, E. E., BOGNER-STRAUSS, J. G., HOEFLER, G., LEVAK-FRANK, S. & KRATKY, D. 2013. Adipose triglyceride lipase is a TG hydrolase of the small intestine and regulates intestinal PPARalpha signaling. *J Lipid Res,* 54**,** 425-35.

OCKNER, R. K., HUGHES, F. B. & ISSELBACHER, K. J. 1969. Very low density lipoproteins in intestinal lymph: origin, composition, and role in lipid transport in the fasting state. *J Clin Invest,* 48**,** 2079-88.

OKAZAKI, H., IGARASHI, M., NISHI, M., TAJIMA, M., SEKIYA, M., OKAZAKI, S., YAHAGI, N., OHASHI, K., TSUKAMOTO, K., AMEMIYA-KUDO, M., MATSUZAKA, T., SHIMANO, H., YAMADA, N., AOKI, J., MORIKAWA, R., TAKANEZAWA, Y., ARAI, H., NAGAI, R., KADOWAKI, T., OSUGA, J. & ISHIBASHI, S. 2006. Identification of a novel member of the carboxylesterase family that hydrolyzes triacylglycerol: a potential role in adipocyte lipolysis. *Diabetes,* 55**,** 2091-7.

ONG, K. T., MASHEK, M. T., BU, S. Y., GREENBERG, A. S. & MASHEK, D. G. 2011. Adipose triglyceride lipase is a major hepatic lipase that regulates triacylglycerol turnover and fatty acid signaling and partitioning. *Hepatology,* 53**,** 116-26.

PADMANABHA DAS, K. M., WECHSELBERGER, L., LIZICZAI, M., DE LA ROSA RODRIGUEZ, M., GRABNER, G. F., HEIER, C., VIERTLMAYR, R., RADLER, C., LICHTENEGGER, J., ZIMMERMANN, R., BORST, J. W., ZECHNER, R., KERSTEN, S. & OBERER, M. 2018. Hypoxia-inducible lipid droplet-associated protein inhibits adipose triglyceride lipase. *J Lipid Res,* 59**,** 531-541.

PAN, X. & HUSSAIN, M. M. 2012. Gut triglyceride production. *Biochim Biophys Acta,* 1821**,** 727-35.

PHAN, C. T. & TSO, P. 2001. Intestinal lipid absorption and transport. *Front Biosci,* 6**,** D299-319.

QUIROGA, A. D., LIAN, J. & LEHNER, R. 2012. Carboxylesterase1/Esterase-x regulates chylomicron production in mice. *PLoS One,* 7**,** e49515.

RADNER, F. P., STREITH, I. E., SCHOISWOHL, G., SCHWEIGER, M., KUMARI, M., EICHMANN, T. O., RECHBERGER, G., KOEFELER, H. C., EDER, S., SCHAUER, S., THEUSSL, H. C., PREISS-LANDL, K., LASS, A., ZIMMERMANN, R., HOEFLER, G., ZECHNER, R. & HAEMMERLE, G. 2010. Growth retardation, impaired triacylglycerol catabolism, hepatic steatosis, and lethal skin barrier defect in mice lacking comparative gene identification-58 (CGI-58). *J Biol Chem,* 285**,** 7300-11.

RADOVIC, B., VUJIC, N., LEOPOLD, C., SCHLAGER, S., GOERITZER, M., PATANKAR, J. V., KORBELIUS, M., KOLB, D., REINDL, J., WEGSCHEIDER, M., TOMIN, T., BIRNER-GRUENBERGER, R., SCHITTMAYER, M., GROSCHNER, L., MAGNES, C., DIWOKY, C., FRANK, S., STEYRER, E., DU, H., GRAIER, W. F., MADL, T. & KRATKY, D. 2016. Lysosomal acid lipase regulates VLDL synthesis and insulin sensitivity in mice. *Diabetologia,* 59**,** 1743-52.

SAMPUGNA, J., QUINN, J. G., PITAS, R. E., CARPENTER, D. L. & JENSEN, R. G. 1967. Digestion of butyrate glycerides by pancreatic lipase. *Lipids,* 2**,** 397-402.

SCHREIBER, R., XIE, H. & SCHWEIGER, M. 2019. Of mice and men: The physiological role of adipose triglyceride lipase (ATGL). *Biochim Biophys Acta Mol Cell Biol Lipids,* 1864**,** 880-899.

SCHWEIGER, M., LASS, A., ZIMMERMANN, R., EICHMANN, T. O. & ZECHNER, R. 2009. Neutral lipid storage disease: genetic disorders caused by mutations in adipose triglyceride lipase/PNPLA2 or CGI-58/ABHD5. *Am J Physiol Endocrinol Metab,* 297**,** E289-96.

SCHWEIGER, M., ROMAUCH, M., SCHREIBER, R., GRABNER, G. F., HUTTER, S., KOTZBECK, P., BENEDIKT, P., EICHMANN, T. O., YAMADA, S., KNITTELFELDER, O., DIWOKY, C., DOLER, C., MAYER, N., DE CECCO, W., BREINBAUER, R., ZIMMERMANN, R. & ZECHNER, R. 2017. Pharmacological inhibition of adipose triglyceride lipase corrects high-fat diet-induced insulin resistance and hepatosteatosis in mice. *Nat Commun,* 8**,** 14859.

SCHWEIGER, M., SCHREIBER, R., HAEMMERLE, G., LASS, A., FLEDELIUS, C., JACOBSEN, P., TORNQVIST, H., ZECHNER, R. & ZIMMERMANN, R. 2006. Adipose triglyceride lipase and hormone-sensitive lipase are the major enzymes in adipose tissue triacylglycerol catabolism. *J Biol Chem,* 281**,** 40236-41.

SEYER, A., CANTIELLO, M., BERTRAND-MICHEL, J., ROQUES, V., NAUZE, M., BEZIRARD, V., COLLET, X., TOUBOUL, D., BRUNELLE, A. & COMERA, C. 2013. Lipidomic and spatio-temporal imaging of fat by mass spectrometry in mice duodenum during lipid digestion. *PLoS One,* 8**,** e58224.

SHIAU, Y. F., BOYLE, J. T., UMSTETTER, C. & KOLDOVSKY, O. 1980. Apical distribution of fatty acid esterification capacity along the villus-crypt unit of rat jejunum. *Gastroenterology,* 79**,** 47-53.

SHIM, J., MOULSON, C. L., NEWBERRY, E. P., LIN, M. H., XIE, Y., KENNEDY, S. M., MINER, J. H. & DAVIDSON, N. O. 2009. Fatty acid transport protein 4 is dispensable for intestinal lipid absorption in mice. *J Lipid Res,* 50**,** 491-500.

SIDDIQI, S., SALEEM, U., ABUMRAD, N. A., DAVIDSON, N. O., STORCH, J., SIDDIQI, S. A. & MANSBACH, C. M., 2ND 2010. A novel multiprotein complex is required to generate the prechylomicron transport vesicle from intestinal ER. *J Lipid Res,* 51**,** 1918-28.

SONI, K. G., MARDONES, G. A., SOUGRAT, R., SMIRNOVA, E., JACKSON, C. L. & BONIFACINO, J. S. 2009. Coatomer-dependent protein delivery to lipid droplets. *J Cell Sci,* 122**,** 1834-41.

SOUED, M. & MANSBACH, C. M., 2ND 1996. Chylomicron remnant uptake by enterocytes is receptor dependent. *Am J Physiol,* 270**,** G203-12.

STAHL, A., HIRSCH, D. J., GIMENO, R. E., PUNREDDY, S., GE, P., WATSON, N., PATEL, S., KOTLER, M., RAIMONDI, A., TARTAGLIA, L. A. & LODISH, H. F. 1999. Identification of the major intestinal fatty acid transport protein. *Mol Cell,* 4**,** 299-308.

STONE, S. J., MYERS, H. M., WATKINS, S. M., BROWN, B. E., FEINGOLD, K. R., ELIAS, P. M. & FARESE, R. V., JR. 2004. Lipopenia and skin barrier abnormalities in DGAT2-deficient mice. *J Biol Chem,* 279**,** 11767-76.

STORCH, J., ZHOU, Y. X. & LAGAKOS, W. S. 2008. Metabolism of apical versus basolateral sn-2-monoacylglycerol and fatty acids in rodent small intestine. *J Lipid Res,* 49**,** 1762-9.

TSO, P., DRAKE, D. S., BLACK, D. D. & SABESIN, S. M. 1984. Evidence for separate pathways of chylomicron and very low-density lipoprotein assembly and transport by rat small intestine. *Am J Physiol,* 247**,** G599-610.

UNGER, R. H., CLARK, G. O., SCHERER, P. E. & ORCI, L. 2010. Lipid homeostasis, lipotoxicity and the metabolic syndrome. *Biochim Biophys Acta,* 1801**,** 209-14.

VAN RIJN, J. M., VAN HOESEL, M., DE HEUS, C., VAN VUGT, A. H. M., KLUMPERMAN, J., NIEUWENHUIS, E. E. S., HOUWEN, R. H. J. & MIDDENDORP, S. 2019. DGAT2 partially compensates for lipid-induced ER stress in human DGAT1-deficient intestinal stem cells. *J Lipid Res*.

VANCE, D. & VANCE, J. 2002. Assembly and secretion of lipoproteins *Biochemistry of Lipids, Lipoproteins, and Membranes (4th edition).* Elsevier Science B.V.

VASQUEZ, K. O., CASAVANT, C. & PETERSON, J. D. 2011. Quantitative whole body biodistribution of fluorescent-labeled agents by non-invasive tomographic imaging. *PLoS One,* 6**,** e20594.

VILLENA, J. A., ROY, S., SARKADI-NAGY, E., KIM, K. H. & SUL, H. S. 2004. Desnutrin, an adipocyte gene encoding a novel patatin domain-containing protein, is induced by fasting and glucocorticoids: ectopic expression of desnutrin increases triglyceride hydrolysis. *J Biol Chem,* 279**,** 47066-75.

VUJIC, N., KORBELIUS, M., LEOPOLD, C., DUTA-MARE, M., RAINER, S., SCHLAGER, S., GOERITZER, M., KOLB, D., EICHMANN, T. O., DIWOKY, C., ZIMMER, A., ZIMMERMANN, R., LASS, A., RADOVIC, B. & KRATKY, D. 2017. Monoglyceride lipase deficiency affects hepatic cholesterol metabolism and lipid-dependent gut transit in ApoE-/- mice. *Oncotarget,* 8**,** 33122-33136.

WALTHER, T. C. & FARESE, R. V., JR. 2009. The life of lipid droplets. *Biochim Biophys Acta,* 1791**,** 459-66.

WANG, D. Q. 2007. Regulation of intestinal cholesterol absorption. *Annu Rev Physiol,* 69**,** 221-48.

WANG, L., GILL, R., PEDERSEN, T. L., HIGGINS, L. J., NEWMAN, J. W. & RUTLEDGE, J. C. 2009. Triglyceride-rich lipoprotein lipolysis releases neutral and oxidized FFAs that induce endothelial cell inflammation. *J Lipid Res,* 50**,** 204-13.

WILLIAMSON, J. R. 1964. ADIPOSE TISSUE. MORPHOLOGICAL CHANGES ASSOCIATED WITH LIPID MOBILIZATION. *J Cell Biol,* 20**,** 57-74.

WINDMUELLER, H. G. & SPAETH, A. E. 1978. Identification of ketone bodies and glutamine as the major respiratory fuels in vivo for postabsorptive rat small intestine. *J Biol Chem,* 253**,** 69-76.

WRENSCH, F., CROUCHET, E., LIGAT, G., ZEISEL, M. B., KECK, Z. Y., FOUNG, S. K. H., SCHUSTER, C. & BAUMERT, T. F. 2018. Hepatitis C Virus (HCV)-Apolipoprotein Interactions and Immune Evasion and Their Impact on HCV Vaccine Design. *Front Immunol,* 9**,** 1436.

WU, J. W., WANG, S. P., ALVAREZ, F., CASAVANT, S., GAUTHIER, N., ABED, L., SONI, K. G., YANG, G. & MITCHELL, G. A. 2011. Deficiency of liver adipose triglyceride lipase in mice causes progressive hepatic steatosis. *Hepatology,* 54**,** 122-32.

XIE, P., GUO, F., MA, Y., ZHU, H., WANG, F., XUE, B., SHI, H., YANG, J. & YU, L. 2014. Intestinal Cgi-58 deficiency reduces postprandial lipid absorption. *PLoS One,* 9**,** e91652.

YAMAGUCHI, T., OMATSU, N., MORIMOTO, E., NAKASHIMA, H., UENO, K., TANAKA, T., SATOUCHI, K., HIROSE, F. & OSUMI, T. 2007. CGI-58 facilitates lipolysis on lipid droplets but is not involved in the vesiculation of lipid droplets caused by hormonal stimulation. *J Lipid Res,* 48**,** 1078-89.

YANG, X., LU, X., LOMBES, M., RHA, G. B., CHI, Y. I., GUERIN, T. M., SMART, E. J. & LIU, J. 2010. The G(0)/G(1) switch gene 2 regulates adipose lipolysis through association with adipose triglyceride lipase. *Cell Metab,* 11**,** 194-205.

YEN, C. L., CHEONG, M. L., GRUETER, C., ZHOU, P., MORIWAKI, J., WONG, J. S., HUBBARD, B., MARMOR, S. & FARESE, R. V., JR. 2009. Deficiency of the intestinal enzyme acyl CoA:monoacylglycerol acyltransferase-2 protects mice from metabolic disorders induced by high-fat feeding. *Nat Med,* 15**,** 442-6.

YEN, C. L. & FARESE, R. V., JR. 2006. Fat breakdown: a function for CGI-58 (ABHD5) provides a new piece of the puzzle. *Cell Metab,* 3**,** 305-7.

YEN, C. L., NELSON, D. W. & YEN, M. I. 2015. Intestinal triacylglycerol synthesis in fat absorption and systemic energy metabolism. *J Lipid Res,* 56**,** 489-501.

ZECHNER, R., KIENESBERGER, P. C., HAEMMERLE, G., ZIMMERMANN, R. & LASS, A. 2009. Adipose triglyceride lipase and the lipolytic catabolism of cellular fat stores. *J Lipid Res,* 50**,** 3-21.

ZECHNER, R., MADEO, F. & KRATKY, D. 2017. Cytosolic lipolysis and lipophagy: two sides of the same coin. *Nat Rev Mol Cell Biol,* 18**,** 671-684.

ZECHNER, R., ZIMMERMANN, R., EICHMANN, T. O., KOHLWEIN, S. D., HAEMMERLE, G., LASS, A. & MADEO, F. 2012. FAT SIGNALS--lipases and lipolysis in lipid metabolism and signaling. *Cell Metab,* 15**,** 279-91.

ZHANG, L. J., WANG, C., YUAN, Y., WANG, H., WU, J., LIU, F., LI, L., GAO, X., ZHAO, Y. L., HU, P. Z., LI, P. & YE, J. 2014a. Cideb facilitates the lipidation of chylomicrons in the small intestine. *J Lipid Res,* 55**,** 1279-1287.

ZHANG, X., XIE, X., HECKMANN, B. L., SAARINEN, A. M., CZYZYK, T. A. & LIU, J. 2014b. Targeted disruption of G0/G1 switch gene 2 enhances adipose lipolysis, alters hepatic energy balance, and alleviates high-fat diet-induced liver steatosis. *Diabetes,* 63**,** 934-46.

ZHU, J., LEE, B., BUHMAN, K. K. & CHENG, J. X. 2009. A dynamic, cytoplasmic triacylglycerol pool in enterocytes revealed by ex vivo and in vivo coherent anti-Stokes Raman scattering imaging. *J Lipid Res,* 50**,** 1080-9.

ZIERLER, K. A., JAEGER, D., POLLAK, N. M., EDER, S., RECHBERGER, G. N., RADNER, F. P., WOELKART, G., KOLB, D., SCHMIDT, A., KUMARI, M., PREISS-LANDL, K., PIESKE, B., MAYER, B., ZIMMERMANN, R., LASS, A., ZECHNER, R. & HAEMMERLE, G. 2013. Functional cardiac lipolysis in mice critically depends on comparative gene identification-58. *J Biol Chem,* 288**,** 9892-904.

ZIMMERMANN, R., STRAUSS, J. G., HAEMMERLE, G., SCHOISWOHL, G., BIRNER-GRUENBERGER, R., RIEDERER, M., LASS, A., NEUBERGER, G., EISENHABER, F., HERMETTER, A. & ZECHNER, R. 2004. Fat mobilization in adipose tissue is promoted by adipose triglyceride lipase. *Science,* 306**,** 1383-6.